

Molecular Force Sensors

Design, Characterization and Applications

Dissertation

Faculty of Physics

Ludwig-Maximilians-Universität München



presented by

Kerstin Blank

München, 30. August 2006

First referee: Prof. Dr. Hermann E. Gaub
Second referee: Prof. Dr. Thomas Carell
Date of the defense: 20. October 2006

***One never notices what has been done.
One can only see what remains to be done.***

Marie Curie (1867-1934)

Table of Contents

1	Summary	7
2	Introduction	9
3	Force measurements	12
	3.1 <i>Thermodynamic and kinetic models</i>	12
	3.2 <i>Techniques for the application and detection of forces</i>	15
	3.2.1 <i>Overview</i>	15
	3.2.2 <i>The atomic force microscope (AFM)</i>	16
	3.2.3 <i>The differential force assay</i>	18
4	Immobilization of biomolecules on surfaces	21
	4.1 <i>Overview</i>	21
	4.2 <i>Covalent immobilization using hetero-bifunctional poly(ethylene glycol) spacers</i>	24
	4.3 <i>Covalent immobilization using “suicide inhibitors”</i>	25
5	Molecular force sensors	28
	5.1 <i>Requirements</i>	28
	5.2 <i>Desoxyribo nucleic acid (DNA)</i>	28
	5.3 <i>Antibody antigen interactions</i>	30
6	Molecular force sensors for the detection of receptor ligand interactions	33
	6.1 <i>Introduction to microarray technology</i>	33
	6.2 <i>Protein microarrays</i>	34
	6.2.1 <i>Technological aspects</i>	34
	6.2.2 <i>Protein microarrays based on antibody antigen interactions</i>	35
	6.2.3 <i>Force-based antibody microarrays</i>	36
7	Molecular force sensors for the manipulation of enzyme activity	37
	7.1 <i>Classical enzyme kinetics</i>	37
	7.2 <i>Influence of forces on enzyme kinetics</i>	39
	7.3 <i>Activity measurements with single enzymes</i>	41
	7.4 <i>Model system for force based manipulation</i>	43
8	Outlook	45
9	References	46
10	Supplement	
11	Curriculum vitae	
12	Acknowledgements	

1 Summary

Mechanical forces play a central role in biological systems. Many different biomolecules generate, transmit and sense forces. The most important group of such biomolecules are proteins which act as molecular force sensors. If they experience a force, which exceeds a certain threshold, they respond in a defined way. This response may either be a change in the binding affinity or in the enzymatic activity.

The effect of external forces on the binding affinity has in the past already been characterized in detail for various classes of biomolecules. A change in binding affinity can be measured directly with the analytical device, which is used to apply the force. However, measuring changes in enzymatic activity requires more sophisticated experimental approaches, such as the ones described in this work.

Once the response of a biomolecule to an external force has been characterized, this knowledge provides the blue print for the design of artificial force sensors, which act in a similar way as naturally occurring force sensors. As soon as a certain threshold force is reached, the artificial force sensors show a desired and defined response.

Within the scope of this work two different artificial force sensors have been designed, characterized and applied to analyze biological systems:

- Force sensors were designed based on DNA duplexes and antibody antigen interactions. The design is based on the unbinding force of the respective interaction.
- Another important aspect, which was considered for the design of the artificial force sensors, was the availability of methods to connect the force sensor with a force transducer (analytical device) and the biological system of interest. Two different protocols were developed to establish the desired connections.
- Two interesting candidates for artificial molecular force sensors - a DNA duplex consisting of a repetitive sequence and an antibody antigen interaction – were characterized. Their response to an externally applied force was determined for various different loading rates with dynamic force spectroscopy.
- The first application utilized a DNA based force sensor for the analysis of receptor ligand interactions. The unbinding force of this force sensor was compared directly to the unbinding forces of different antibody antigen interactions. The experiment was implemented in a parallel format, the so-called differential force assay, which was developed within the scope of this work.

- It was shown that this new assay format could be used to solve specificity problems in multiplexed diagnostic assays, which employ antibody antigen interactions. This could be achieved by utilizing the force sensor for the local application of antibodies onto surface bound antigens.
- For the second application an antibody antigen interaction was used as a force sensor for the force-based manipulation of the activity of an enzyme. For this experiment, the force sensor was required to prevent damage on the enzyme caused by too high forces.
- A model system was established, which will allow the measurement of the formation of a product while applying the force to the enzyme. This included the preparation and immobilization of the enzyme and the attachment of the force sensor to the enzyme.

The usage of artificial force sensors opens up new possibilities for the force based analysis and manipulation of biological systems. First, they can facilitate the analysis of naturally occurring force sensors by manipulating these with an artificial force sensor. Second, as has been shown within the scope of this work, an artificial force sensor can be applied for the analysis of other biological systems, which do not respond to forces in their natural environment. And finally, applications of artificial force sensors are not restricted to biological systems, but they could serve as building blocks for nanostructures.

2 Introduction

The classical way of investigating the function of biological systems relies on the analysis of molecular interactions and molecular mechanisms under equilibrium conditions. From this point of view the regulation of cellular functions is based on the binding of a ligand to its receptor, which results in a change of the conformation of the receptor. This conformational change alters the rate of a biochemical reaction or can favor another reaction pathway. However, in the last few years many examples point out that tensile, compressive and shearing forces might play a similar and fundamental role for the regulation of biochemical pathways as the binding of a ligand to its receptor (Vogel and Sheetz, 2006; Wang and Thampatty, 2006). It is assumed that molecular force sensors detect the mechanical force and convert it into a biochemical signal. Furthermore, cells do not only convert mechanical information into biochemical information. They can also utilize biochemical information to generate forces (Fig.1).

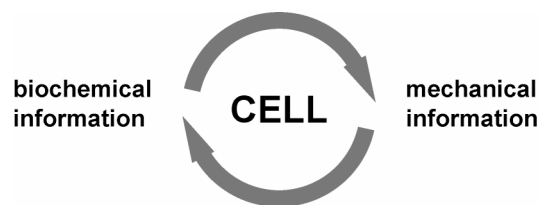


Figure 1. Cells have many mechanisms to convert biochemical information into mechanical information (e.g. molecular motors) and the other way round (e.g. mechanosensitive ion channels). All these processes rely on conformational changes of certain proteins.

This conversion of biochemical energy into mechanical work is done by molecular motors. The mode of action of molecular motors is well characterized. In contrast, almost nothing is known about the conversion of mechanical forces into biochemical information. (Fig.2). In many cases the whole process of force sensing, transduction and response is known in general, but the mechanism of the force sensor cannot be explained in detail. This is quite surprising because e.g. the receptors for hearing detect mechanical forces. The main reason for this lack of information is that only in recent years methods like the atomic force microscope, optical tweezers and molecular dynamics simulations have been developed for the analysis of these force sensors.

Recently, a few reports have been published which describe a detailed characterization of the mechanism of a force sensor. In all cases the applied force leads to a conformational change of a protein. The external force can result in a change of the binding affinity (FimH), of the catalytic activity (titin kinase, fibronectin), or of the pore size of a channel protein (MscL).

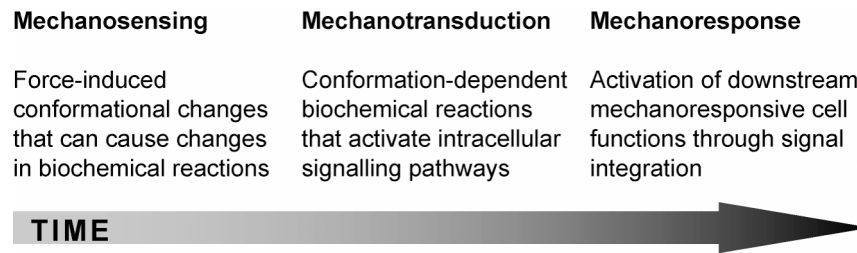


Figure 2. Process how cells react to mechanical forces. Specially adapted sensor molecules detect the force. This force is converted into a biochemical signal, which triggers or changes a signalling cascade. Finally, the cell processes the information and reacts in an appropriate way. (adapted from Vogel, 2006)

In general, the binding affinity between a receptor and its ligand becomes weaker if an external force acts on the molecular bond (chapter 3.1). However, in certain cases the applied force can lead to a conformational change in the receptor molecule resulting in a strengthening of the respective bond (catch bond). This phenomenon was shown to be responsible for the adhesion of bacteria, which becomes stronger if the bacteria are subjected to shear forces (Thomas et al., 2002; Thomas et al., 2006). This is the case when they bind to surfaces under flow conditions. The adhesion is mediated by so-called fimbriae, which are hair-like structures on the surface of the bacterium. One fimbrium consists of many individual monomers, which assemble into the respective structure. The structural domain, which is responsible for the adhesion is located at the end of each fimbrium. In the case of type 1 fimbriae from the bacterium *Escherichia coli* this domain is called the FimH domain. It consists of a ligand binding part and another part, which connects FimH to the rest of the fimbrium. Both parts are connected with a linker. Mutational studies combined with molecular dynamics simulations suggest that the force-induced extension of this linker regulates the affinity of the distally located ligand-binding site allosterically. This mechanism allows the bacteria to adhere firmly to surfaces during periods of high flow, while still permitting reversible adhesion and bacterial spreading during periods of low flow.

In the example described above the structure of the binding site is probably rearranged. More substantial conformational changes in the whole protein are required for the activation of titin kinase and fibronectin. Titin kinase is a catalytically active protein (enzyme) whose active site is hidden if no force acts on the molecule. Titin kinase is part of the muscle protein titin, which is responsible for the passive elasticity of the muscle. If a muscle is stretched titin takes up the load and can transmit force onto the titin kinase. As has been shown with molecular dynamics simulations this force can remove the so-called autoinhibitory tail and the active site becomes exposed (Gräter et al., 2005). After exposure of the active site the titin kinase is able to bind to other proteins, which are most probably involved in muscle gene expression (Lange et al., 2005). Whereas titin kinase is an enzyme, the physiological function of fibronectin is different. Fibronectin is a structural protein.

However, if fibronectin is stretched specific peptide sequences can change their conformation or become exposed. Some of these sequences are involved in binding to other proteins. Other sequences are considered to exhibit a possible catalytic activity. From this point of view fibronectin is extremely interesting. Force induced conformational changes might switch a protein with pure mechanical function into a protein with enzymatic activity. Unfortunately, no experimental data exists proving that this force induced exposure of these sequences indeed results in an enzymatic activity (Vogel, 2006).

Another class of molecules which are activated by a force induced conformational change are mechanosensitive ion channels (MS channels). These channels are transmembrane proteins, which transduce a mechanical stimulus into an electrochemical response by opening a pore in the cell membrane. The large mechanosensitive channel (MscL) of bacteria normally exists in a closed conformation and can be activated directly by a mechanical stimulus. The channel is a pentamer consisting of five identical subunits. Each monomer consists of 2 transmembrane helices and additional domains, which are not packed into the membrane. Upon changes in the tension profile of the membrane these helices move away from the central axis similar to the opening of an iris of a camera (Sukharev et al., 2001; Perozo et al., 2002). This movement generates a large water filled pore. Although the opening of the channel has been analyzed in detail, nothing is known about how MscL senses the force, which is generated by the membrane tension. It is considered that MscL possesses a defined force sensor. But the exact location and the mechanism is not known yet (Perozo, 2006).

All of the above mentioned examples show that force can act as an allosteric regulator similar to biochemical inhibitors or activators. It is expected that many similar systems of force sensing and transduction will be discovered in the near future. These natural force sensors will require new methods for their characterization but they will also inspire the design of artificial force sensors. Artificial force sensors can find broad applications for the analysis of biological systems. They can be combined with existing technologies and expand their range of possible applications. For example, an artificial force sensor can provide a defined threshold force, which cannot be controlled accurately with a macroscopic device alone.

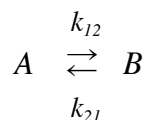
The following sections will explain the basic principles for the force based analysis of biomolecular functions and will describe the required methods to apply and measure forces at the molecular level. One section deals with the design of artificial force sensors and describes examples of biomolecular interactions, which are good candidates for artificial force sensors. Finally, two examples are described which show the application of artificial force sensors for the analysis of biological systems.

3 Force measurements

In order to understand the requirements for artificial molecular force sensors, this chapter summarizes the models describing the stability of receptor ligand interactions in the absence and presence of an externally applied force. Furthermore, the macroscopic devices used to apply forces to molecules are summarized and the two methods used in this work will be described in more detail.

3.1 Thermodynamic and kinetic models

Many transitions, which occur in biological systems, can be approximated with the simplest model system represented by only two states A and B. The states A and B are separated by a transition state T characterized by an energy barrier (Fig. 3a). The two states represent for example the folded and the unfolded state of a protein, a receptor ligand system in its bound and unbound state or two different conformations of a molecule. The transition between these two states occurs with the rate constants k_{12} and k_{21} .



The rate constants depend exponentially on the height of the energy barrier (ΔG_1 or ΔG_2 respectively) between these states:

$$k_{12} = \nu_1 \cdot e^{\frac{-\Delta G_1}{k_B T}} \quad (\text{eq. 3.1})$$

$$k_{21} = \nu_2 \cdot e^{\frac{-\Delta G_2}{k_B T}} \quad (\text{eq. 3.2})$$

with ν_1 and ν_2 the attempt frequency according to Kramers,
 k_B the Boltzmann constant,
 and T the absolute temperature

According to the law of mass action the equilibrium constant K can be calculated as follows

$$K = \frac{k_{12}}{k_{21}} = \frac{[B]}{[A]} \quad (\text{eq. 3.3})$$

and therefore can be used to determine the free energy difference between the two states A and B:

$$\Delta G_1 - \Delta G_2 = -k_B T \cdot \ln K \quad (\text{eq. 3.4})$$

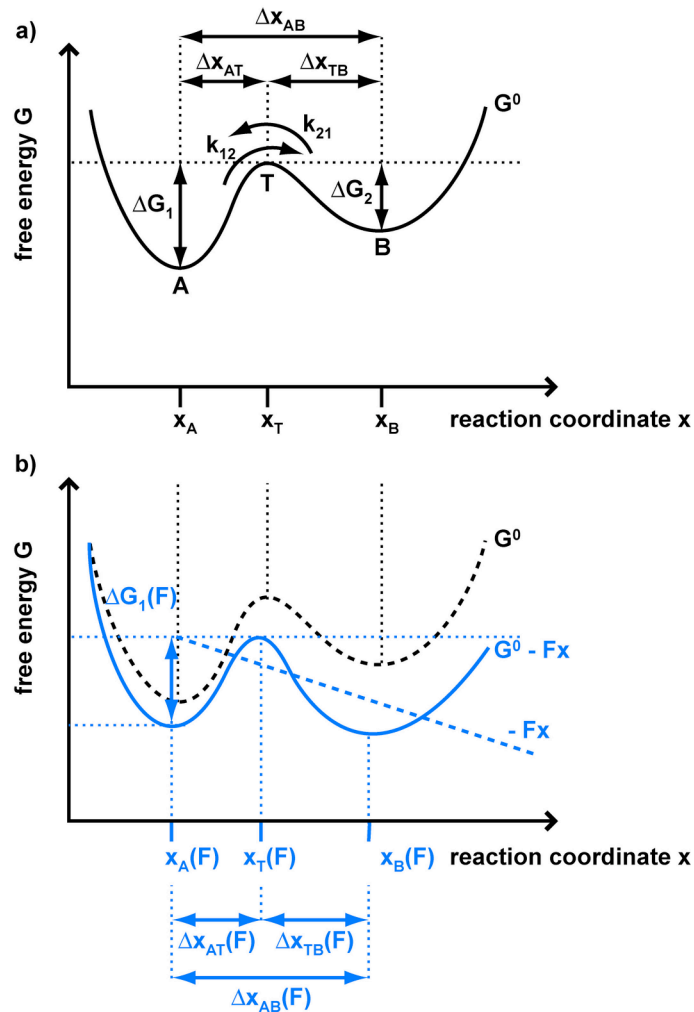


Figure 3. The effect of force on the free energy of a two-state system. a) Potential landscape of a two state-system without an externally applied force. A and B are two different states of a molecule or a molecular interaction. T represents the transition state. k_{12} and k_{21} are constants describing the rates of the transition from one state to the other. ΔG_1 and ΔG_2 describe the difference in free energy between state A or B and the transition state. Δx refers to the width of the potentials. b) Comparison of the system with (solid blue curve) and without an externally applied force (dashed black curve). The application of force lowers the free energy of both the transition state and state B relative to state A by $-Fx$ (dashed blue curve). As a result, the rate k_{12} and therefore the population of state B increases. The positions of the free energy minima and the maximum shift along the reaction coordinate. Their relative shifts depend on the local curvature of the free energy surface.

If a force is applied to the system, which acts along the reaction coordinate x , one has to distinguish two fundamentally different cases (Guthold et al., 2001). If the system can access all its energy states within the time scale of the experiment, the force does not shift the equilibrium of the transition and the transition is fully reversible. In this case the rate at which the force is applied (the “loading rate”) will not change the force at which the transformation occurs. For reactions, which proceed at equilibrium, the data obtained from the force measurements can be used to determine the free enthalpy of the reaction. If the time scale of the experiment is

faster than the time scales of the transformation the system is no longer in equilibrium. In non-equilibrium transitions the externally applied force causes a thermodynamically irreversible change. The influence of the external force on such a system was first described by Bell (Bell, 1978). The model was further developed by Evans (Evans and Ritchie, 1999). The now well-established Bell-Evans model can be applied broadly for the data analysis of force measurements. The most important aspects are summarized in the following. The model describes how the energy landscape is tilted by the externally applied force resulting in a reduction of the free energy of the transition state. For the reason of simplicity the potential width Δx_{AT} is assumed to be independent of the applied force. This assumption is valid for deep potentials. Based on this assumption eq. 3.5 describes the exponential increase of the rate $k_{12}(F)$ of the transition from state A to B with an externally applied force.

$$k_{12}(F) = \nu_1 \cdot e^{-\frac{(\Delta G_1 - F \cdot \Delta x_{AT})}{k_B T}} \quad (\text{eq. 3.5})$$

The probability $N(t)$ for the system to be in state A can be calculated by solving eq. 3.6.

$$\frac{dN(t)}{dt} = k_{12}(F) \cdot N(t) \quad (\text{eq. 3.6})$$

This results in a distribution of unbinding forces

$$p(F) = \frac{k_{12}(F)}{\dot{F}} \cdot N\left(\frac{F}{\dot{F}}\right) \quad (\text{eq. 3.7})$$

The most probable unbinding force can be given by

$$F(\dot{F}) = \frac{k_B T}{\Delta x_{AT}} \cdot \ln\left(\frac{\dot{F}}{k_{12}(0)} \cdot \frac{\Delta x_{AT}}{k_B T}\right) \quad (\text{eq. 3.8})$$

$$\text{with the loading rate } \dot{F} = \frac{dF}{dt}$$

Eq. 3.8 relates the measured force with the transition rate at zero force $k_{12}(0)$. For example, this transition rate can refer to the dissociation rate of a receptor ligand system. Additionally, the width of the potential Δx_{AT} can be obtained. Both values can be determined from a plot of the most probable unbinding force versus the ln of the corresponding loading rate. For a two level system this plot shows a straight

line. The potential width can be obtained from the slope and the transition rate from the intercept with the x-axis at zero force.

The most important conclusion from eq. 3.8 is that the unbinding force depends on the loading rate. At slow loading rates the system has more attempts driven by thermal fluctuations to reach the energy barrier than at faster loading rates. Therefore, at slow loading rates, the transition will occur at lower forces and at fast loading rates the transition will occur at higher forces.

3.2 Techniques for the application and detection of forces

Having shown the influence of external forces e.g. on the binding potential of receptor ligand interactions this chapter will describe the most common techniques used to apply and measure forces. For all techniques the molecules of interest have to be connected to a macroscopic device. One binding partner is attached to the force transducer and the other to a translation stage, which brings the binding partner in the correct position for the establishment of an interaction. After a short overview of the techniques the working principle of the atomic force microscope is described in detail. Additionally, a technique developed within the scope of this work is introduced.

3.2.1 Overview

The techniques differ from each other mainly by the method of applying and detecting the forces, as well as the type of surface to which the binding partners are coupled. The most common techniques are: Atomic force microscopy (Florin et al., 1994), optical tweezers (Ashkin, 1997), magnetic tweezers (Smith et al., 1992), the biomembrane force probe (Evans et al., 1995), glass microneedles (Kamimura and Takahashi, 1981) and hydrodynamic techniques such as the application of shear flow to the bond of interest (Tees et al., 1993; Alon et al., 1995). The forces generated and sensed are in the range of several pN up to several nN. None of these techniques can cover the whole range of possible forces. The force range and the working principle of the different techniques are summarized in table 1. For all these techniques except of the differential force assay the force acting on the molecular interaction is compared with the response of a micro-sized object such as a bead or a cantilever. In contrast, in the differential force assay the molecular interaction is compared with another molecular interaction. This exhibits several advantages, which will be described in chapter 3.2.3.

Table 1. Techniques used in single molecule force spectroscopy

technique	force range	throughput	working principle
atomic force microscope (AFM)	> 1 pN	low	The bending of a micro-fabricated cantilever is detected by the deflection of a laser beam.
optical tweezers (OT)	0.1 pN – 150 pN	low	A micrometer-sized bead is trapped in an electric field gradient of a laser focus by optical forces. Displacement of the bead from the center of the laser focus is converted into forces.
magnetic tweezers	10 fN – 100 pN	medium	Magnetic forces are applied through a micrometer-sized magnetic bead. The displacement of the bead is converted into forces.
biomembrane force probe (BFP)	0.5 pN -1000 pN	low	A red blood cell or a vesicle is aspirated by micropipette suction. The deformation of the cell/vesicle is used to quantify the force, which is acting on the cell/vesicle.
glass microneedles	> 0.1 pN	low	An optical fiber is deflected perpendicular to the fiber axis. The deflection can be converted into forces.
hydrodynamic techniques	1 – 250 pN	medium	Hydrodynamic flow or surface tension is used to exert forces directly on the sample molecules or on a bead. In contrast to other techniques, bond lifetimes are measured instead of forces.
differential force assay	0.1 pN – 1000 pN	medium-high	The molecular bond of interest is compared directly with another molecular bond. After building up a chain of molecular bonds this chain is loaded with force and the weakest bond ruptures first.

3.2.2 The atomic force microscope (AFM)

Originally invented for the characterization of surfaces by Binnig, Quate and Gerber (Binnig et al., 1986) the technology has experienced many improvements. The AFM combines a high spatial precision with a high force resolution. Therefore, it was a logical consequence that the technology did not only find applications for the characterization of surfaces but also was used for the measurement of forces between individual biomolecules (Florin et al., 1994). Now, the AFM is one of the most common devices for the measurement of biomolecular interactions, also called force spectroscopy. A schematic setup of an AFM is shown in Fig. 4.

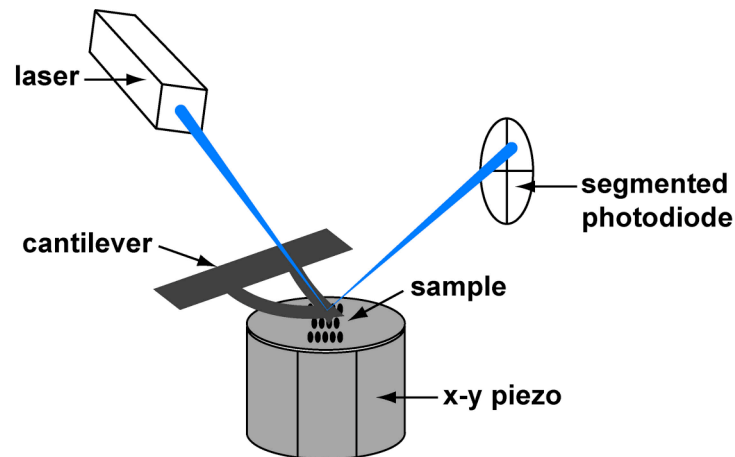


Figure 4. Setup of an atomic force microscope. The sample is mounted onto an x-y piezo table, which allows the positioning of the sample relative to the cantilever. The cantilever is mounted in a way that it can be moved in z-direction. The cantilever possesses a very sharp tip. This tip is brought in contact with the sample. When performing force spectroscopy, the contact time is sufficiently long to allow the tip itself or bound molecules to interact with the sample. Then, the cantilever is retracted. In the case of an interaction, the cantilever bends. This bending can be monitored with a laser, whose deflection is detected using a segmented photodiode.

In a typical force spectroscopy experiment one binding partner is anchored to a surface mounted on the x-y piezo table whereas the other binding partner is immobilized on the tip of the cantilever. The tip of the cantilever is brought into contact with the surface to allow the binding partners to interact. In the next step the cantilever is retracted thereby applying a force to the molecular bonds resulting in forced-induced transformations or bond rupture. In the case of bond rupture the cantilever relaxes back into its equilibrium position. The force applied to the molecular interaction is known throughout the whole process. It is determined by the measurement of the deflection of the cantilever by means of the optical detection system. The force can be calculated from the deflection and the spring constant of the cantilever. As described in chapter 3.1 the unbinding force of a molecular interaction is dependent on the loading rate. This rate can be varied by changing the retract speed of the cantilever (dynamic force spectroscopy).

As the dissociation is influenced by thermal fluctuations, one unbinding event is a stochastic process. Therefore, many rupture events have to be recorded to provide sufficient statistics to obtain the most probable rupture force. The measured force extension curves are analyzed to obtain the rupture force and the corresponding loading rate, which can be calculated from the retract speed and the slope of the force extension curve at the moment of the bond rupture. These values obtained from various force extension curves are plotted in histograms and fitted with a Gaussian distribution. The maxima of these distributions represent the most probable rupture force and the corresponding loading rate. To analyze the obtained data, the force is plotted versus the \ln of the loading rate. From this plot the values for the potential width Δx_{AT} and the natural off-rate $k_{12}(0)$ can be obtained using

equation 3.8. (This method of evaluating the data can also be used for any other technique as described in chapter 3.2.1.)

Although the measurement of unbinding forces with the AFM can be applied broadly and provides the desired information in many cases the technology still has some drawbacks. First, the throughput is relatively low. Only one molecular interaction can be characterized at one time and many force extension curves have to be recorded one after the other to provide the required statistics. Second, the instrument is susceptible to external perturbations, just as sound or temperature drift. Third, the force sensitivity is limited by the size of the cantilever (Viani et al., 1999). Therefore, the comparison of two different molecular interactions yields huge errors. The differential force assay described in the next chapter represents an attractive alternative for the comparison of molecular interactions circumventing all the problems mentioned above.

3.2.3 The differential force assay

The differential force assay compares the molecular interaction of interest directly with either another known or an unknown molecular interaction. This is attractive for many reasons. The main advantage is the use of another molecular interaction as a force sensor. For AFM experiments it has been shown that smaller cantilevers have a higher force resolution and a better sensitivity. This is due to the fact that smaller cantilevers experience less thermal noise which is one of the main determinants of the signal to noise ratio. However, the use of smaller cantilevers is hindered by the limits of the optical detection system and the fabrication of the cantilevers. Therefore, the use of molecules as force sensors is a logical consequence and single molecules are the smallest force sensors one can think of. In addition the use of a molecular interaction as a force sensor provides a symmetric set-up. In AFM experiments the interaction of interest is compared with a spring (cantilever). In the differential force assay it is compared with another molecular interaction. This set-up resembles a balance. If one uses a balance the difference is measured directly (Fig. 5). A balance is less influenced by external disturbances and is therefore much more accurate.

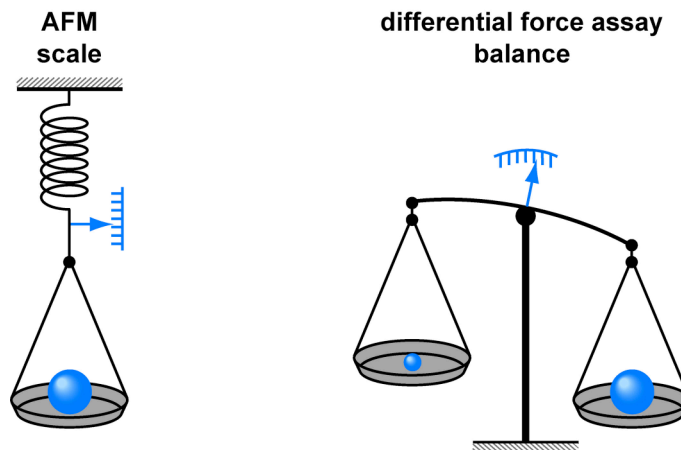


Figure 5. Comparison of the principle of a differential force assay with conventional methods (e.g. AFM) for the detection of intermolecular forces. In conventional methods the sample of interest is connected to a spring. In the case of an AFM, the response of this spring is detected as the deflection of the cantilever. If two samples have to be compared they have to be measured sequentially and each measurement is sensitive to external perturbations, e.g. temperature. If one uses a differential force assay, the two samples are compared directly. Influences from the environment influence both samples in the same way. Therefore, this type of measurement has a smaller error and allows the measurement of smaller differences.

Besides these advantages described above, another aspect makes the application of a differential force assay extremely attractive. In the differential force assay the molecules are immobilized on a surface just as in the AFM experiments. The molecules, which form the force sensor, are coupled to the surface of an elastomer. The elastomer allows the contact of the two surfaces to establish a connection between all the molecules. This set-up allows the measurement of various identical molecular interactions in parallel. Therefore, the required statistics can be obtained from only one experiment. In addition, different molecular interactions can be localized on different positions on the surfaces allowing parallel measurements of many interactions of interest. Many different realizations of a differential force assay are possible. Two principally different set-ups can be distinguished. In one set-up many unknown molecular interactions are compared to a well-characterized molecular interaction providing a reference force. As a result the assay provides the information if the unbinding force of the unknown interaction is higher or lower than the reference force. This set-up is shown in Fig. 6. In the other realization two unknown molecular interactions are compared directly.

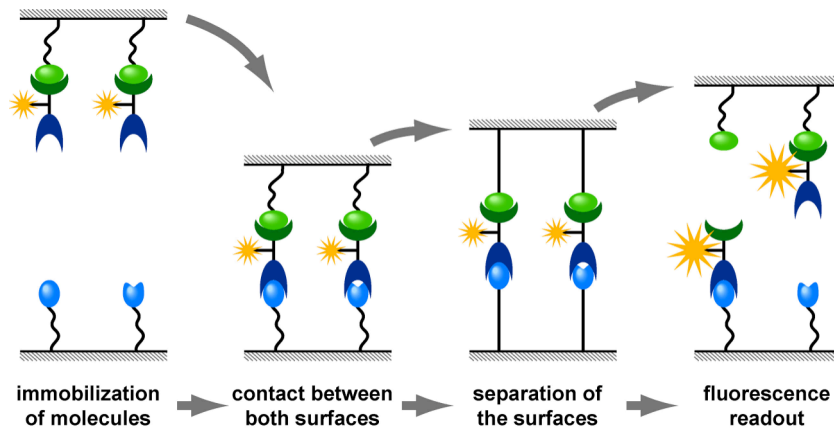


Figure 6. Example of one possible experimental set-up of a differential force assay. The strengths of two different molecular interactions (blue; same receptor – different ligands) are compared with a reference bond (green). The two ligands to be analyzed are immobilized on a surface at different positions. The ligand of the reference bond is immobilized on another surface. The corresponding receptors are connected to the same fluorescence label. This fluorescent complex is bound to the ligand of the reference bond on the respective surface. The surfaces are brought into contact allowing the blue ligands to bind to their receptor. In the next step, the surfaces are separated. The assembled chain of molecular interactions is loaded with a force. This force is constant along the chain. After stretching the molecules of the chain, the weakest bond ruptures with a higher probability. The distribution of the fluorescent complex is finally measured and yields the desired information. For example, if the left bond is stronger than the right bond a higher fluorescence will be measured at this position on the surface.

Two different examples have been realized within the scope of this work. The first example has been implemented to prove the high sensitivity of the differential force assay. In this set-up two different DNA duplexes have been compared with each other. It is described in more detail in the publication P9. In the second example a known reference force was used to detect the specificity of antibody antigen interactions. This set-up is described in chapter 6 in more detail.

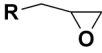
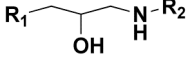
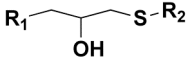
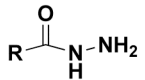
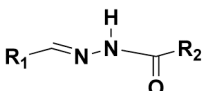
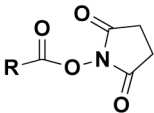
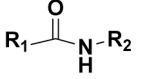
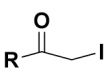
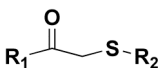
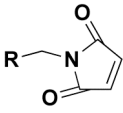
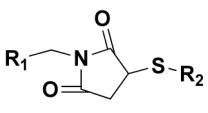
4 Immobilization of biomolecules on surfaces

A prerequisite for the force-based characterization of biomolecules is their immobilization on the macroscopic device, which is used to apply the external force. The immobilization procedure should be easy to carry out and possess a high specificity. The bond has to be stable over the time scale of the experiment. This also applies to the immobilized biomolecule. In addition, the biomolecule should not be destroyed by the immobilization procedure and have a good steric accessibility. The possibility of controlling the density of actively immobilized biomolecules is of great advantage.

4.1 Overview

In principle, three different strategies are feasible and have been used successfully: Physical adsorption was used to bind proteins, e.g. titin, to AFM cantilevers (Rief et al., 1997). The most commonly applied procedure is the covalent coupling to chemically activated surfaces (Hermanson, 1995). For example, antibodies can be coupled to glass surfaces using this approach (Neuert et al., 2006). The third strategy is based on the specific recognition of different receptor ligand systems. In this case, the receptor is bound to the surface and the ligand is attached to the biomolecule. This attachment can either be achieved with chemical coupling of the ligand to the biomolecule or with the usage of fusion proteins. Fusion proteins are constructed on the genetic level by attaching the sequence of the affinity ligand to the sequence of the protein of interest. Then these recombinant hybrids can be expressed as fusion proteins with the attached “tag” at the N- or C-terminus of the protein of interest (Hearn and Acosta, 2001; Terpe, 2003). The fusion protein approach has the advantage that the “tag” is attached at a well-defined position. One prominent example is the so-called His tag, which binds to Ni^{2+} -ions complexed with nitrilotriacetic acid (NTA). For example, this system was used to bind His tagged recombinant antibody fragments to AFM cantilevers (Berquand et al., 2005). Useful strategies for chemical coupling and suitable receptor ligand systems are summarized in table 2.

Table 2. Summary of methods for the immobilization of biomolecules

surface	biomolecule	bond	reaction conditions
epoxy 	amino $R-NH_2$	secondary amine 	reaction is pH dependent $pH > 9$
epoxy 	thiol $R-SH$	thioester 	reaction is pH dependent $7.5 < pH < 8.5$
aldehyde 	amino $R-NH_2$	Schiff base $R_1=N-R_2$	labile Schiff base interaction can be chemically stabilized by reduction
aldehyde 	hydrazide 	hydrazone 	more stable than aldehyde + amine reduction is not essential
activated esters 	amino $R-NH_2$	amide 	reaction is pH dependent half life of NHS ester can be critical for the yield
iodoacetyl 	thiol $R-SH$	thioester 	specificity for SH-groups is pH dependent slightly alkaline pH required
maleimide 	thiol $R-SH$	thioester 	specificity for SH-groups is pH dependent at high pH possible reaction of amino groups
thiol $R-SH$	disulfide derivative $R_1-S-S-X$	disulfide $R_1-S-S-R_2$	bond is not stable under reducing conditions
biotin	(strept)avidin	specific recognition non-covalent very low k_{off}	binding in a broad range of different buffers

surface	biomolecule	bond	reaction conditions
antibody	antigen	specific recognition non-covalent	binding dependent on the respective antibody
capture molecule e.g. Ni ²⁺ -NTA	affinity tag e.g. his tag	specific recognition non-covalent	binding dependent on the system used
suicide inhibitor	enzyme	specific recognition covalent	reaction dependent on the enzyme

All the methods summarized in table 2 have specific advantages and disadvantages. It has to be taken into account that a certain fraction of molecules could be inactivated as a result of their immobilization or previous chemical modification. Frequent problems are denaturation of the molecule, destruction of the active site by direct chemical modification, steric hindrance caused by neighboring molecules or the surface, strain induced by multipoint attachment or a shift of the isoelectric point of the biomolecule. Most of these problems can be overcome by means of a spacer between the biomolecule and by site-specific immobilization. The use of a spacer avoids direct contact between the biomolecule and the surface preventing potential denaturation and steric hindrance. Site-specific immobilization avoids multi-point attachment and ensures that the active site is located sufficiently far away from the point of attachment (Turkova, 1999).

When an external force should be applied to the biomolecules it has to be considered that a thermodynamically stable bond is not necessarily stable, if an external force is applied to the bond. If no external force is applied to the biomolecule the free energy of the bond determines its stability. It is normally sufficient to consider only the type of spacer and the position of the attachment point on the molecule. Either covalent chemical coupling or receptor ligand interactions can be used. Most of the receptor ligand interactions possess a sufficient stability to ensure that the bond is stable during the experiment. However, if an external force is applied to these complexes, the lifetime of the complex is no longer dependent on the equilibrium free energy. The applied force changes the energy landscape (as described in chapter 3.1). Therefore, the bond might rupture at a relatively low force and result in a low yield of the measurement. Furthermore, dependent on the binding potentials of the interaction of interest and the receptor ligand interaction used for the immobilization it cannot be excluded that both interactions rupture with a certain probability (Neuert et al., 2006). From this point of view only covalent bonds are tolerable in experiments with molecular force sensors. The strength of covalent bonds is in the range of 1-2 nN (Grandbois et al., 1999), whereas the strength of typical receptor ligand interactions is in the range of 10-250 pN

(Florin et al., 1994; Rief et al., 1999). This difference is large enough to ensure that only the bond of interest breaks, if a force is applied.

Considering all the aspects described above, two examples for immobilization procedures are described in the following sections, which fulfill many important criteria. One example describes a protocol for the covalent immobilization via heterobifunctional poly(ethylene glycol) spacers. The second example is based on the reaction of the enzyme hAGT with a so-called "suicide inhibitor". It is particularly useful for the immobilization of proteins. hAGT fusion proteins have been shown to be active in many different applications.

4.2 Covalent immobilization using hetero-bifunctional poly(ethylene glycol) spacers

The usage of spacers for the attachment of biomolecules to surfaces has many advantages. First, it prevents the molecule from interacting with the surface. Especially if the surface is hydrophobic the biomolecule could adsorb non-specifically and become inactivated. Second, the spacer allows the molecule to move relatively free in solution. Therefore the spacer prevents steric hindrance and reduces mass transport effects. Third, it can be used to change the surface properties and introduce the required functional groups for the attachment of the biomolecule. And finally it serves as an elastic module if a force is applied to the molecule.

The molecule poly(ethylene glycol) (PEG) is an ideal spacer which shows all the above mentioned advantages. PEG has unique properties. If PEG is coupled to a surface at a sufficiently high density the surface becomes resistant to the adsorption of proteins and other biomolecules (Sofia and Merrill, 1997; Alcantar et al., 2000). PEG is a linear polymer with a relatively narrow length distribution. It is available in a broad range of different lengths allowing the adjustment of the distance between the surface and the biomolecule for the particular application. And finally, PEG can be synthesized with many different reactive groups (Veronese, 2001; Roberts et al., 2002). Monofunctional PEGs are activated at one end and bifunctional PEGs carry a reactive group at both ends. Either these groups are identical (homo-bifunctional) or the PEG is synthesized with different reactive groups (hetero-bifunctional). Hetero-bifunctional PEG spacers are especially useful for the immobilization of biomolecules. The spacer can be coupled to the surface with one reactive group. The free reactive group can be used to couple the biomolecule in the next step (Fig. 7).

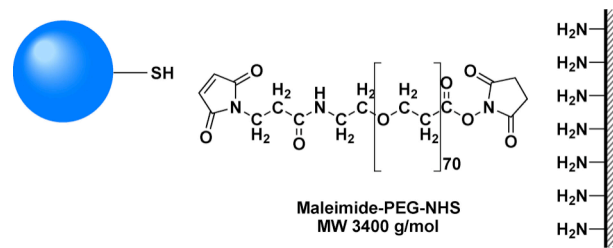


Figure 7. Example for the immobilization of a biomolecule on a surface using NHS-PEG-maleimide. First, the hetero-bifunctional NHS-PEG-maleimide is coupled to an amino-modified surface. The NHS-group reacts with an amino group. As the maleimide group is not involved in the coupling reaction it can be used in the next step. Then, the thiolated biomolecule is coupled. Because thiol groups are very rare among the reactive groups on biomolecules this strategy allows a site-specific immobilization in most of the cases.

The usage of the hetero-bifunctional NHS-PEG-maleimide is a very general strategy to achieve the site-specific immobilization of many different biomolecules. The NHS-group is coupled to an amino-functionalized surface. In the next step the maleimide group can be used to couple any type of biomolecule, which possesses a thiol group. Thiol groups on biomolecules are very attractive for coupling procedures. In the case of proteins, thiol groups of the amino acid cysteine are very rare on the surface of proteins. Therefore, the chance is high that a protein has only one cysteine on its surface. This single natural cysteine can then be used for coupling at a defined position. Alternatively, if the protein does not possess a single cysteine it can be introduced by mutation. In the case of other biomolecules, just as oligonucleotides or peptides, a thiol group can be introduced during the synthesis of the molecule. The application of this procedure for the site-specific immobilization of an enzyme is demonstrated in the publication P3.

4.3 Covalent immobilization using “suicide inhibitors”

Suicide inhibitors are a special group of enzyme inhibitors. They bind into the active site of the enzyme and are recognized as a substrate. In the next step the enzyme catalyzes the transformation of the inhibitor. But, in contrast to a normal substrate the product is not released from the active site but remains covalently bound in the active site thereby inactivating the enzyme. Because of the covalent nature of the attachment suicide inhibitors are interesting tools for various applications. Recently it has been shown that enzymes can be covalently attached to surfaces displaying an appropriate suicide inhibitor (Hodneland et al., 2002; Kindermann et al., 2003). If the enzyme is genetically fused to another protein this protein is attached to the surface together with the enzyme. This results in a highly specific and covalent attachment of the protein. Therefore, the usage of suicide inhibitors is an interesting option for the attachment of proteins for force measurements.

Most of the known suicide inhibitors are artificial substrate analogues, which have been synthesized for a special group of enzymes e.g. proteases and lipases. In contrast, the natural reaction of human O⁶-alkylguanine-DNA alkyltransferase (hAGT; EC 2.1.1.63) with its substrate yields a chemically modified active site resulting in an inactive enzyme (Rasimas et al., 2003). In its natural environment hAGT is a DNA repair protein. Many homologues in different species have been discovered indicating that hAGT plays a very important role in maintaining the integrity of the genome. It repairs alkylated guanine bases thereby preventing incorrect base pairing. This is achieved by transferring the alkyl group of the substrate O⁶-alkylguanine to one of its cysteine residues. This stoichiometric transfer results in dealkylated guanine and an alkylated enzyme. As hAGT lacks the ability to dealkylate itself it only participates in one single reaction. It is inactivated irreversibly and undergoes a conformational change, which triggers its proteolytic degradation.

hAGT is a monomeric protein of 207 amino acids. Its structure has been solved in 2000 (Daniels et al., 2000; Wibley et al., 2000). It consists of two domains. The function of the N-terminal domain is unknown. It possesses a binding site for a Zn²⁺ ion. Binding of Zn²⁺ is considered to be important for the stability of the protein. However, hAGT is also active without a bound Zn²⁺ ion. The C-terminal domain contains a DNA binding motif and the active site. hAGT possesses five cysteine residues of which Cys145 is the site of the alkyl transfer. Cys5 and Cys35 participate in the creation of the Zn²⁺ binding site. For Cys62 and Cys151 no obvious structural or functional role is known. Both termini of hAGT are located far away from the active site.

The substrate specificity of hAGT is relatively low. It also reacts with the nucleobase O⁶-benzylguanine (BG) either in its free form or incorporated into oligonucleotides. Furthermore, BG derivatives with substituted benzyl rings are accepted as substrates. In this reaction the substituted benzyl group is transferred to the active site of hAGT. The benzyl ring can be substituted at the 4-position with a wide variety of labels such as dyes, cross-linkers and affinity tags without significantly influencing the reaction (Keppler et al., 2003). The possibility of labeling hAGT with a variety of different labels and the option of making N-terminal and C-terminal fusion proteins allows the labeling of any protein via the reaction of hAGT with this label. Using this approach, hAGT can be used to attach a protein of interest to a force sensor or for the immobilization of a protein on a surface displaying BG (Fig. 8).

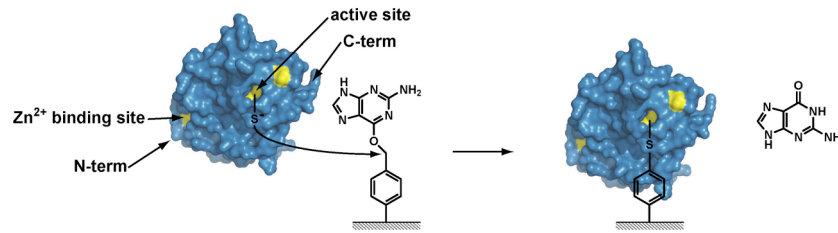


Figure 8. Reaction of hAGT with O⁶-benzylguanine (BG) modified surfaces. hAGT (PDB no. 1QNT) reacts with different derivatives of BG. It cleaves the bond between the benzyl group and guanine. The reaction yields free guanine. The benzyl group remains covalently attached to a cysteine in the active site of hAGT. If BG has been attached to a surface beforehand, the enzyme remains bound to the surface. This mechanism can be employed to attach a protein of interest to the surface. For this purpose, fusion proteins can be produced with recombinant DNA techniques. The protein of interest can be attached at the N-terminus or the C-terminus of hAGT.

Thereby hAGT reacts specifically with BG resulting in a covalent immobilization of the protein of interest on the surface (Kindermann et al., 2003; Sielaff et al., 2006). As BG is chemically inert there are no side reactions and the immobilization is highly specific. Therefore only hAGT is involved in the immobilization reaction. hAGT acts as a spacer and leaves the protein of interest accessible for interactions with other molecules. Furthermore, because of the high specificity of the immobilization it can be performed in crude extracts eliminating the need for the purification of the protein of interest. Using the crude extracts directly can be of a certain advantage for applications where the density of the proteins on the surfaces is not relevant. The application of the immobilization of hAGT fusion proteins for AFM measurements is demonstrated in the publication P5.

5 Molecular force sensors

Molecular force sensors have the potential to find broad applications either as tools to characterize the function of naturally occurring force sensors or alternatively as analytical tools for the measurement of molecular interactions or the systematic manipulation of biomolecules. As summarized in the last two chapters it is always necessary to attach the biological system of interest to various types of surfaces. Molecular force sensors can be designed in a certain way to allow the defined immobilization and to provide a defined reference force. For example, they can be used as force sensors in the differential force assay (chapters 3.2.3 and 6). Alternatively, they can be used to transmit forces between an analytical device just as the AFM and the molecule of interest. If the force reaches the threshold value, which is defined by the sensors, the bond will open and prevent damage on the molecule caused by too high forces (chapter 7).

5.1 Requirements

To fulfill these functions, force sensors have to accomplish the following requirements. They have to provide possibilities for the attachment of the force sensor to the surface and to the molecule of interest. In an ideal case the attachment to the molecule is achieved at a defined position and can be carried out easily. It is of capital importance, that the attachment of the force sensor does not change the structure and the function of the molecule of interest. Additionally, the stability of the force sensor has to be characterized at equilibrium conditions and at various different loading rates, e.g. with the AFM.

5.2 Desoxyribo nucleic acid (DNA)

The mechanical properties of double stranded DNA have been investigated with different methodologies and over a broad range of forces. These experiments revealed different regimes of the reaction of DNA to externally applied forces (Strick et al., 2000; Bustamante et al., 2003). Up to a force of 10 pN the process is governed by entropic forces. Between 10 pN and 65 pN DNA stretches like any spring. At 65 pN a phase transition from B-DNA to S-DNA occurs (B-S transition) (Rief et al., 1999; Guthold et al., 2001). If the force is increased further the double strand melts into two single strands (melting transition). These experiments have been performed with rather long DNA molecules (> 1000 bp).

However, short DNA sequences are required (< 50 bp) to use DNA as a force sensor. First, the DNA is required in a relatively high concentration and it needs specific reactive groups attached to its ends in order to couple it to the surface and to the molecule of interest. This can only be achieved with solid phase synthesis of oligonucleotides. Second, when using oligonucleotides the sequence and length of the DNA is known exactly and provides the possibility of fine-tuning the strength and orientation of the force sensor (Fig. 9).

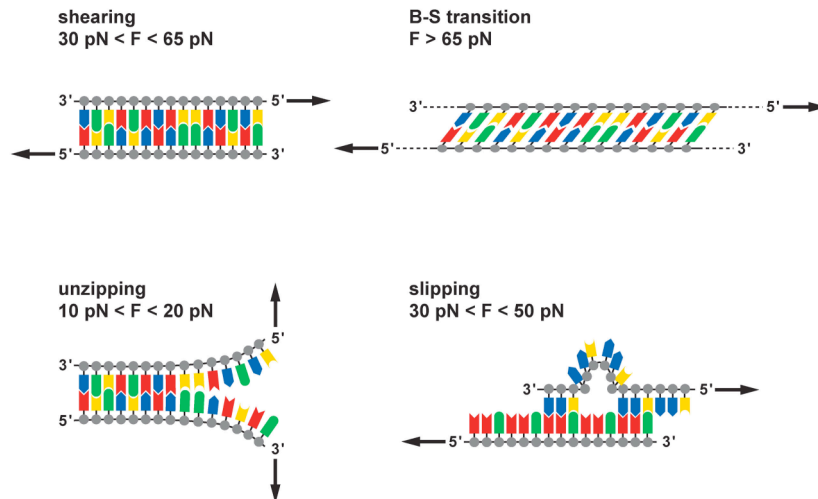


Figure 9. Different unbinding mechanisms of DNA if an externally applied force acts on the duplex. The mechanism is dependent on the length and the sequence of the DNA as well as the direction and rate of the applied force. Every strand of the DNA has an orientation, which is given by the structure of the chemical bonds in the backbone of the DNA (linkages between desoxyribose and phosphate groups). Therefore, each DNA strand has a 3' end and a 5' end. Looking at a relatively short DNA duplex (10 base pairs to approximately 30 base pairs), this duplex opens up in a zipper mode (bottom left) if one strand is pulled at the 3' end and if the other strand is pulled at the 5' end. If both strands are loaded at the 5' end all base pairs have to open up at the same time. The strands are sheared apart yielding a higher force compared with the unzipping mechanism (top left). For longer DNA duplexes, pulling at the 5' end of both strands results in a structural change (B-S transition) before the strands finally dissociate. This structural change happens at approximately 65 pN (top right). In the case of repetitive DNA sequences loops can form and propagate along the DNA. This slipping mechanism can be observed with and without an externally applied force (bottom right).

The mechanisms shown in Fig. 9 have been investigated in detail. It has been shown that for short oligonucleotides (10 bp, 20 bp and 30 bp) the force for DNA shearing depends on the stability (ΔG) of the DNA duplex and on the applied loading rate (Strunz et al., 1999). In these experiments, no B-S transition was observed because the rupture of the duplexes occurred at forces below 65 pN and the process of bond rupture followed the Bell-Evans model. Therefore, at a defined loading rate the holding force of the duplex can be tuned by changing the length and the base composition. Although the B-S transition has only been observed for long DNA molecules it is expected to occur also for short duplexes as soon as the

stability and the loading rate are so high, that the rupture force is in the range of 65 pN. Above 65 pN the holding forces are expected to be less predictable as the B-S transition and the melting transition cannot be described with the Bell-Evans model. This has to be considered if DNA is used as a force sensor.

If repetitive DNA sequences are sheared apart another unbinding mechanism has been predicted theoretically (Neher and Gerland, 2004). It is considered that the DNA can form bulge loops propagating along the DNA strand resulting in a displacement of the strands relative to each other. By applying a shear force to the duplex the displacement occurs favorably in one direction finally resulting in thermal unbinding of the two strands. Within the scope of this work, experiments have been performed with the AFM, which prove the existence of this unbinding mechanism (publication P2). The slipping process has been characterized in more detail for 20 bp and 30 bp duplexes and provides another force sensor with a cut-off force in the range of 40 pN.

Additionally, a principally different unbinding mechanism has been shown. DNA can be pulled apart in an unzipping process. In contrast to the shearing processes described above, the bases are separated sequentially. The forces required to separate the strands are also sequence dependent (Rief et al., 1999; Krautbauer et al., 2003) but are much lower compared with the forces needed for shearing the DNA. The forces required to unzip the DNA are independent of the loading rate. This might be an advantage if DNA is used as a force sensor especially if the loading rate is not known in the respective experimental set-up. The application of this kind of force sensor for the detection of receptor ligand interactions is summarized in chapter 6.

In summary, the use of DNA as a force sensor has the advantage that the stability of many different configurations was characterized in many different types of experiments. Therefore, DNA interactions provide a range of different force sensors with well-characterized holding forces. However, the usage of DNA has some drawbacks. In the organism proteins are the molecules which perform most of the functions, e.g. in force transduction. In order to analyze the function of proteins it is not straightforward to attach a force sensor consisting of DNA to the molecule of interest. The attachment of DNA to a protein requires huge amounts of purified DNA and protein and sophisticated protocols for the chemical coupling.

5.3 Antibody antigen interactions

For the characterization of proteins it is much more convenient to utilize the interaction between different proteins as a force sensor. The main advantage of this approach is the possibility of preparing fusion proteins of the protein of interest and the force sensor. Antibody antigen interactions are ideal candidates for this purpose. Different antibody antigen interactions have been characterized with the AFM (Schwesinger et al., 2000; Neuert et al., 2006) and exhibit holding forces in a useful range.

Antibodies are available from various sources. Monoclonal antibodies are one possible source. Recombinant antibodies such as Fab fragments or single chain Fv (scFv) fragments provide more flexibility (Plückthun, 1994). The different formats are shown in Fig. 10. Recombinant antibodies are selected from large libraries using e.g. phage display (Winter et al., 1994) or ribosome display (Plückthun et al., 2000). They can be produced in large amounts in *Escherichia coli* providing the possibility of making modifications on the genetic level (Ge et al., 1995).

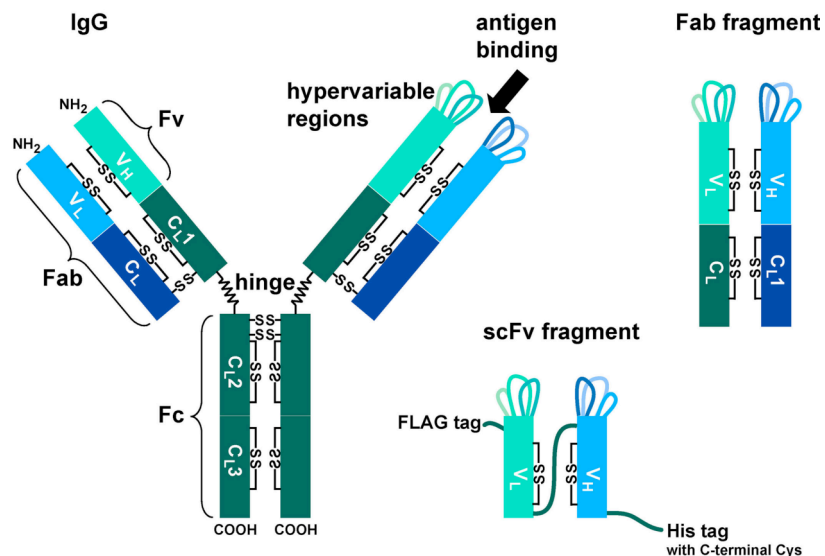


Figure 10. Different antibody formats. The IgG molecule represents the most common format of monoclonal antibodies. It consists of two identical heavy chains and two identical light chains. One light chain binds to one heavy chain. The chains are connected via disulfide bonds, which stabilize the molecule. The variable domain of one light chain V_L and the variable domain of the corresponding heavy chain V_H build the antigen binding site. Therefore, an IgG molecule possesses two identical binding sites for antigens. In more detail, each variable domain contains three hypervariable regions or CDRs, which are responsible for antigen binding. Therefore, the smallest antigen binding structure is the Fv fragment, which consists of V_L and V_H . The Fc part of the antibody is involved in the immune response in the body. For applications where only the antigen binding function is required, it can be an advantage to use smaller fragments of the antibody like Fab or scFv fragments. In the scFv fragment the V_H and V_L domains are connected via a peptide linker, which stabilizes the molecule.

Especially well-suited as force sensors are antibody fragments, which bind a peptide antigen. The use of recombinant antibody technology offers the possibility to optimize the binding constants of the antibody to the antigen providing a range of different clones. The peptide antigen can be easily fused to the protein of interest on the genetic level. As the peptide is relatively small it is assumed that it does not interfere with the protein of interest. In addition, the peptide sequence can be modified. Therefore, the availability of different clones in combination with modified peptides most likely provides a series of molecular interactions spanning a range of different holding forces. The system shown in Fig. 11 is considered to be useful for

the generation of such a series of force sensors. Different antibody fragments have been selected and the equilibrium constants have been measured (Hanes et al., 1998; Zahnd et al., 2004) in the group of Prof. Andreas Plückthun at the University of Zurich. Within the scope of this work three clones have been characterized with the AFM to obtain their holding forces at different loading rates. The results are submitted for publication (P1). In the future, modifications of the peptide will be analyzed to extend the number of combinations, which can be used as force sensors. One clone of this series is currently used as a force sensor for the manipulation of the activity of an enzyme (chapter 7).

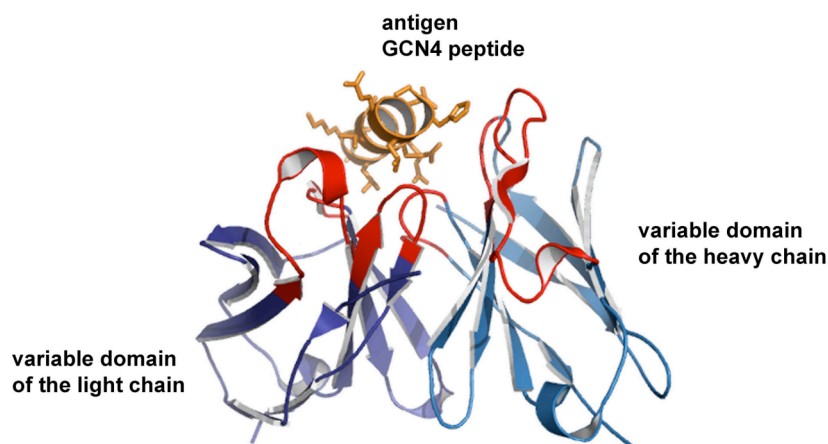


Figure 11. Structure of the anti-GCN4 antibody fragment complexed with its antigen (PDB no. 1P4B). The framework regions of the two domains are shown in blue. The loops of the CDRs, which are responsible for antigen binding, are shown in red. The antibody fragment was crystallized with a truncated version of the original peptide. This truncated version binds to the antibody fragment in an α -helical conformation, lying flat in the binding site. It is shown in yellow.

6 Molecular force sensors for the detection of receptor ligand interactions

Receptor ligand interactions are key processes in biological systems for example in the immune system or in cell signaling. Therefore, their analysis is of great importance for the understanding of biological systems. In addition, receptor ligand interactions can be utilized to detect biologically relevant molecules. For example, the presence of a certain DNA or RNA sequence in a sample of interest can be detected with hybridization assays like Southern or Northern blots. Immunological assays based on the specificity of antibodies for their respective antigen are commonly applied for the detection of proteins.

6.1 Introduction to microarray technology

Microarray technology is an advancement of the methods mentioned above. It allows the detection of many analytes in a highly parallel (multiplexed) fashion. In a microarray experiment many (20 to >1000) receptors (e.g. DNA oligonucleotides or antibodies) are immobilized at spatially defined positions on a surface. Therefore, the specificity of each receptor is exactly defined by the position of the respective molecule on the array. A sample with unknown content is incubated on this array and the ligands bind to the array at those positions where a specific interaction with a receptor can occur. The bound ligands are detected either by attaching a label to the ligand or with so-called label free detection methods such as surface plasmon resonance.

The first report on microarray technology showed the specific detection of certain messenger RNAs from *Arabidopsis thaliana* (Skena et al., 1995). In the following years the area of DNA microarrays developed extremely fast. Today the detection of 20.000 different DNA sequences on one microarray has evolved to a broadly applied standard technology. This is due to the fact that receptors can be easily fabricated and immobilized on the surface. In addition, the hybridization of DNA is highly specific. In contrast, microarrays for the detection of proteins are still a field of intensive research.

6.2 Protein microarrays

The analysis of the protein content of a biological sample in a microarray format is far more complicated. Different proteins show very diverse physicochemical properties. Therefore, a general strategy for their production, purification and immobilization does not exist. As a result, the main bottleneck for the broad application is the availability of suitable receptors. With respect to this problem, protein microarrays can be divided into two different classes: protein detecting arrays and functional protein arrays. Functional protein arrays attempt to obtain information about the biological function of certain proteins such as enzymatic activity. Protein detecting arrays measure the abundance and/or the concentration of different analytes. In general, protein detecting arrays are easier to fabricate as they are related with immunoassays – a well established technology.

6.2.1 Technological aspects

In order to establish and to carry out a protein array experiment many different technological aspects (Fig. 12) have to be considered (Kusnezow and Hoheisel, 2002; MacBeath, 2002; Cutler, 2003; Tomizaki et al., 2005; Kingsmore, 2006).

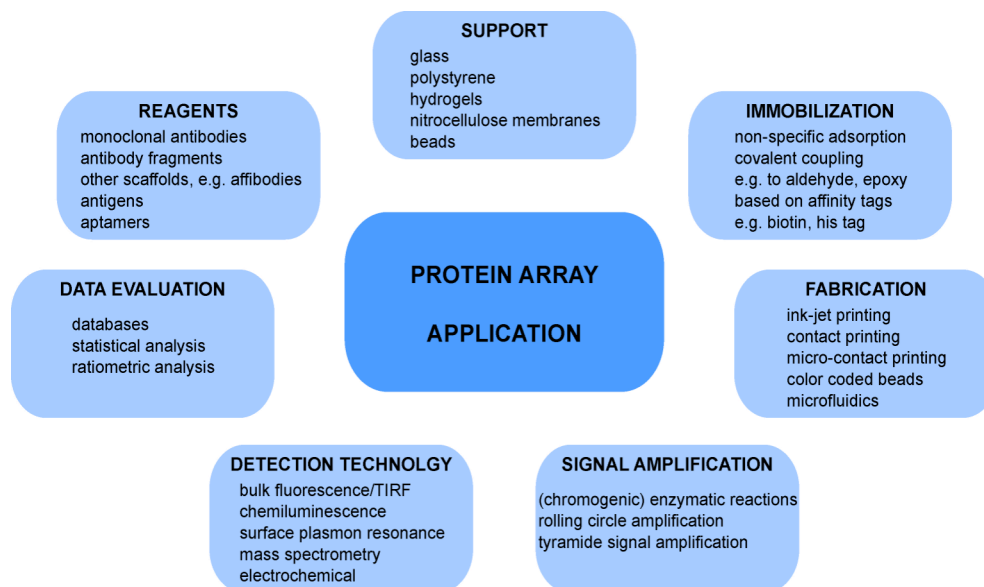


Figure 12. Summary of the different components necessary to establish a protein array experiment. For each component many different solutions have been developed. For each experiment a different combination of these components might be necessary to achieve the desired result.

The choice of a certain technology, e.g. for the immobilization of the receptor molecules, depends on the demands on the experiment. To design a protein array experiment the following aspects have to be considered: number of receptors, specificity, sensitivity, dynamic range, stability, reproducibility, and ease of handling.

6.2.2 Protein microarrays based on antibody antigen interactions

The most prominent realization of protein microarrays utilizes antibody antigen interactions. As immunoassays are a standard procedure many different antibodies and antigens are available for using them as receptors on an array. In principle the different forms of immunoassays can be realized on the array in a multiplexed fashion (Fig. 13). Depending on the particular application either the antibodies or the antigens are immobilized. Sandwich immunoassays are the most common format. In a conventional immunoassay optimized for the detection of one antigen a sandwich assay provides high specificity. Two antibodies are used, which bind the same antigen at different positions. Using this set-up, the probability that a different antigen is bound falsely by these two antibodies is extremely low.

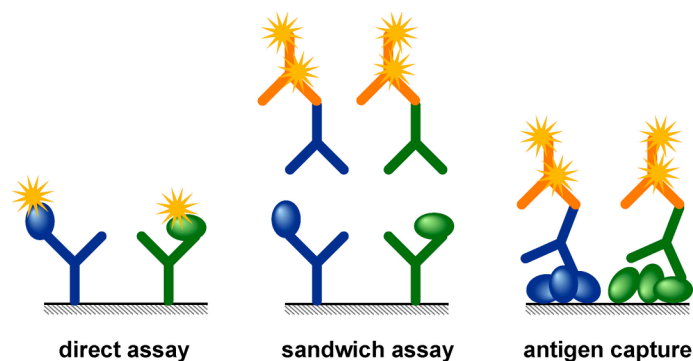


Figure 13. Different formats of antibody based microarrays. Either the antibodies or the antigens can be immobilized on a surface. Immobilized antibodies allow for the detection of an antigen either in a direct assay or in a sandwich assay. In a direct assay the antigen is labeled directly with a marker. Alternatively the antigen can be detected with label free detection methods. In a sandwich assay the antigen itself is not labeled. Instead, a labeled detection antibody, which is specific for the antigen, is incubated on the surface. The binding of this antibody is detected with a so-called secondary antibody, which carries the label. In the third format the antigen is immobilized on the surface. And the presence of an antibody in a sample is detected after incubation with a labeled secondary antibody.

However, it turned out that multiplexing of sandwich assays is associated with many problems. Whereas the detection antibody provides high specificity in a single assay, it yields an increasing number of false positives and an increasing background signal with a higher degree of multiplexing. This is the result of the experimental procedure: After binding the antigens to the receptors the array is incubated with a cocktail containing all the detection antibodies. This incubation step is followed by a second incubation step to bind the labeled secondary antibodies. The problems arise from the possibility of the detection antibodies and the secondary antibody to bind everywhere on the array. In more detail, the problems can be attributed to the following effects: First, antibodies are known to exhibit crossreactivity (Michaud et al., 2003). Crossreactivity is defined as the property of an antibody to bind not only to the antigen against which it has been elicited but also to other related or non-related antigens. Therefore, if either an antibody used as a

receptor or as a detection antibody is crossreactive it will be impossible to distinguish which antigen has been detected. Second, with an increasing degree of multiplexing more detection antibodies have to be added to the cocktail resulting in a higher total antibody concentration. With a higher antibody concentration more non-specific interactions with the surface will occur leading to a higher background signal and a reduced sensitivity.

6.2.3 Force-based antibody microarrays

These problems can be eliminated if the detection antibodies are applied to the position of the respective receptor only. Using this strategy, the detection antibody does not have any contact with other positions on the array. Therefore, it will only measure the presence and the concentration of the desired antigen on the respective position. This local application of detection antibodies was realized in the format of a differential force assay (chapter 3.2.3). The receptor and the antigen were bound to one surface. The detection antibodies were coupled to the second surface via force sensors. DNA duplexes in unzipping conformation were used as the force sensors. They provide a high thermodynamic stability and a low mechanical stability under an externally applied force. In addition the unzipping process is not dependent on the loading rate. This is a big advantage, as the loading rate is not known in the differential force assay. As the force, which is required for unzipping the DNA duplex, is always lower than the unbinding force of the antibody antigen interaction the set-up ensures that the force sensor will always open if a specific interaction between the detection antibody and the antigen is present. The opening of the force sensor results in the transfer of a fluorescent label on the antigen. This label is finally detected and the fluorescence intensity is proportional to the concentration of the antigen. The experimental realization of this set-up is shown in much greater detail in the publications P6, P7, P8 and P9.

7 Molecular force sensors for the manipulation of enzyme activity

Enzymes are the catalysts in most biological processes. Enzyme catalysis can produce rate accelerations as large as a factor of 10^{19} compared with the uncatalyzed reaction (Garcia-Viloca et al., 2004). This high catalytic efficiency combined with a high substrate specificity is still a topic of intensive research for biochemists and recently biophysicists. In most of the cases enzymes are proteins. More than 100 years ago Fischer proposed that the substrate is bound to the active site of the enzyme in a “lock and key” mechanism. Later, Haldane suggested that the “key does not fit the lock perfectly but exercises a certain strain on it” (Haldane, 1930). In 1946 Pauling’s explanation for the catalytic mechanism of an enzyme was that “the substrate molecule is attracted to the enzyme, and caused by the forces of attraction to assume the strained state which favors the chemical reaction” (Pauling, 1946). The ideas of Haldane and Pauling lead to the conclusion that an enzyme has to be so flexible that it can bind to the substrate and undergo a conformational change after binding the substrate (induced fit). Indeed conformational changes have been shown for many different enzymes (Garcia-Viloca et al., 2004). Recent findings show that enzymes do not show an induced fit only but can fluctuate between many different conformations at every step of the reaction suggesting that an enzyme is a highly dynamical entity.

7.1 Classical enzyme kinetics

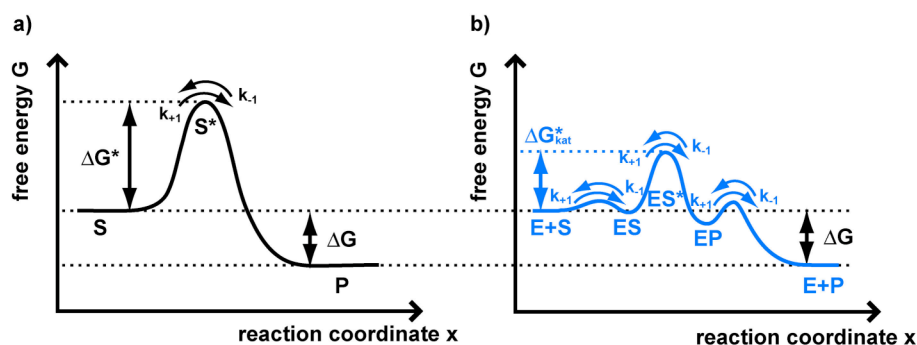
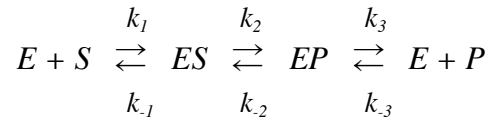


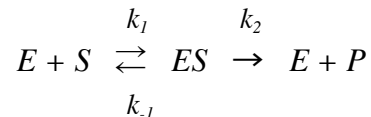
Figure 14. Comparison of an uncatalyzed and an enzyme catalyzed chemical reaction. a) uncatalyzed reaction. The substrate S has to reach a transition state S^* before it converts into the product P. The free energy difference ΔG^* between S and S^* is relatively high. b) enzyme catalyzed reaction. The addition of an enzyme lowers the free energy difference ΔG^*_{kat} but not the difference in the free energy ΔG between the substrate and the product. This is the reason why an enzyme accelerates the reaction. An enzyme catalyzed reaction proceeds in three steps. First, the enzyme binds to the substrate and forms the complex ES. This complex is transformed into the activated complex ES^* . After the substrate was converted into a product the product first remains bound to the enzyme to yield EP. Finally, the product is released from the enzyme and the enzyme can bind a new substrate molecule.

As mentioned above enzymes are able to speed up chemical reactions by many orders of magnitude. The origin of this huge rate acceleration lies in the effect that enzymes lower the activation barrier ΔG^* to reach the transition state of the reaction. The difference in the free energy ΔG between the substrate and the product and therefore the equilibrium constant of the reaction remains unchanged (Fig. 14).

As shown in Fig. 14 b) an enzyme-catalyzed reaction follows the following reaction scheme:



Assuming that the barrier between EP and E+P is low and that the reaction rate k_2 is very small the reaction scheme can be written as follows:



The first step can be attributed to the binding of the substrate to the enzyme. Mostly, this step is rapid, reversible and does not result in any chemical changes. The second step – the catalytic step – refers to the chemical conversion of the substrate. This step follows the first order rate constant k_2 .

The following equations describe the changes of the concentrations of the substrate [S], the enzyme [E], the complex of enzyme and substrate [ES] and the product [P] during the reaction:

$$\frac{d[S]}{dt} = -k_1[E][S] + k_{-1}[ES] \quad (\text{eq. 7.1})$$

$$\frac{d[E]}{dt} = -k_1[E][S] + (k_{-1} + k_2)[ES] \quad (\text{eq. 7.2})$$

$$\frac{d[ES]}{dt} = k_1[E][S] - (k_{-1} + k_2)[ES] \quad (\text{eq. 7.3})$$

$$\frac{d[P]}{dt} = k_2[ES] \quad (\text{eq. 7.4})$$

$$[E] = [E_T] - [ES] \text{ with the total concentration of enzyme } E_T$$

Assuming that the production and the turnover of the enzyme substrate complex proceeds with the same rate (steady-state conditions)

$$\frac{d[ES]}{dt} = 0$$

and that the binding of the substrate to the enzyme is not rate-limiting, which is given by $[S] \gg [E]$, the Michaelis-Menten equation is obtained. The Michaelis-Menten equation describes the hyperbolic dependence of the reaction velocity v from the concentration of the substrate $[S]$:

$$v = \frac{v_{\max}[S]}{[S] + K_M} \quad (\text{eq. 7.5})$$

with $v_{\max} = k_2 \cdot [E_T]$ the maximum velocity of the reaction

and $K_M = (k_{-1} + k_2)/k_1$ the Michaelis-Menten constant

Whereas the Michaelis-Menten equation is a good phenomenological description of the production rate the underlying molecular mechanisms for the lowering of the activation barrier are still a topic of intensive research. Only in recent years it became possible to study the catalytic mechanism of enzymes in more detail. A detailed analysis of catalytic mechanisms requires information about the structure of the enzyme and the substrate. As more and more structural data is available it has been possible to explain the mechanisms for lowering the activation barrier for a number of enzymes (Garcia-Viloca et al., 2004). In most cases conformational changes are associated with changes in electrostatic interactions, hydrogen bonding or desolvation effects. Thereby the contacts between enzyme and substrate can be optimized by the conformational change or the interaction with the substrate can cause the conformational change. In some cases the conformational change can be caused by a strain, which is induced in the enzyme upon substrate binding. If this strain is only relieved at the transition state the conformational change contributes to the lowering of the activation barrier. This mechanism, called strain-induced catalysis, will be the topic of the next chapter.

7.2 Influence of forces on enzyme catalysis

The idea that strain is induced in the enzyme was already proposed by Haldane and Pauling. As mentioned above it was shown that the release of the strain in the transition state has a contribution to the lowering of the activation energy. Although there is clearly a contribution in some systems it is not considered to be a general mechanism. It is believed that enzymes are flexible molecules and cannot generate sufficient strain (Villa and Warshel, 2001). However, many enzymes undergo

conformational changes due to substrate binding. Furthermore, it is considered that the large size of enzymes is presumably a manifestation of the requirement to limit flexibility (Narlikar and Herschlag, 1997). Bustamante et al. (Bustamante et al., 2004) believe that the generation of strain has a significant contribution. From their point of view the contribution is not evident because of the lack of methods for the direct analysis of the forces generated during enzymatic action.

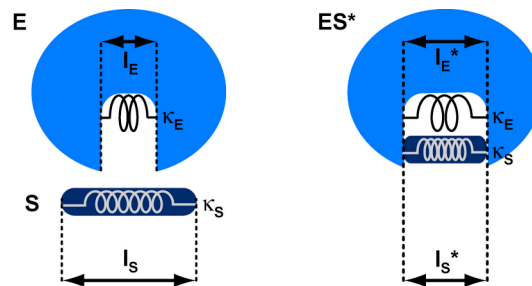


Figure 15. Spring model of an enzyme substrate interaction. In the unbound conformation (left) the binding site of the enzyme has a defined geometry with the length l_E . The substrate has the length l_S . Formation of the activated enzyme substrate complex ES^* induces strain between the binding pocket of the enzyme and its substrate. Both enzyme and substrate are distorted resulting in a new geometry of the bond. The effective lengths l_E^* and l_S^* are determined by the relative stiffnesses of the enzyme κ_E and the substrate κ_S . (adapted from Bustamante et al., 2004)

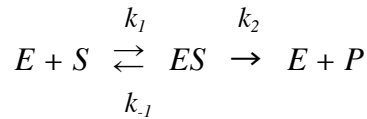
The basic mechanical principle of strain-induced catalysis is summarized in Fig. 15. According to Bustamante et al. the process of lowering the activation barrier can be described as follows: Upon binding of the substrate, the enzyme is not perfectly complementary to the substrate. Therefore the enzyme undergoes a conformational change utilizing a gradient of binding energy (potential energy). This gradient of binding energy is translated in a series of motions. These motions generate a force, which acts on the enzyme and the substrate until the transition state is reached and the product can be formed.

However, if it is really the generated force or the optimization of interactions between enzyme and substrate, which result in a lowering of the activation barrier, cannot be distinguished easily. But, even if the strain itself does not have a major contribution to the lowering of the activation barrier it is highly likely that an externally applied force will have an influence on the activity of the enzyme. In chapter 3.1 it has been shown that forces influence the conformations of proteins. If conformational changes are necessary for enzyme activity external forces will influence the equilibrium between the conformations.

7.3 Activity measurements with single enzymes

In order to analyze the influence of external forces on the activity of enzymes single enzymes will have to be analyzed for example with the AFM. Therefore, the following chapter will introduce the basic concepts for the analysis of single enzyme data and give a short overview of the information, which can be gained from single enzyme measurements.

At the single molecule level the concentration of an enzyme is no longer relevant. The enzymatic reaction is considered to be a stochastic event. Therefore, for single molecule experiments the probabilities for the enzyme to be in one of the possible states along the reaction pathway are considered. To describe one complete enzymatic turnover again the following reaction scheme is used.



The following equations can be used to describe the time dependent probabilities for the enzyme to be either in its free state E or to be bound in the enzyme substrate complex ES :

$$\frac{dP_E(t)}{dt} = -k_1[S]P_E(t) + k_{-1}P_{ES}(t) + k_2P_{ES}(t) \quad (\text{eq. 7.6})$$

$$\frac{dP_{ES}(t)}{dt} = k_1[S]P_E(t) - k_{-1}P_{ES}(t) - k_2P_{ES}(t) \quad (\text{eq. 7.7})$$

The different states cannot be measured in a single enzyme experiment. The parameter, which can be measured, is the time the enzyme molecule needs for one complete turnover cycle. This time is also called the “waiting time” τ . If a huge number of turnover cycles is measured a waiting time distribution is obtained, which is the basis for the analysis of the dynamic behavior of the enzyme.

Relating the waiting time distribution to the differential equations and solving them for the initial conditions $P_E(0) = 1$ and $P_{ES}(0) = 0$ at $t = 0$ and the constraint $P_E(t) + P_{ES}(t) = 1$ one obtains the following relationship between the mean waiting time $\langle \tau \rangle$ and the substrate concentration $[S]$ (Kou et al., 2005):

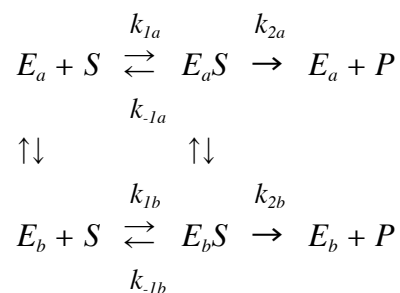
$$\frac{1}{\langle \tau \rangle} = \frac{k_2[S]}{[S] + K_M} \quad (\text{eq. 7.8})$$

Comparing this equation to the classical Michaelis-Menten equation it is evident, that the reciprocal of the mean waiting time is related to the enzymatic velocity measured in an ensemble measurement. This relation originates from the

equivalence between time averaging over a long time trace and ensemble averaging over a large number of identical molecules (English et al., 2006).

The above relation shows that experiments with single enzymes can yield the same result as ensemble measurements. However, this is not always the case. Enzymes are dynamic entities exhibiting distributions and fluctuations of catalytic rate constants. These effects can be analyzed in single molecule experiments only. The most important features of enzymes, which are hidden in ensemble measurements, are static and dynamic disorder (Xie and Lu, 1999). Static disorder is the result of differences in the activity of individual enzyme molecules. The existence of static disorder was shown for lactate dehydrogenase first (Xue and Yeung, 1995). A solution of the enzyme and its substrate was filled in a narrow capillary. The enzyme concentration was adjusted to ensure that single enzyme molecules are separated by a relatively large distance. The accumulation of product was measured after an incubation time of one hour. The amount of the product varied by a factor of 4. This result could be reproduced with the same enzyme molecules showing that the enzymes indeed possess different activities. Dynamic disorder refers to fluctuations of the rate constants of the reaction caused by transitions among different enzyme conformers. Dynamic disorder has been shown for different enzymes. The first experiment proving the existence of dynamic disorder was carried out with cholesterol oxidase (Lu et al., 1998). Later it was shown for staphylococcal nuclease (Ha et al., 1999), horseradish peroxidase (Edman et al., 1999), bacteriophage λ exonuclease (van Oijen et al., 2003), lysozyme (Lu, 2004), the lipase B of *Candida antarctica* (Velonia et al., 2005) and β -galactosidase (English et al., 2006). It is considered to be a general property of enzymes (Xie, 2001).

The fluctuations resulting in dynamic disorder can occur on a time scale comparable to or longer than the time scale of the enzymatic reaction, so that the rate of the product formation is no longer governed by a single rate constant but effectively by a distribution of rate constants. The simplest case is shown in the reaction scheme below where E_a shows very high catalytic activity and E_b shows low catalytic activity:



Depending on the rates of the enzymatic reaction and the rates for the interconversion between the different conformations of the enzyme two general cases can be distinguished. If k_{2a} is slow compared to the interconversion rates, k_{2a} is rate limiting and no dynamic disorder will be observed. However, if the interconversion rates are slower than k_{2a} the enzyme can remain in the highly active conformation for several turnovers and then convert into the less active conformation and remain in this conformation for a while. The effect that long waiting times are followed by long waiting times and short waiting times are followed by short waiting times is a non-Markovian behavior. Therefore, dependent on the combination of the rate constants memory effects can be observed. Interestingly, if the constants of the basic Michaelis-Menten equation are replaced by the weighted averages of the distributions of the conformers the equation is still valid. This has been shown theoretically and experimentally for the enzyme β -galactosidase (English et al., 2006). Information about dynamic disorder can be obtained from the time trajectories of the enzymatic turnover events. The rate constants can be obtained from a multiexponential fit to the probability density function of the waiting times. Alternatively the autocorrelation function of the waiting times shows the range of the timescales of the fluctuations (Xie, 2001; Kou et al., 2005; Min et al., 2005; English et al., 2006).

7.4 Model system for force based manipulation

Having established that it is highly likely that an enzyme will respond to an externally applied force and the theory for the analysis of single enzyme data, a model system is introduced in the next chapter, which will allow the observation of force induced changes of the enzyme activity. Lipase B from *Candida antarctica* (CalB) is an interesting candidate (Uppenberg et al., 1994, Uppenberg, 1995 #21; Anderson et al., 1998). The enzyme has low substrate specificity and can convert different fluorogenic substrates into fluorescent products (Fig. 16). Furthermore, it has been shown that CalB displays dynamic disorder (Velonia et al., 2005). Therefore, if an externally applied force can shift the equilibrium between the different conformations of CalB this effect should be immediately visible. The effect of the force can be analyzed by comparing time traces of the generated fluorescence signal measured with and without an externally applied force.

In order to be able to monitor the enzymatic turnover during the application of the external force the enzyme needs to be immobilized on a glass surface in a site-specific manner. This allows the measurement of the activity of surface bound enzymes with a total internal reflection fluorescence (TIRF) microscope. In addition a force sensor (chapter 5) is attached to the enzyme at a defined position. This force sensor transmits the force from the AFM cantilever to the enzyme and opens if the force reaches a certain threshold. This threshold force is assumed to prevent the unfolding of the enzyme. Using this set-up the enzyme can be manipulated with an

external force simultaneously monitoring fluorescence bursts on the surface, which are the result of single turnover events.

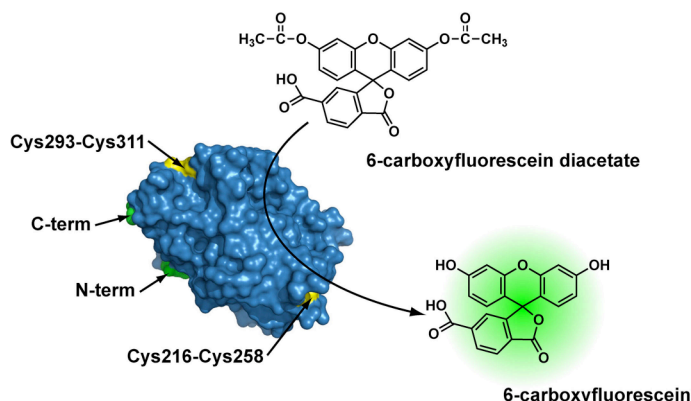


Figure 16. Model system consisting of CalB and the fluorogenic substrate carboxyfluorescein diacetate (CFDA). The lipase CalB (PDB no. 1LBT) has a low substrate specificity. It does not catalyze the hydrolysis of natural fat only but it also converts the artificial substrate CFDA. The substrate itself is not fluorescent. But, enzymatic cleavage yields the fluorescent product carboxyfluorescein. The generation of the product can be measured in bulk measurements and in single molecule measurements. The structure of CalB shows the termini of the protein. These can be used to modify the protein to achieve coupling to a surface or a force sensor. They are located in an appropriate distance from the active site. Additionally, two surface exposed disulfide bonds are shown. They can be modified genetically or chemically.

In order to establish this complex set-up CalB had to be modified on the genetic level. First, it was necessary to clone and express CalB in *Escherichia coli*. The results of this study are summarized in the publication P4. Second, it was necessary to introduce a reactive site for the site-specific immobilization of CalB on the glass surface. This was achieved by introducing a cysteine residue at the C-terminus, which can be utilized for coupling to a surface displaying maleimide groups. The optimized protocol is summarized in the publication P3. Third, a peptide sequence was attached to the N-terminus. This peptide is one part of the force sensor. The force sensor is described in more detail in chapter 5.3 and in the publication P1. Due to the complexity of the set-up the fluorescence measurements (with and without an externally applied force) are not the subject of this thesis. First measurements without force again proved the presence of dynamic disorder. Measurements with an applied external force will be carried out in the near future. Therefore, the question if an enzyme reacts to an external force and how it reacts cannot be answered yet.

8 Outlook

The results presented in this work demonstrate that receptor ligand interactions can be applied as molecular force sensors in a broad range of different applications. After their characterization with standard technologies like AFM they can be immobilized on surfaces and connected to different kinds of biomolecules. They provide a threshold force, which can be used as a reference in a differential force assay. Alternatively they can be applied to load molecules with a force allowing the observation of the response of this molecule to the applied force. It is believed that molecular force sensors will find broad applications for the analysis of the mechanisms of naturally occurring molecular force sensors. Especially the antibody peptide interaction presented here has a huge potential for this type of experiments as the peptide can be fused to the molecule of interest on the genetic level easily. Furthermore, force sensors cannot be used for the characterization of naturally occurring force sensors only but also for the analysis of molecules which are not responding to force in their natural environment. As has been pointed out for the manipulation of the enzyme, force can shift the equilibrium between different conformations of a protein. Therefore, the analysis of the effect of force on the function of a protein can reveal a more detailed picture of the energy landscape of the folded protein. In addition, the use of molecular force sensors is not restricted to the analysis of biomolecules. They are expected to play an important role in bottom up approaches in nanotechnology. Appropriately designed force sensors allow to pick up a molecule of interest and to release it at a defined position. If the force sensor is attached to an AFM cantilever, the procedure can be repeated many times and the accuracy of the positioning is in the nanometer range due to the high spatial resolution of the AFM.

9 References

- Alcantar, N.A., Aydil, E.S., and Israelachvili, J.N. (2000) Polyethylene glycol-coated biocompatible surfaces. *J. Biomed. Mater. Res.* 51(3):343-351.
- Alon, R., Hammer, D.A., and Springer, T.A. (1995) Lifetime of the P-selectin-carbohydrate bond and its response to tensile force in hydrodynamic flow. *Nature* 374(6522):539-542.
- Anderson, E.M., Larsson, K.M., and Kirk, O. (1998) One biocatalyst - many applications: The use of *Candida antarctica* B-Lipase in organic synthesis. *Biocatal. Biotransfor.* 16:181-204.
- Ashkin, A. (1997) Optical trapping and manipulation of neutral particles using lasers. *Proc. Natl. Acad. Sci. USA* 94(10):4853-4860.
- Bell, G.I. (1978) Models for the specific adhesion of cells to cells. *Science* 200(4342):618-627.
- Berquand, A., Xia, N., Castner, D.G., Clare, B.H., Abbott, N.L., Dupres, V., Adriaensen, Y., and Dufrene, Y.F. (2005) Antigen binding forces of single antilysozyme Fv fragments explored by atomic force microscopy. *Langmuir* 21(12):5517-5523.
- Binnig, G., Quate, C.F., and Gerber, C. (1986) Atomic Force Microscope. *Phys. Rev. Lett.* 56(9):930-933.
- Bustamante, C., Bryant, Z., and Smith, S.B. (2003) Ten years of tension: single-molecule DNA mechanics. *Nature* 421(6921):423-427.
- Bustamante, C., Chemla, Y.R., Forde, N.R., and Izhaky, D. (2004) Mechanical processes in biochemistry. *Annu. Rev. Biochem.* 73:705-748.
- Cutler, P. (2003) Protein arrays: the current state-of-the-art. *Proteomics* 3(1):3-18.
- Daniels, D.S., Mol, C.D., Arvai, A.S., Kanugula, S., Pegg, A.E., and Tainer, J.A. (2000) Active and alkylated human AGT structures: a novel zinc site, inhibitor and extrahelical base binding. *EMBO J.* 19(7):1719-1730.
- Edman, L., Foldes-Papp, Z., Wennmalm, S., and Rigler, R. (1999) The fluctuating enzyme: a single molecule approach. *Chemical Physics* 247(1):11-22.
- English, B.P., Min, W., van Oijen, A.M., Lee, K.T., Luo, G., Sun, H., Cherayil, B.J., Kou, S.C., and Xie, X.S. (2006) Ever-fluctuating single enzyme molecules: Michaelis-Menten equation revisited. *Nat. Chem. Biol.* 2(2):87-94.
- Evans, E., and Ritchie, K. (1999) Strength of a weak bond connecting flexible polymer chains. *Biophys. J.* 76(5):2439-2447.

- Evans, E., Ritchie, K., and Merkel, R. (1995) Sensitive force technique to probe molecular adhesion and structural linkages at biological interfaces. *Biophys. J.* 68(6):2580-2587.
- Florin, E.L., Moy, V.T., and Gaub, H.E. (1994) Adhesion forces between individual ligand-receptor pairs. *Science* 264(5157):415-417.
- Garcia-Viloca, M., Gao, J., Karplus, M., and Truhlar, D.G. (2004) How enzymes work: analysis by modern rate theory and computer simulations. *Science* 303(5655):186-195.
- Ge, L., Knappik, A., Pack, P., Freund, C., and Plückthun, A. (1995) Expressing Antibodies in *Escherichia coli*. In: *Antibody Engineering*. Borrebaeck, C.A.K. (editor). Oxford University Press, New York. 229-266.
- Grandbois, M., Beyer, M., Rief, M., Clausen-Schaumann, H., and Gaub, H.E. (1999) How strong is a covalent bond? *Science* 283(5408):1727-1730.
- Gräter, F., Shen, J., Jiang, H., Gautel, M., and Grubmüller, H. (2005) Mechanically induced titin kinase activation studied by force-probe molecular dynamics simulations. *Biophys. J.* 88(2):790-804.
- Guthold, M., Superfine, R., and Taylor, R.M. (2001) The rules are changing: force measurements on single molecules and how they relate to bulk reaction kinetics and energies. *Biomed. Microdevices* 3(1):9-18.
- Ha, T., Ting, A.Y., Liang, J., Caldwell, W.B., Deniz, A.A., Chemla, D.S., Schultz, P.G., and Weiss, S. (1999) Single-molecule fluorescence spectroscopy of enzyme conformational dynamics and cleavage mechanism. *Proc. Natl. Acad. Sci. USA* 96(3):893-898.
- Haldane, J.B.S. (1930) *Enzymes*. Longmans, London.
- Hanes, J., Jermutus, L., Weber-Bornhauser, S., Bosshard, H.R., and Plückthun, A. (1998) Ribosome display efficiently selects and evolves high-affinity antibodies in vitro from immune libraries. *Proc. Natl. Acad. Sci. USA* 95(24):14130-14135.
- Hearn, M.T., and Acosta, D. (2001) Applications of novel affinity cassette methods: use of peptide fusion handles for the purification of recombinant proteins. *J. Mol. Recognit.* 14(6):323-369.
- Hermanson, G.T. (1995) *Bioconjugate Techniques*. Academic Press, San Diego, CA.
- Hodneland, C.D., Lee, Y.S., Min, D.H., and Mrksich, M. (2002) Selective immobilization of proteins to self-assembled monolayers presenting active site-directed capture ligands. *Proc. Natl. Acad. Sci. USA* 99(8):5048-5052.
- Kamimura, S., and Takahashi, K. (1981) Direct measurement of the force of microtubule sliding in flagella. *Nature* 293(5833):566-568.

- Keppler, A., Gendreizig, S., Gronemeyer, T., Pick, H., Vogel, H., and Johnsson, K. (2003) A general method for the covalent labeling of fusion proteins with small molecules in vivo. *Nat. Biotechnol.* 21(1):86-89.
- Kindermann, M., George, N., Johnsson, N., and Johnsson, K. (2003) Covalent and selective immobilization of fusion proteins. *J. Am. Chem. Soc.* 125(26):7810-7811.
- Kingsmore, S.F. (2006) Multiplexed protein measurement: technologies and applications of protein and antibody arrays. *Nat. Rev. Drug. Discov.* 5(4):310-320.
- Kou, S.C., Cherayil, B.J., Min, W., English, B.P., and Xie, X.S. (2005) Single-molecule Michaelis-Menten equations. *J. Phys. Chem. B* 109(41):19068-19081.
- Krautbauer, R., Rief, M., and Gaub, H.E. (2003) Unzipping DNA oligomers. *Nano Lett.* 3(4):493-496.
- Kusnezow, W., and Hoheisel, J.D. (2002) Antibody microarrays: promises and problems. *Biotechniques* Suppl:14-23.
- Lange, S., Xiang, F., Yakovenko, A., Vihola, A., Hackman, P., Rostkova, E., Kristensen, J., Brandmeier, B., Franzen, G., Hedberg, B., Gunnarsson, L.G., Hughes, S.M., Marchand, S., Sejersen, T., Richard, I., Edstrom, L., Ehler, E., Udd, B., and Gautel, M. (2005) The kinase domain of titin controls muscle gene expression and protein turnover. *Science* 308(5728):1599-1603.
- Lu, H.P. (2004) Single-molecule spectroscopy studies of conformational change dynamics in enzymatic reactions. *Curr. Pharm. Biotechnol.* 5(3):261-269.
- Lu, H.P., Xun, L., and Xie, X.S. (1998) Single-molecule enzymatic dynamics. *Science* 282(5395):1877-1882.
- MacBeath, G. (2002) Protein microarrays and proteomics. *Nat. Genet.* 32 Suppl:526-532.
- Michaud, G.A., Salcius, M., Zhou, F., Bangham, R., Bonin, J., Guo, H., Snyder, M., Predki, P.F., and Schweitzer, B.I. (2003) Analyzing antibody specificity with whole proteome microarrays. *Nat. Biotechnol.* 21(12):1509-1512.
- Min, W., English, B.P., Luo, G., Cherayil, B.J., Kou, S.C., and Xie, X.S. (2005) Fluctuating enzymes: lessons from single-molecule studies. *Acc. Chem. Res.* 38(12):923-931.
- Narlikar, G.J., and Herschlag, D. (1997) Mechanistic aspects of enzymatic catalysis: lessons from comparison of RNA and protein enzymes. *Annu. Rev. Biochem.* 66:19-59.
- Neher, R.A., and Gerland, U. (2004) Dynamics of force-induced DNA slippage. *Phys. Rev. Lett.* 93(19):198102.

- Neuert, G., Albrecht, C., Pamir, E., and Gaub, H.E. (2006) Dynamic force spectroscopy of the digoxigenin-antibody complex. *FEBS Lett.* 580(2):505-509.
- Pauling, L. (1946) Molecular Architecture and Biological Reactions. *Chem. Eng. News* 24(10):1375-1377.
- Perozo, E. (2006) Gating prokaryotic mechanosensitive channels. *Nat. Rev. Mol. Cell Biol.* 7(2):109-119.
- Perozo, E., Cortes, D.M., Sompornpisut, P., Kloda, A., and Martinac, B. (2002) Open channel structure of MscL and the gating mechanism of mechanosensitive channels. *Nature* 418(6901):942-948.
- Plückthun, A. (1994) Recombinant Antibodies. In: Immunochemistry. van Oss, C.J., van Regenmortel, M.H.V. (editors) Marcel Dekker, Inc., New York. 201-236.
- Plückthun, A., Schaffitzel, C., Hanes, J., and Jermutus, L. (2000) In vitro selection and evolution of proteins. *Adv. Protein Chem.* 55:367-403.
- Rasimas, J.J., Pegg, A.E., and Fried, M.G. (2003) DNA-binding mechanism of O⁶-alkylguanine-DNA alkyltransferase. Effects of protein and DNA alkylation on complex stability. *J. Biol. Chem.* 278(10):7973-7980.
- Rief, M., Clausen-Schaumann, H., and Gaub, H.E. (1999) Sequence-dependent mechanics of single DNA molecules. *Nat. Struct. Biol.* 6(4):346-349.
- Rief, M., Gautel, M., Oesterhelt, F., Fernandez, J.M., and Gaub, H.E. (1997) Reversible unfolding of individual titin immunoglobulin domains by AFM. *Science* 276(5315):1109-1112.
- Roberts, M.J., Bentley, M.D., and Harris, J.M. (2002) Chemistry for peptide and protein PEGylation. *Adv. Drug. Deliv. Rev.* 54(4):459-476.
- Schena, M., Shalon, D., Davis, R.W., and Brown, P.O. (1995) Quantitative monitoring of gene expression patterns with a complementary DNA microarray. *Science* 270(5235):467-470.
- Schwesinger, F., Ros, R., Strunz, T., Anselmetti, D., Güntherodt, H.J., Honegger, A., Jermutus, L., Tiefenauer, L., and Plückthun, A. (2000) Unbinding forces of single antibody-antigen complexes correlate with their thermal dissociation rates. *Proc. Natl. Acad. Sci. USA* 97(18):9972-9977.
- Sielaff, I., Arnold, A., Godin, G., Tugulu, S., Klok, H.A., and Johnsson, K. (2006) Protein function microarrays based on self-immobilizing and self-labeling fusion proteins. *ChemBioChem* 7(1):194-202.
- Smith, S.B., Finzi, L., and Bustamante, C. (1992) Direct mechanical measurements of the elasticity of single DNA molecules by using magnetic beads. *Science* 258(5085):1122-1126.

- Sofia, S.J., and Merrill, E.W. (1997) Protein Adsorption on Poly(ethylene oxide)-Grafted Silicon Surfaces. In: Poly(ethylene glycol) Chemistry and Biological Applications. Harris, J.M., Zalipsky, S. (editors) ACS Symposium Series, Washington, DC. 342-360.
- Strick, T., Allemand, J., Croquette, V., and Bensimon, D. (2000) Twisting and stretching single DNA molecules. *Prog. Biophys. Mol. Biol.* 74(1-2):115-140.
- Strunz, T., Oroszlan, K., Schäfer, R., and Güntherodt, H.J. (1999) Dynamic force spectroscopy of single DNA molecules. *Proc. Natl. Acad. Sci. USA* 96(20):11277-11282.
- Sukharev, S., Betanzos, M., Chiang, C.S., and Guy, H.R. (2001) The gating mechanism of the large mechanosensitive channel MscL. *Nature* 409(6821):720-724.
- Tees, D.F., Coenen, O., and Goldsmith, H.L. (1993) Interaction forces between red cells agglutinated by antibody. IV. Time and force dependence of break-up. *Biophys. J.* 65(3):1318-1334.
- Terpe, K. (2003) Overview of tag protein fusions: from molecular and biochemical fundamentals to commercial systems. *Appl. Microbiol. Biotechnol.* 60(5):523-533.
- Thomas, W., Forero, M., Yakovenko, O., Nilsson, L., Vicini, P., Sokurenko, E., and Vogel, V. (2006) Catch-bond model derived from allostery explains force-activated bacterial adhesion. *Biophys. J.* 90(3):753-764.
- Thomas, W.E., Trintchina, E., Forero, M., Vogel, V., and Sokurenko, E.V. (2002) Bacterial adhesion to target cells enhanced by shear force. *Cell* 109(7):913-923.
- Tomizaki, K.Y., Usui, K., and Mihara, H. (2005) Protein-detecting microarrays: current accomplishments and requirements. *ChemBioChem* 6(5):782-799.
- Turkova, J. (1999) Oriented immobilization of biologically active proteins as a tool for revealing protein interactions and function. *J. Chromatogr. B* 722(1-2):11-31.
- Uppenberg, J., Hansen, M.T., Patkar, S., and Jones, T.A. (1994) The sequence, crystal structure determination and refinement of two crystal forms of lipase B from *Candida antarctica*. *Structure* 2(4):293-308.
- van Oijen, A.M., Blainey, P.C., Crampton, D.J., Richardson, C.C., Ellenberger, T., and Xie, X.S. (2003) Single-molecule kinetics of lambda exonuclease reveal base dependence and dynamic disorder. *Science* 301(5637):1235-1238.
- Velonia, K., Flomenbom, O., Loos, D., Masuo, S., Cotlet, M., Engelborghs, Y., Hofkens, J., Rowan, A.E., Klaffer, J., Nolte, R.J., and de Schryver, F.C. (2005) Single-enzyme kinetics of CALB-catalyzed hydrolysis. *Angew. Chem. Int. Ed. Engl.* 44(4):560-564.

- Veronese, F.M. (2001) Peptide and protein PEGylation: a review of problems and solutions. *Biomaterials* 22(5):405-417.
- Viani, M.B., Schäffer, T.E., Chand, A., Rief, M., Gaub, H.E., and Hansma, P.K. (1999) Small cantilevers for force spectroscopy of single molecules. *J. Appl. Phys.* 86(4):2258-2262.
- Villa, J., and Warshel, A. (2001) Energetics and dynamics of enzymatic reactions. *J. Phys. Chem. B* 105(33):7887-7907.
- Vogel, V. (2006) Mechanotransduction involving multimodular proteins: converting force into biochemical signals. *Annu. Rev. Biophys. Biomol. Struct.* 35:459-488.
- Vogel, V., and Sheetz, M. (2006) Local force and geometry sensing regulate cell functions. *Nat. Rev. Mol. Cell Biol.* 7(4):265-275.
- Wang, J.H., and Thampatty, B.P. (2006) An introductory review of cell mechanobiology. *Biomech. Model. Mechanobiol.* 5(1):1-16.
- Wibley, J.E., Pegg, A.E., and Moody, P.C. (2000) Crystal structure of the human O(6)-alkylguanine-DNA alkyltransferase. *Nucleic Acids Res.* 28(2):393-401.
- Winter, G., Griffiths, A.D., Hawkins, R.E., and Hoogenboom, H.R. (1994) Making antibodies by phage display technology. *Annu. Rev. Immunol.* 12:433-455.
- Xie, S.N. (2001) Single-molecule approach to enzymology. *Single Mol.* 2(4):229-236.
- Xie, X.S., and Lu, H.P. (1999) Single-molecule enzymology. *J. Biol. Chem.* 274(23):15967-15970.
- Xue, Q., and Yeung, E.S. (1995) Differences in the chemical reactivity of individual molecules of an enzyme. *Nature* 373(6516):681-683.
- Zahnd, C., Spinelli, S., Luginbühl, B., Amstutz, P., Cambillau, C., and Plückthun, A. (2004) Directed in vitro evolution and crystallographic analysis of a peptide-binding single chain antibody fragment (scFv) with low picomolar affinity. *J. Biol. Chem.* 279(18):18870-18877.

10 Supplement

P1 _____ S3

Application of Dynamic Force Spectroscopy for the Analysis of Affinity Matured Recombinant Antibody Fragments

J. Morfill, K. Blank, C. Zahnd, B. Luginbühl, F. Kühner, K. E. Gottschalk, A. Plückthun and H. E. Gaub

Proceedings of the National Academy of Sciences USA (2006) submitted

P2 _____ S16

Force induced DNA slippage

F. Kühner, J. Morfill, R. Neher, K. Blank and H. E. Gaub

Biophysical Journal (2006) submitted

P3 _____ S24

Site-Specific Immobilization of Genetically Engineered Variants of *Candida antarctica* Lipase B

K. Blank, J. Morfill and H. E. Gaub

ChemBioChem, published online 26 July 2006

P4 _____ S29

Functional expression of *Candida antarctica* lipase B in *Escherichia coli*

K. Blank, J. Morfill, H. Gumpff and H. E. Gaub

Journal of Biotechnology, published online 17 May 2006

P5 _____ S40

Covalent immobilization of recombinant fusion proteins with hAGT for single molecule force spectroscopy

S. Kufer, H. Dietz, C. Albrecht, K. Blank, A. Kardinal, M. Rief and H. E. Gaub

European Biophysics Journal (2005) 35: 72-78

P6 _____ S48

Double chip protein arrays using recombinant single-chain Fv antibody fragments

I. Gilbert, S. Schiffmann, S. Rubenwolf, K. Jensen, T. Mai, C. Albrecht, A. Lankenau, G. Beste, K. Blank, H. E. Gaub and H. Clausen-Schaumann

Proteomics (2004) 4: 1417-1420

P7 _____ S53

Double-chip protein arrays: force-based multiplex sandwich immunoassays with increased specificity

K. Blank, A. Lankenau, T. Mai, S. Schiffmann, I. Gilbert, S. Hirler, C. Albrecht, M. Benoit, H. E. Gaub and H. Clausen-Schaumann

Analytical and Bioanalytical Chemistry (2004) 379:974-981

P8 _____ S62

A force-based protein biochip

K. Blank, T. Mai, I. Gilbert, S. Schiffmann, J. Rankl, R. Zivin, C. Tackney, T. Nicolaus, K. Spinnler, F. Oesterhelt, M. Benoit, H. Clausen-Schaumann and H. E. Gaub

Proceedings of the National Academy of Sciences USA (2003) 100:11356-11360

P9 _____ S68

DNA: A Programmable Force Sensor

C. Albrecht, K. Blank, M. Lalic-Mülthaler, S. Hirler, T. Mai, I. Gilbert, S. Schiffmann, T. Bayer, H. Clausen-Schaumann and H. E. Gaub

Science (2003) 301: 367-370

Further publications, which are not part of this thesis:

Crystal structure of the anti-His tag antibody 3D5 single-chain fragment complexed to its antigen

M. Kaufmann, P. Lindner, A. Honegger, K. Blank, M. Tschopp, G. Capitani, A. Plückthun and M. G. Grütter

Journal of Molecular Biology (2002) 318: 135-147

Self-immobilizing recombinant antibody fragments for immunoaffinity chromatography: generic, parallel and scalable protein purification

K. Blank, P. Lindner, B. Diefenbach and A. Plückthun

Protein Expression and Purification (2002) 24: 313-322

P1

Application of Dynamic Force Spectroscopy for the Analysis of Affinity Matured Recombinant Antibody Fragments

J. Morfill, K. Blank, C. Zahnd, B. Luginbühl, F. Kühner, K. E. Gottschalk,
A. Plückthun and H. E. Gaub

Proceedings of the National Academy of Sciences USA (2006) submitted

Classification: Biological Sciences / Biophysics

Application of Dynamic Force Spectroscopy for the Analysis of Affinity Matured Recombinant Antibody Fragments

Julia Morfill[†], Kerstin Blank[†], Christian Zahnd[‡], Beatrice Luginbühl[‡], Ferdinand Kühner[†], Kay Gottschalk[†], Andreas Plückthun[‡], Hermann E. Gaub[†]

[†] Lehrstuhl für Angewandte Physik & Center for Nanoscience, LMU München, Amalienstrasse 54, 80799 München, Germany

[‡] Biochemisches Institut, Universität Zürich, Winterthurerstrasse 190, 8057 Zürich, Switzerland

Corresponding author: Prof. Dr. Hermann E. Gaub
hermann.gaub@physik.uni-muenchen.de
Tel.: +49-89-2180-3173
Fax: + 49-89-2180-2050

Number of text pages: 19
Number of figures: 4
Number of tables: 1
Number of words (abstract): 248
Number of characters: 30986

Abstract

In recent years the importance of recombinant antibodies has increased dramatically. For many applications high affinity antibodies are needed to fulfill desired functions. In general it is assumed that the dissociation rate of the antibody of interest has to be optimized. Using conventional methods just as surface plasmon resonance (SPR), the exact measurement of low dissociation rates however is critical due to the detection limit and the required time for the assay. Therefore, we applied dynamic force spectroscopy (DFS) to determine the dissociation rates of three clones of a recombinant antibody fragment and compared our values with the data obtained from SPR measurements. The three clones have been taken from different steps of an affinity maturation process and therefore are closely related. The antibodies exhibit very high affinities (K_D of 2.6 nM to 5 pM). Within the experimental error both measurement methods yield the same values for the dissociation rates (k_{off} between 0.0039 s^{-1} and 0.00049 s^{-1}). This proves that DFS is an attractive alternative to SPR if the unbinding process of a molecular interaction needs to be characterized. Many problems, which appear in SPR measurements just as rebinding and avidity effects cannot occur if DFS is used. Besides this advantage DFS further yields additional information about the width of the binding potential. In the study presented here, it was found that the potential width and therefore the unbinding pathway are not affected by the mutations whereas one mutation has a significant influence on the dissociation rate.

Introduction

In recent years recombinant antibodies have become increasingly important as therapeutic agents, for proteomics applications and for diagnostic assays. In addition, they might prove usefulness as building blocks for the self-assembly of nanostructures. Depending on the particular application, antibodies with high affinity are needed in most of the cases. For example, virus, toxin or cytokine neutralizing antibodies require a high affinity to block the action of as many molecules as possible (1-4). In diagnostic assays, especially when low abundance proteins want be detected, the use of high-affinity reagents is necessary to obtain the required sensitivity (5). In principle, antibodies with a higher affinity (characterized by a lower dissociation constant $K_D = k_{off}/k_{on}$) can be obtained either by increasing the association rate (k_{on}) or by decreasing the dissociation rate (k_{off}). Because of the diffusion control of the association reaction, the upper limit of k_{on} is thought, in general, to be not faster than $10^6 \text{ M}^{-1} \text{ s}^{-1}$ to $10^7 \text{ M}^{-1} \text{ s}^{-1}$ for antibody antigen interactions in solution (6, 7). In contrast, k_{off} can vary over several orders of magnitudes (10^{-1} s^{-1} to 10^{-6} s^{-1}). Therefore, it is considered that k_{off} is the main determinant of the equilibrium constant for most antibody antigen interactions (8, 9).

Many different approaches have been developed for the *in vitro* affinity maturation of recombinant antibody fragments such as single chain Fv (scFv) or Fab fragments (1-4, 10-15). If a number of clones has been selected, they need to be characterized with regard to their affinity improvement. Mostly, the determination of the dissociation constant yields sufficient information. However, in selected cases it is necessary to measure the kinetic rate constants of the binding and unbinding process. This is of particular importance if the affinity improvement wants to be correlated with the position and type of the acquired mutation(s) of the clone of interest to obtain more detailed information on structure function relationships. Several different methods exist for the determination of the dissociation constant. It can be measured with ELISA (16), surface plasmon resonance (SPR) (17), fluorescence titration (9), and fluorescence activated cell sorting (FACS) (13). The exact measurement of the kinetic constants is far more complicated. Mostly, SPR is used for this purpose. To obtain exact

values, especially for k_{off} , one has to take care about possible rebinding effects on the surface during the dissociation phase. In addition, in the case of slow dissociation rates (k_{off} below 10^{-5} s^{-1}) an accurate determination of k_{off} is difficult due to the small amount of analyte dissociating. The measurement is disturbed by drift of the SPR instrument (18).

Dynamic force spectroscopy (DFS) is an alternative method to obtain information about the unbinding process of receptor-ligand interactions. This measurement method has been used for a broad range of different biological systems including antibody-antigen interactions (9, 19). DFS makes use of the effect that k_{off} is increased if an external force is applied. Measuring the rupture forces of a receptor-ligand interaction for different loading rates allows the extrapolation to the dissociation rate at zero force, which represents the natural k_{off} . Furthermore, this measurement method yields additional information about the width of the binding potential Δx . This additional information might be useful for the interpretation of the influence of different mutations of various antibody clones on the (un)binding kinetics and the geometry of the binding site.

In this report we have analyzed three different clones of scFv fragments with DFS. They represent a series of clones obtained from different steps of an affinity maturation process using ribosome display (15, 20). They all bind the same peptide antigen, which is a random coil in solution. The crystal structure of a related clone complexed with the antigen is published (15). As the peptide forms an α -helical structure in the complex with the antibody the peptide is considered to undergo a conformational change upon binding and unbinding. To our knowledge, this is the first report describing a detailed structure based analysis of a system where both the antibody and the antigen can react to the externally applied force. For the DFS measurements an atomic force microscope (AFM) was used and the rupture forces were measured over a broad range of different loading rates. From these results k_{off} and Δx were calculated with two analysis methods, which are based on the well-established Bell-Evans-model (21-23). The k_{off} values from DFS were compared with the k_{off} values determined with SPR. Based on these results one possible unbinding process is discussed with respect to the amino acid substitutions of the clones.

Materials and Methods

Cloning, expression and purification of the antibody fragments

The three clones were expressed with a C-terminal His tag followed by a cysteine to allow the site-specific immobilization of the scFv fragments. The plasmids for the periplasmic expression of the clones were based on the pAK series (24). The gene for coexpression of the periplasmic chaperone Skp was introduced (25). The His tag was replaced by a tag of six histidines followed by two glycines and a cysteine. For the expression and purification of the clones the protocol of Hanes et al. (20) was slightly modified. Briefly, the plasmids were transformed in the *E. coli* strain SB536. Cells were grown at 25 °C in SB medium (20 g l⁻¹ tryptone, 10 g l⁻¹ yeast extract, 5 g l⁻¹ NaCl, 50 mM K₂HPO₄) containing 30 µg ml⁻¹ chloramphenicol. Expression was induced with 1 mM Isopropyl-β-D-thiogalactopyranosid (IPTG) at an OD₆₀₀ between 1.0 and 1.5. The cells were harvested 3 h after induction by centrifugation. Cell disruption was achieved by French Press lysis. The scFv fragments were purified using two chromatography steps. After a Ni²⁺-NTA column (Qiagen, Hilden, Germany) using standard protocols the eluted fraction was directly loaded onto an affinity column with immobilized antigen. The fractions from the affinity column were dialyzed against coupling buffer (50 mM sodium phosphate pH 7.2, 50 mM NaCl, 10 mM EDTA) and concentrated using Centricon YM-10 (Millipore, Eschborn, Germany). The actual concentration of the purified scFv fragments was determined by measuring the absorbance at 280 nm. The extinction coefficients of the different clones have been calculated using the program Vector NTI (Invitrogen, Karlsruhe, Germany). The purified clones were adjusted to a final concentration of 0.8 mg ml⁻¹ and stored in aliquots at -80 °C.

Preparation of slides and cantilevers

The scFv fragments were immobilized on an amino-functionalized slide using a hetero-bifunctional poly(ethylene glycol) spacer (NHS-PEG-maleimide MW = 5000 g/mol; Nektar, Huntsville, Alabama). The peptide CGGGRMKQLEPKVEELLPKNYHLENEVARLKLKLVGER (Jerini Peptide Technologies GmbH, Berlin, Germany) was coupled to the cantilever via the same PEG spacer (Fig. 1). The cantilevers (Bio-lever, Olympus, Tokio, Japan) were cleaned

and functionalized as described (19). Instead of epoxy-functionalized cantilevers, amino-modified surfaces were prepared using 3-aminopropyl-dimethylethoxysilane (ABCR GmbH, Karlsruhe, Germany). Commercially available amino functionalized slides (Slide A, Nexterion, Mainz, Germany) were used. From now on, both surfaces were treated in parallel as described (26). Briefly, they were incubated in borate buffer pH 8.5 for one hour. This step was necessary to deprotonate the amino groups for coupling to the NHS groups of the PEG. The PEG was dissolved in a concentration of 50 mM in borate buffer at pH 8.5 and incubated on the surfaces for one hour. In parallel, the peptide and one of the scFv fragments were reduced using TCEP beads (Perbio Science, Bonn, Germany) in order to generate free thiols. After washing both surfaces with ultrapure water, a solution of the peptide (200 μ M) was incubated on the cantilever and a solution of the scFv fragment (0.13 mg/ml) was incubated on the slide for one hour. Finally, both surfaces were rinsed with PBS (phosphate buffered saline) to remove non-covalently bound material and stored in PBS until use.

Dynamic force spectroscopy

All force measurements were performed with a MFP-1D atomic force microscope (AFM) (Asylum Research, Santa Barbara, USA) at room temperature in PBS. Cantilever spring constants ranged from 6 to 8 pN/nm (A-Bio-Lever) and were measured as described previously (27, 28). During one experiment the approach and retract velocity were held constant, whereas the applied force was adjusted by changing the distance between the cantilever tip and the surface to obtain single binding events. To achieve good statistics, several hundreds of approach-retract cycles have been carried out. To obtain a broad loading rate distribution, several experiments were performed each at a different retract velocity ranging from 50 nm/s to 10 μ m/s.

Data extraction

The obtained data was converted into force-extension curves. From these force-extension curves, the rupture force (the force at which the antibody-antigen complex ruptures), the rupture length and the corresponding loading rate were determined using the program Igor Pro 5.0 (Wavemetrics, Lake Oswego, OR) and a custom-written set of

procedures. The rupture force was determined as described previously (22, 23). The loading rate was determined using the freely jointed chain fit to the force-extension curve, according to previous studies (29).

Data analysis

To analyze the obtained data set of one experiment, which was recorded at a constant retract velocity, the rupture forces, lengths and logarithmic loading rates were plotted in three histograms. These histograms were analyzed with two methods based on the Bell-Evans-model (21-23). Using the first method, the force and the loading rate histogram were fitted with a Gaussian distribution to determine the maximum of the respective histograms. The maxima of the experimentally received histograms were determined for each data set. Finally the maxima of the Gaussian distributions were plotted into a force versus logarithmic loading rate diagram. The maximum force F_{max} (from the Gaussian distribution) represents the most probable force F^* :

$$(1) \quad F^* = \frac{k_B \cdot T}{\Delta x} \ln \frac{\dot{F} \cdot \Delta x}{k_B \cdot T \cdot k_{off}}$$

with k_B = the Boltzmann constant, T = the temperature, Δx = the potential width, k_{off} = the natural dissociation rate at zero force and $\dot{F} = \frac{dF}{dt}$ = the loading rate. From a linear fit in the force versus logarithmic loading rate diagram and equation (1) k_{off} and Δx of the antibody-antigen complex can be determined. The second method requires normalized histograms. To obtain k_{off} and Δx of the antibody antigen complex, the normalized force histogram was compared with the probability density function $p(F)$ (22, 23):

$$(2) \quad p(F) = k_{off} \cdot \exp\left(\frac{F \cdot \Delta x}{k_B \cdot T}\right) \frac{1}{F} \exp\left(-k_{off} \int_0^F dF' \exp\left(\frac{F' \cdot \Delta x}{k_B \cdot T}\right) \frac{1}{F'}\right)$$

Results

The clones used in our study are closely related and have been published previously (15, 20). They all bind a peptide antigen, which has been derived from the transcription factor GCN4. For a better understanding, we briefly summarize the positions (Table 1) and the influence of the mutations. The antibody clones only differ in a few amino acids. The mutated amino acids do not directly interact with the antigen although three of them are located in the complementarity determining regions. Mutation L42 (N→S; Aho numbering scheme (30)), which has been introduced into clone C11L34 reduces the flexibility of CDR L1 and may allow a more favourable domain orientation. Mutation L107 (A→V) of clone 52SR4 lies in close proximity to mutation L42 and might therefore contribute to this effect. Therefore, these two mutations influence the loop and the relative domain orientation and thereby optimize the binding geometry. Most likely, mutation L135 (N→D; clone 52SR4) has a different effect. The exchange of asparagine to aspartic acid introduces a negatively charged residue. This charged residue might be able to establish an electrostatic interaction with the peptide as the peptide has a positive charge at the corresponding position. Mutations L13 (T→S; clone 52SR4) and H30 (S→L; clone 52SR4) are considered to be neutral.

To analyze the interaction of the clones with their antigen (peptide), DFS measurements were performed using an atomic force microscope (AFM). For this purpose the experimental system was designed to minimize the impact of non-specific interactions and to maximize the probability of detecting specific and single antibody-peptide interactions. An effective approach for differentiating between specific and non-specific interactions implicates the attachment of antibody and peptide to the elastic spacer PEG. Therefore the antibody was coupled to a surface with covalently attached PEG and the peptide was immobilized onto the cantilever tip in the same way (Fig. 1). In all experiments the surface was approached with the tip of the cantilever, allowing the antibody-peptide complex to bind. Subsequently the cantilever was retracted and the antibody-peptide complex was loaded with an increasing force until the complex finally ruptured and the cantilever relaxed back into its equilibrium position. The force applied to this complex was recorded as a function of the distance

between the cantilever tip and the surface. Figure 2 shows a force-extension curve of the interaction between clone C11 and the peptide. To obtain good statistics several hundreds of force-extension curves for all the three clones have been recorded, to determine the rupture force, the rupture length and the corresponding loading rate. Figure 3 shows the experimentally observed rupture force, length and loading rate distributions for the interaction of clone C11 with the peptide. Using the first analysis method (see Materials and Methods), the rupture force histogram in figure 3a exhibits a maximum force F_{max} of 55.6 pN. Figures 3b and 3c show the rupture length and the corresponding logarithmic loading rate histograms. The histogram of the logarithmic loading rate was fitted with a Gaussian distribution, which refers to a maximum of 7.9 pN s^{-1} . For a complete analysis of the experimental results, all data sets for the three clones were examined with the first analysis method. Figure 4 refers to this analysis method and therefore shows the maxima of the Gaussian distributions gained from the experimentally received force histograms plotted against the appropriate maxima of the logarithmic loading rate histograms. These data points were fitted with a linear fit. Using equation (1) Δx and k_{off} for the different clones were determined and listed in table 1.

Additionally, the obtained rupture force distribution (Fig. 3a) was analyzed with the second analysis method based on the probability density function $p(F)$ as described in the methods section. The two analysis methods were compared for all three clones. But only one data set of clone C11 measured at a low loading rate is shown here (Fig. 3). The values obtained for clone C11 are: $\Delta x = 0.9 \text{ nm}$ and $k_{off} = 2 \cdot 10^{-3} \text{ s}^{-1}$. Comparing the values for both methods we conclude that for small retract velocities the values for Δx and k_{off} are identical within the experimental error (19).

Within the calculated error the Δx values for the three clones are identical. Comparing the k_{off} values, clone C11L34 has an 8 times slower rate than clone C11. This is the result of one single mutation at the end of CDR L1 of the V_L domain. Clone C11L34 and clone 52SR4 differ in four amino acids. These mutations do not have any significant influence on k_{off} . The values for k_{off} obtained from the SPR measurements are also summarized in table 1. Within the experimental error, both methods yield the same values for k_{off} for all three clones.

Unfortunately, k_{on} cannot be calculated from the obtained k_{off} values and the published equilibrium constants. The samples for the measurement of the equilibrium constants K_D have been equilibrated at 4 °C (15, 20) whereas the values for k_{off} were determined at 25 °C. As the temperature dependence of the constants is not known, we can only qualitatively estimate differences in k_{on} . Comparing clones C11L34 and 52SR4 we could not detect a significant difference in k_{off} . However, clone 52SR4 has a lower K_D than clone C11L34 suggesting that k_{on} has to be different.

Discussion

The experiments described here were performed to obtain high statistics in order to be able to compare the k_{off} values and their experimental error obtained from the DFS measurements with the achieved values from the SPR measurements. For this purpose, both binding partners, antibody and peptide, were immobilized site-specifically and covalently in the DFS measurements. The use of identical chemistry on both sides (cantilever tip and surface) and the use of PEG as a spacer reduces the probability of non-specific binding events to a minimum. Therefore, a high frequency of specific interactions allowed the measurement of a high number of force-extension curves at various different loading rates. As a result the k_{off} values determined with the two different measurement methods (DFS and SPR) are identical within the experimental error.

The data obtained from the DFS measurements was analyzed with two methods based on the Bell-Evans-model. The first method requires DFS measurements at various different loading rates whereas the second method analyzes the shape of the rupture force histogram at one loading rate. The three antibodies used in this study gained similar k_{off} and Δx values for both analysis methods for slow retract velocities. Using the second analysis method the experimental effort can be reduced significantly as the desired values can be obtained from one experiment at one loading rate. However, if the second analysis method is used retract velocities in the lower range should be used in order stay close to equilibrium.

To summarize the above findings DFS is an attractive alternative to SPR if the unbinding process of a receptor-ligand interaction wants to be characterized. The measurements can be easily standardized and the experimental effort is similar. We believe that in certain cases DFS has several advantages compared to SPR measurements. SPR measurements become unreliable for very low values of k_{off} . This is not the case for DFS measurements. In addition rebinding and avidity effects, which might result in lower k_{off} values in SPR measurements, cannot occur in DFS measurements. These binding events can be excluded in DFS measurements by a carefully designed experiment and during data evaluation. Whereas the advantages described above are mainly of practical interest, the following

aspect is even more important. DFS yields additional information about the unbinding process. The width of the potential Δx is another important parameter, which provides information about the unbinding pathway.

In the study presented here, the clones have an identical potential width. The potential width is considered to represent a geometrical value, which is related to the distance how far the complex can be stretched until it finally ruptures. This leads to the conclusion that neither the geometry of the binding sites nor the unbinding pathways were affected by the mutations introduced during the affinity maturation process. Compared with other protein-ligand interactions the obtained value for Δx is in the upper range. As the peptide is a random coil in solution and has an α -helical structure in complex with the antibody, the most likely unbinding path refers to a slow unfolding upon the forced unbinding process. During this process one or both binding partners can be deformed in the direction of the applied force. If a certain point is reached the deformation is so huge that the complex dissociates. This would mean that a more rigid binding site possesses a higher resistance to the applied force. This effect would then reflect a lower k_{off} value. Indeed the only relevant mutation, which improves k_{off} is the mutation in clone C11L34 which is considered to reduce the flexibility of CDR L1. This interpretation can also be supported with the fact, that the flexibility of the binding pocket is reduced during the affinity maturation process *in vivo* (31) This finding is an interesting aspect of the affinity maturation process. However, more data from more different clones would be needed to investigate if evolution generally results in more rigid binding sites.

This particular antibody antigen interaction might be useful for a broad range of further investigations and applications. First, it is an ideal model system to investigate forced unbinding processes in more detail. It therefore would be interesting to analyze, if the site of attachment of the peptide changes the unbinding pathway. In addition the analysis of truncated or mutated peptides will yield additional valuable information. As the structure of the complex is known molecular dynamics simulations can provide further insights. Secondly, as the antigen is a peptide it can be fused to proteins at the genetic level. Using this strategy,

the peptide provides a handle for the immobilization of the protein just like any other tag. Therefore, it is an ideal candidate to replace e.g. the digoxigenin system (19). It is superior to established affinity conjugation systems used for force measurements: The handle will be attached at a defined position and the bond strength can be modified by simply choosing another antibody or by changing the peptide sequence. Thirdly, the system can be used for the self-assembly of nanostructures. The peptide can be fused to any other protein or can be bound to surfaces using so called "genetically engineered proteins for inorganics (GEPI)" (32). If in addition a bispecific recombinant antibody (33) is used antibody displaying surfaces for virtually any antigen can be produced by self assembly.

Acknowledgements

The authors thank Julia Sedlmair and Holger Hesse for help in measuring this huge amount of data points as well as Gregor Neuert, Hauke Clausen-Schaumann, Matthias Rief, Robert Lugmaier, Ludmila Mendeleevitch and Thomas Nicolaus for helpful discussions. This work was supported by the European Union and the Deutsche Forschungsgemeinschaft.

References

1. Yang, W. P., Green, K., Pinz-Sweeney, S., Briones, A. T., Burton, D. R. & Barbas, C. F., 3rd (1995) *J. Mol. Biol.* **254**, 392-403.
2. Chen, Y., Wiesmann, C., Fuh, G., Li, B., Christinger, H. W., McKay, P., de Vos, A. M. & Lowman, H. B. (1999) *J. Mol. Biol.* **293**, 865-81.
3. Maynard, J. A., Maassen, C. B., Leppla, S. H., Brasky, K., Patterson, J. L., Iverson, B. L. & Georgiou, G. (2002) *Nat. Biotechnol.* **20**, 597-601.
4. Wu, H., Pfarr, D. S., Tang, Y., An, L. L., Patel, N. K., Watkins, J. D., Huse, W. D., Kiener, P. A. & Young, J. F. (2005) *J. Mol. Biol.* **350**, 126-44.
5. Kusnezow, W. & Hoheisel, J. D. (2002) *Biotechniques Suppl.* **14**, 14-23.
6. Northrup, S. H. & Erickson, H. P. (1992) *Proc. Natl. Acad. Sci. USA* **89**, 3338-42.
7. Maynard, J. & Georgiou, G. (2000) *Annu. Rev. Biomed. Eng.* **2**, 339-76.
8. Plückthun, A., Schaffitzel, C., Hanes, J. & Jermutus, L. (2000) *Adv. Protein Chem.* **55**, 367-403.
9. Schwesinger, F., Ros, R., Strunz, T., Anselmetti, D., Güntherodt, H. J., Honegger, A., Jermutus, L., Tiefenauer, L. & Plückthun, A. (2000) *Proc. Natl. Acad. Sci. USA* **97**, 9972-7.
10. Schier, R., Bye, J., Apell, G., McCall, A., Adams, G. P., Malmqvist, M., Weiner, L. M. & Marks, J. D. (1996) *J. Mol. Biol.* **255**, 28-43.
11. Chen, G., Dubrawsky, I., Mendez, P., Georgiou, G. & Iverson, B. L. (1999) *Protein Eng.* **12**, 349-56.
12. Boder, E. T., Midelfort, K. S. & Wittrup, K. D. (2000) *Proc. Natl. Acad. Sci. USA* **97**, 10701-5.
13. van den Beucken, T., Pieters, H., Steukers, M., van der Vaart, M., Ladner, R. C., Hoogenboom, H. R. & Hufton, S. E. (2003) *FEBS Lett.* **546**, 288-94.
14. Graff, C. P., Chester, K., Begent, R. & Wittrup, K. D. (2004) *Protein Eng. Des. Sel.* **17**, 293-304.

15. Zahnd, C., Spinelli, S., Luginbühl, B., Amstutz, P., Cambillau, C. & Plückthun, A. (2004) *J. Biol. Chem.* **279**, 18870-7.
16. Friguet, B., Chaffotte, A. F., Djavadi-Ohanian, L. & Goldberg, M. E. (1985) *J. Immunol. Methods* **77**, 305-19.
17. Nieba, L., Krebber, A. & Plückthun, A. (1996) *Anal. Biochem.* **234**, 155-65.
18. Schier, R., McCall, A., Adams, G. P., Marshall, K. W., Merritt, H., Yim, M., Crawford, R. S., Weiner, L. M., Marks, C. & Marks, J. D. (1996) *J. Mol. Biol.* **263**, 551-67.
19. Neuert, G., Albrecht, C., Pamir, E. & Gaub, H. E. (2006) *FEBS Lett.* **580**, 505-9.
20. Hanes, J., Jermutus, L., Weber-Bornhauser, S., Bosshard, H. R. & Plückthun, A. (1998) *Proc. Natl. Acad. Sci. USA* **95**, 14130-5.
21. Bell, G. I. (1978) *Science* **200**, 618-27.
22. Evans, E. & Ritchie, K. (1999) *Biophys. J.* **76**, 2439-47.
23. Friedsam, C., Wehle, A. K., Kühner, F. & Gaub, H. E. (2003) *J. Phys. Condens. Matter* **15**, S1709-S1723.
24. Krebber, A., Bornhauser, S., Burmester, J., Honegger, A., Willuda, J., Bosshard, H. R. & Plückthun, A. (1997) *J. Immunol. Methods* **201**, 35-55.
25. Bothmann, H. & Plückthun, A. (1998) *Nat. Biotechnol.* **16**, 376-80.
26. Blank, K., Morfill, J. & Gaub, H. E. (2006) *ChemBioChem in press*.
27. Butt, H. J. & Jaschke, M. (1995) *Nanotechnology* **6**, 1-7.
28. Hugel, T. & Seitz, M. (2001) *Macromol. Rapid Commun.* **22**, 989-1016.
29. Oesterhelt, F., Rief, M. & Gaub, H. E. (1999) *New J. Phys.* **1**, 6.1-6.11.
30. Honegger, A. & Plückthun, A. (2001) *J. Mol. Biol.* **309**, 657-70.
31. Jimenez, R., Salazar, G., Yin, J., Joo, T. & Romesberg, F. E. (2004) *Proc. Natl. Acad. Sci. USA* **101**, 3803-8.
32. Sarikaya, M., Tamerler, C., Jen, A. K., Schulten, K. & Baneyx, F. (2003) *Nat. Mater.* **2**, 577-85.
33. Holliger, P., Prospero, T. & Winter, G. (1993) *Proc. Natl. Acad. Sci. USA* **90**, 6444-8.
34. Kühner, F. & Gaub, H. E. (2006) *Polymer* **47**, 2555-2563.

Figures

Figure 1

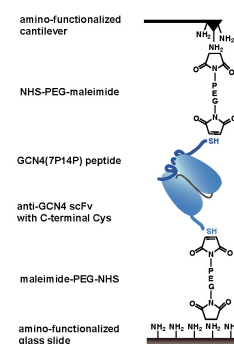


Figure 1. Experimental setup. The antibody fragments possessing a C-terminal cysteine were covalently immobilized onto amino-functionalized glass slides using a hetero-bifunctional poly(ethylene glycol) spacer. The same coupling chemistry was used for the immobilization of the peptide to the cantilever.

Figure 2

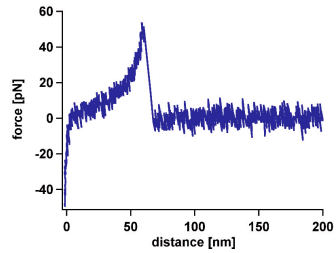


Figure 2. Example of a typical force-extension curve. The force-extension curve shows the rupture event of the antibody C11-peptide complex, experimentally recorded at a retract velocity of 1000 nm/s. The values for the rupture force, rupture length and corresponding loading rate were obtained from these force-extension curves.

Figure 3

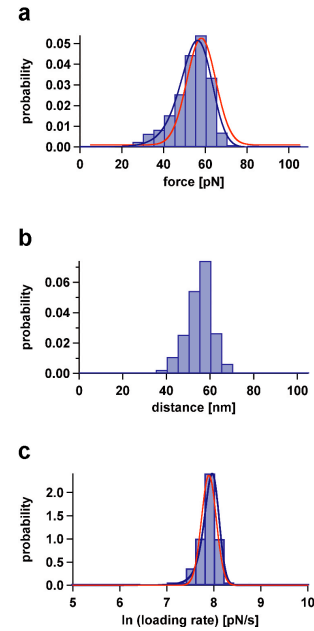


Figure 3. Example of the obtained rupture force, length and loading rate distributions.

(a) Rupture force histogram of the antibody C11-peptide complex. The rupture force histogram contains 859 rupture events and was fitted with a Gaussian curve (red). Additionally, the obtained rupture force distribution was compared with the calculated probability density function $p(F)$ (dark blue) with $\Delta x = 0.9$ nm and $k_{off} = 2 \cdot 10^{-3}$ s $^{-1}$ as described above. To consider the detection noise, the probability density function $p(F)$ was convolved with a Gaussian distribution. The standard deviation of the Gaussian distribution equals the typical noise value of the used cantilever (34). Within the experimental error the values for Δx and k_{off} are identical for both analysis methods (experimental data received from the first

analysis method is shown in figure 6). (b) Rupture length histogram of the antibody C11-peptide complex. (c) Logarithmic loading rate histogram of the antibody C11-peptide complex. The logarithmic loading rate histogram was fitted with a Gaussian curve (red). Additionally, the obtained logarithmic loading rate distribution was compared with the calculated probability density function $p(F)$ (dark blue).

Figure 4

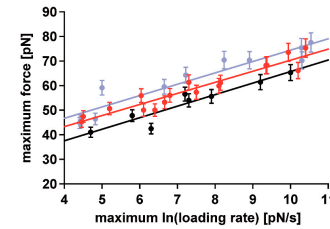


Figure 4. Diagram showing the most probable rupture force F_{\max} against the logarithm of the appropriate loading rate for all three antibody-peptide complexes. Each data point in the diagram represents the maximum rupture force F_{\max} , gained from the Gaussian fit to the rupture force distribution and the logarithm of the appropriate loading rate, gained from a Gaussian fit to the logarithmic loading rate distribution. The black data points correspond to the antibody C11-peptide complex. These data points were fitted with a straight line. From this linear fit a $\Delta x = (0.88 \pm 0.12)$ nm and a $k_{\text{off}} = (3.9 \pm 5.7) \cdot 10^{-3} \text{ s}^{-1}$ were obtained. The blue data set was measured for the forced dissociation of the antibody C11L34-peptide complex. From the linear fit a $\Delta x = (0.90 \pm 0.10)$ nm and a $k_{\text{off}} = (4.9 \pm 7.2) \cdot 10^{-4} \text{ s}^{-1}$ were achieved. Finally, the antibody 52SR4-peptide complex, pictured with red data points and the red linear fit gained a $\Delta x = (0.92 \pm 0.07)$ nm and a $k_{\text{off}} = (8.2 \pm 7.9) \cdot 10^{-4} \text{ s}^{-1}$.

Table 1

Summary of the binding constants of the different clones

clone	mutations	Δx in nm	k_{off} in s^{-1} (AFM)	k_{off} in s^{-1} (SPR)
C11	none	0.88 ± 0.12	$(3.9 \pm 5.7) \cdot 10^{-3}$	$2 \cdot 10^{-3}$
C11L34	L42 (N→S)	0.90 ± 0.10	$(4.9 \pm 7.2) \cdot 10^{-4}$	$3 \cdot 10^{-4}$
52SR4	L13 (T→S) L42 (N→S) L107 (A→V) L135 (N→D) H30 (S→L)	0.92 ± 0.07	$(8.2 \pm 7.9) \cdot 10^{-4}$	$1.5 \cdot 10^{-4}$

P2

Force induced DNA slippage

F. Kühner, J. Morfill, R. Neher, K. Blank and H. E. Gaub

Biophysical Journal (2006) submitted

Force induced DNA slippage

Ferdinand Kühner*, Julia Morfill*, Richard A. Neher[†], Kerstin Blank* and Hermann E. Gaub*

*Lehrstuhl for Applied Physics and Center for NanoScience, Ludwig-Maximilians Universität München, Munich, Germany; [†]Arnold Sommerfeld Center for Theoretical Physics and Center for Nanoscience, Ludwig-Maximilians Universität München, Munich, Germany

ABSTRACT DsDNA containing repetitive sequences displays richer dynamics than heterogeneous sequences. In the genome the number of repeat units of repetitive sequences, known as microsatellites, may vary during replication by DNA slippage and their expansion gives rise to serious disorders. We studied the mechanical properties of repetitive DNA using dynamic force-spectroscopy and found striking differences compared with ordinary sequences. Repetitive sequences dissociate at lower forces and elongate above a certain threshold force. This yield force was found to be rate dependent. Following the rapid stretching of the DNA-duplex, the applied force relaxes by stepwise elongation of this duplex. Conversely, contraction of the DNA-duplex can be observed at low forces. The stepwise elongation and shortening is initiated by single slippage events and single-molecule experiments might help to explain the molecular mechanisms of microsatellites formation. In addition to the biological importance, the remarkable properties of repetitive DNA can be useful for different nano-mechanical applications.

INTRODUCTION

DNA represents a popular building block for the assembly of nanoscale structures and devices (1). Despite the fact that the structure and dynamics of DNA were extensively studied, many of the discovered intra-molecular processes with complex dynamics and distinct biological function still lack satisfactory explanation. Microsatellites formation and bulge loop propagation in repetitive sequences are prominent examples (2). Two complementary DNA strands with a heterogeneous sequence, can only bind in a well-defined, unique conformation. Thermodynamic fluctuations lead to excitations in the double stranded DNA, which result in fast opening and closing of short stretches of base pairs (3, 4). These fluctuations remain localized and do not propagate.

In contrast, double stranded DNA, containing short repetitive sequences, so-called microsatellites, displays a more complex dynamic behavior (5-9) with potential applications in nanotechnology. Two complementary strands can hybridize in a number of different conformations in which sufficiently long stretches are aligned to build up thermodynamically stable structures. Rapid transitions between these different conformations may occur. This bulge loop formation and propagation (see Fig. 1) is called DNA slippage. It is considered to play a central role in the evolution of microsatellites, which can be found throughout the genome (10).

The repeat units of these microsatellites usually consist of one to six bases e.g. $(A)_N$, $(GT)_N$ or $(GTT)_N$. The corresponding length of the microsatellites, i.e. the number of consecutive identical repeat units N , changes rapidly in evolution, presumably due to DNA slippage events during replication. Because of this length variability, the microsatellites are frequently used as genetic markers e.g. for forensic purposes, or to determine the genetic similarity between different populations. On the other hand, certain human neurodegenerative diseases, such as fragile X or Huntington, are related to expansions of trinucleotide repeats of microsatellites beyond certain thresholds (11).

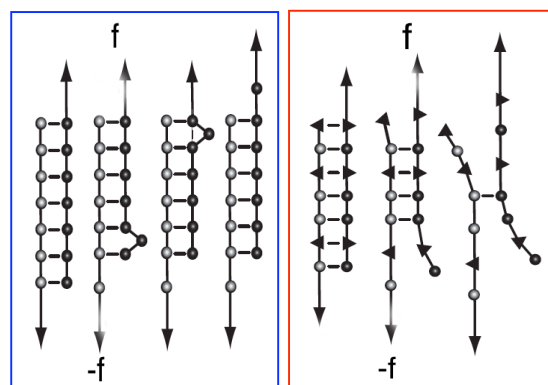


FIGURE 1. Comparison of the behavior of repetitive (left) and heterogeneous (right) DNA sequences under an externally applied force. Repetitive DNA sequences can form bulge loops. These bulge loops can propagate to the other end of the DNA duplex and therefore cause a lengthening of the molecule. In contrast, this dissociation path is not available for heterogeneous DNA sequences. Heterogeneous DNA sequences simply dissociate in an all or none mode.

DNA slippage has been studied *in vitro* (2, 12). It could be shown that DNA bulge loop formation at the end of the duplex occurs on a time-scale of microseconds. As a result, the two strands can be shifted relative to each other by the propagation of a bulge loop towards the other end of the duplex (comp. Fig. 1). In recent years, single molecule techniques have been successfully used to study the mechanical properties of single DNA molecules. For example, the elasticity (13-16) and unzipping of lambda phage DNA (17, 18), the interactions between proteins and double stranded DNA (19, 20) and the dissociation forces of short DNA duplexes (21, 22) have been measured using different experimental setups. Recently, a theoretical work suggested to study DNA slippage using an atomic force microscope (AFM) (23): The two complementary strands of a DNA duplex with a repetitive sequence are predicted to move relative to each other if the externally applied force exceeds a threshold force, the critical slipping force f_c . The rate of this motion of the two DNA strands relative to each

other is determined by the diffusion of bulge loops from one end to the other, see Fig. 1. The critical force f_c is given by the simplified relation

$$(1) \quad f_c = \frac{\epsilon_b}{2l_s - l_d}$$

,where ϵ_b is the binding free energy of one repeat unit, l_s is the effective length of one unit when unbound and stretched by the force f and l_d the length of the hybridized repeat unit. For a tri-nucleotide (GTT) the base pairing energy is $\epsilon_b \approx 7-8k_B T$, the length of three base pairs in the duplex is $l_d \approx 1$ nm and the effective length of three single stranded bases is $l_s \approx 1.5$ nm. Inserting these values in equation (1) a critical force f_c of roughly 20 pN can be predicted. The slipping process can be characterized with the following parameters: the slipping rate, which describes the speed of the movement of the bulge loops along the DNA duplex; the slipping length, which describes the length increase or decrease, which is determined by the number of bases in one repeat unit; the critical slipping force, which describes the threshold for the appearance of slipping.

Here we report on an investigation of the response of short DNA duplexes to an externally applied shear force and compare these repetitive sequences with heterogeneous sequences with respect to their slipping rate, slipping length and slipping force with the intent to test the concept of bulge loop mediated elongation. The dependence of the dynamics on the number of repeat units and the number of bases in one repeat unit is investigated.

RESULTS

For the AFM experiments, the complementary DNA strands were covalently anchored via poly(ethylene glycol) (PEG) spacers. One strand was bound to the surface of a glass slide (24) and the complementary strand was coupled to the cantilever tip, respectively (25).

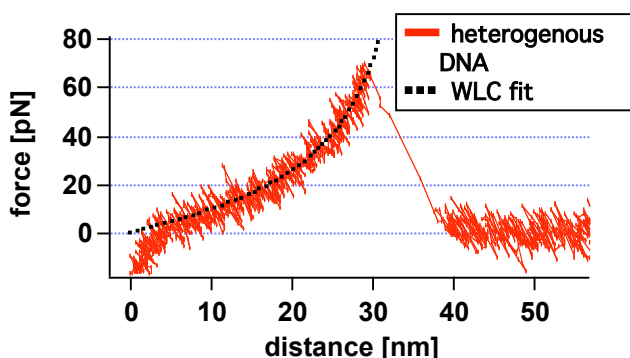


FIGURE 2. Example of a force-extension curve of a heterogeneous DNA duplex. While retracting the cantilever from the surface the polymer spacer and the DNA duplex are set under stress. The elastic behavior of the polymer-DNA duplex is well described by the WLC fit (black dashed line). At a force of 62 pN the double stranded DNA dissociates and the cantilever drops back to its relaxed state.

In all experiments the slide was approached with the tip of the cantilever, allowing the two single strands to hybridize and form a duplex. Subsequently, the cantilever was retracted and the DNA duplex was loaded with a gradually

increasing force until it finally ruptured and the cantilever relaxed back into its equilibrium position. The force applied to the DNA duplex via the PEG spacers was recorded as a function of the distance between the cantilever tip and the surface (Figure 2). This curve could be fitted with the Worm Like Chain (WLC) model, which describes the enthalpic and entropic behavior of polymers under an applied force (26).

Since most biologically relevant interactions are comparable in strength to thermal energies, force-induced processes such as the separation of receptor–ligand systems or in our case here DNA duplexes are fluctuation-assisted processes (27). The distribution of the unbinding forces is therefore significantly broadened (28). At a given force rate and at a fixed bond energy, a shift of the histograms directly reflects the difference in the effective width of the binding potentials (29, 30) and indicates different unbinding pathways in the energy landscape.

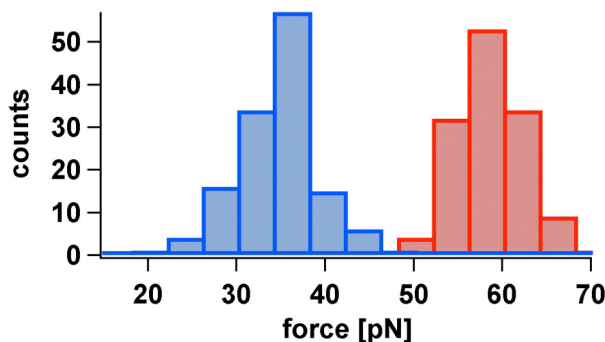


FIGURE 3. Histograms of the unbinding forces of DNA duplexes with a heterogeneous $(X)_{30}$ and a repetitive $(GT)_{15}$ sequence measured at similar pulling speeds. The duplex with the repetitive sequence dissociates at markedly lower forces, although it has the same binding energy as the one with the heterogeneous sequence. The force distribution of the repetitive DNA is truncated at a force of 40 pN. This gives evidence for an additional unbinding path, which is favored by the externally applied force.

To investigate, whether DNA duplexes with repetitive sequences have different unbinding pathways and therefore show different unbinding forces than those with heterogeneous sequences, both kinds of systems were analyzed. Figure 3 shows the resulting distributions of the rupture forces of a heterogeneous and a repetitive DNA sequence $(GT)_{15}$ recorded at approximately the same pulling speed. Although both sequences have similar thermodynamic properties, which correlate mainly with the GC content of the sequence, their rupture force distributions differ drastically. The histogram for the repetitive DNA sequence (blue) is shifted towards lower dissociation forces and is truncated for forces higher than 40 pN. We conclude, that an additional dissociation path is available for the repetitive sequence. Note that the repetitive sequence might also bind fractional and therefore result in lower dissociation forces. But without an additional unbinding path this effect would lead to a broadened force distribution containing also higher forces similar to those of the heterogeneous sequence.

Having established, that repetitive DNA has characteristics, which are absent in heterogeneous sequences, two repetitive sequences with a different number of bases per repeat

unit were compared with a heterogeneous sequence. Studying the unbinding mechanism of $(GTT)_{10}$ and $(GT)_{15}$ should reveal a more detailed insight in the unbinding mechanism.

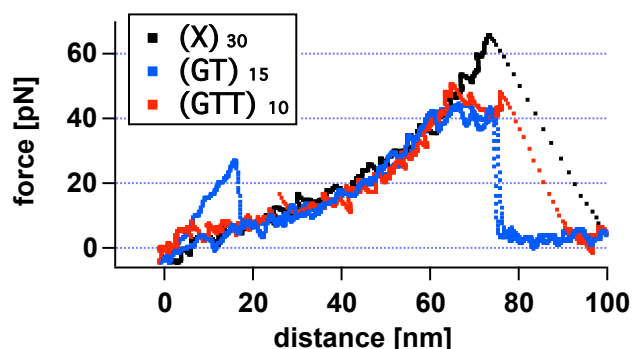


FIGURE 4. Force-extension curves for a heterogeneous $(X)_{30}$ and the repetitive $(GT)_{15}$ and $(GTT)_{10}$ sequences. In contrast to the force-extension curve of the heterogeneous DNA sequence, which follows the WLC behavior, the repetitive DNA duplexes elongate at a force (slipping force) of about 35-40 pN before they finally dissociate (rupture force).

The theoretically predicted unbinding path represents a stepwise elongation of the repetitive DNA duplex by moving both strands against each other (compare figure 1), as soon as the externally applied force exceeds a certain threshold (critical slipping force f_c). Such an elongation can indeed be observed in the recorded force-extension curves. Figure 4 shows several typical force-extension curves obtained for both the repetitive and the heterogeneous DNA sequence. From this data it is evident, that force-extension curves for repetitive DNA deviate from the WLC behavior at forces above 40 pN, whereas the curves for heterogeneous DNA follow the WLC fit up to much higher forces. Apparently, the repetitive DNA gets elongated at forces between 35 pN and 40 pN. In the following we will use the expression 'slipping' force for the value of the applied force beyond which the DNA duplex starts to slip or creep.

While the results described above, show further proof that repetitive sequences slip, the following experiment was carried out to examine the dependence of the slipping process on the length of the elementary repeat unit and the number of repeats. These experiments were carried out using $(GTT)_{10}$, $(GT)_{10}$ and $(GT)_{15}$ sequences. These DNA duplexes were probed at different pulling speeds because the slipping forces are expected to be speed dependent. As they differ only by a few pN, each data set was recorded with one cantilever to avoid calibration errors. In figure 5 the maxima of the slipping force distributions are plotted against the pulling speed of the cantilever. As can be seen in this figure, the slipping force shows a weaker dependence on the pulling speed for di-nucleotide than for tri-nucleotide repeat units. Furthermore, the slipping forces are lower for the shorter repetitive sequence $(GT)_{10}$ than for the sequence containing 15 repeat units. Close to the critical force f_c ,

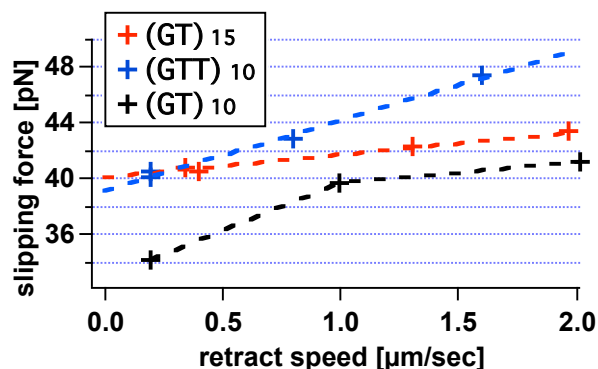


FIGURE 5. Pulling speed dependence of the slipping forces for different repetitive DNA sequences¹. The maximum of the slipping force is plotted against the pulling speed of the cantilever. The slipping force is dependent on the pulling speed and shows a linear time dependency as a first approximation.

theory predicts, that the slipping velocity $v(f)$ increases linearly with force. We therefore expanded the velocity and neglected higher order terms according to $v(f)=dv/df \cdot (f-f_c)$. The variable $u_0 = dv/df$ represents the effective slipping mobility, which depends on the microscopic slipping rate and the number of repeat units, f_c is the critical force and f the externally applied force. In our experiments, we correlated the slipping velocity v with the retract speed of the cantilever and measured the resulting slipping force.

From a linear fit, we achieve a slipping mobility u_0 of 580 nm/s-pN for a di-nucleotide and 250 nm/s-pN for a tri-nucleotide sequence. This is in agreement with the theoretical predictions and with bulk experiments that observed faster expansions for shorter repeat units. To form a bulge loop in a di-nucleotide sequence, fewer base pairs have to open up than in a tri-nucleotide sequence and hence the rate to create these defects is smaller for longer repeat units. However the additional length increase per step for longer repeat units does not compensate the lower rate.

The experimental results so far confirm that repetitive DNA strands can slide against each other and that the slipping force can be determined for different pulling speeds. The values obtained for the slipping mobility are in good agreement with theoretical predictions. However, the time resolution in an usual force-extension measurement is not sufficient to see individual steps, which would give direct evidence of the stepwise microscopic sliding mechanism.

Initial force clamp (31) measurements (data not shown) performed with the AFM showed only a lengthening of the different DNA duplexes at forces of 35-40 pN, but failed to resolve the expected individual steps. Therefore, a new measurement protocol was implemented, whose time resolution is limited only by the relaxation of the cantilever. These measurements were carried out as follows: i) The cantilever was lowered, to allow the DNA to hybridize and form a duplex. ii) The cantilever was gradually retracted from the surface allowing a certain force, well below the slipping force, to build up. iii) Then in one step, the cantilever was retracted additional 3-7 nm away from the sur-

¹ To avoid spring calibration errors every data set for one sequence is performed in a single experiment with the same cantilever.

face. As a result of this distance jump, the force acting on the DNA duplex rises almost instantaneously to a new higher value. Initially, the contour length, which gives the total length under force, does not change. If, in response, the DNA duplex elongates through slipping, an increase of the contour length is observed. In addition, the applied force drops, which can be detected by the cantilever.

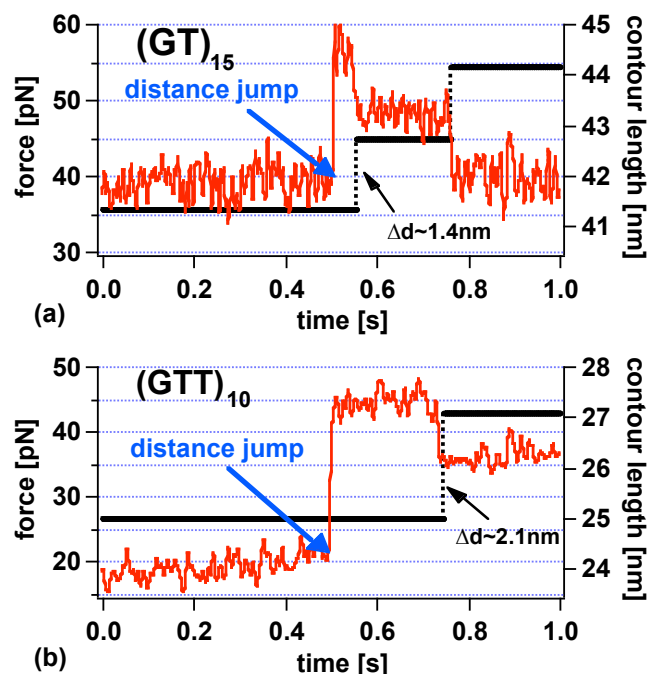


FIGURE 6. Force versus time (red) and contour length versus time curve (black) of repetitive $(GT)_{15}$ and $(GTT)_{10}$ DNA duplexes, held initially at a force under the critical slipping force. After 0.5 seconds a distance jump of the cantilever was performed resulting in a force step above the critical force, but leaves the contour length of the molecule constant. In figure (a) the contour length of the GT-DNA complex relaxes in two discrete elongation steps and the force acting on the duplex drops below the critical slipping force. In figure (b) the contour length (black curve) of the GTT-DNA complex elongates in one discrete step and the force drops under the critical slipping force.

Figure 6 (a) shows two curves, force versus time and distance versus time, for a 15 times repetitive di-nucleotide DNA duplex $(GT)_{15}$ recorded with the measurement protocol described above. First, the force acting on the DNA molecule is fluctuating around 38 pN, a value close to the previously observed slipping force. At the blue arrow in the force-time graph a 4 nm distance jump was performed. As a result of the distance jump the force (red) increases to nearly 57 pN, but the contour length stays constant. Within a fraction of a second the measured force decreases to a value below 40 pN in discrete steps. The final force is again close to the observed slipping force. This rapid and discrete decrease of the force can only be explained through the stepwise lengthening of the DNA molecule, compensating the performed distance jump. These observations show, that a single relaxation process increases the contour length of the di-nucleotide DNA system by approximately 1.4 ± 0.3 nm which can be well explained by sliding of one repeat unit ($dl = 2l_s - l_d = 4 \cdot 0.5 \text{ nm} - 2 \cdot 0.34 \text{ nm} = 1.4 \text{ nm}$). Regrettably, only a limited number of steps may be observed, since the probability to hold these DNA du-

plexes under such a high force for a long time is very low and decreases further with every step.

Figure 6 (b) shows the equivalent experiment for a trinucleotide $(GTT)_{10}$ sequence. As expected, the contour length increase of approximately 2.1 ± 0.3 nm is higher than for the dinucleotide sequence. Analogous experiments performed with the heterogeneous sequence did not show any discrete steps (data not shown).

To exclude the possibility, that the observed steps are artifacts of multiple binding the following arguments are pointed out. First of all the overall elasticity of the measured PEG polymer spacer would be much stiffer. Secondly the presumption of three bound molecules in parallel mimicking the three steps of the single molecule shown in figure 5 would require the respective PEG polymer spacers to differ in length by less than 2 nm. This would mean that the total force acting on the cantilever would be distributed on three duplexes and as a consequence the lifetime for the duplexes would be much longer than our experimental findings. Dissociation of one duplex increases the split force applied to the remaining duplexes and reduces their lifetime drastically. For this reason multiple binding as potential artifact can be excluded with very high certainty.

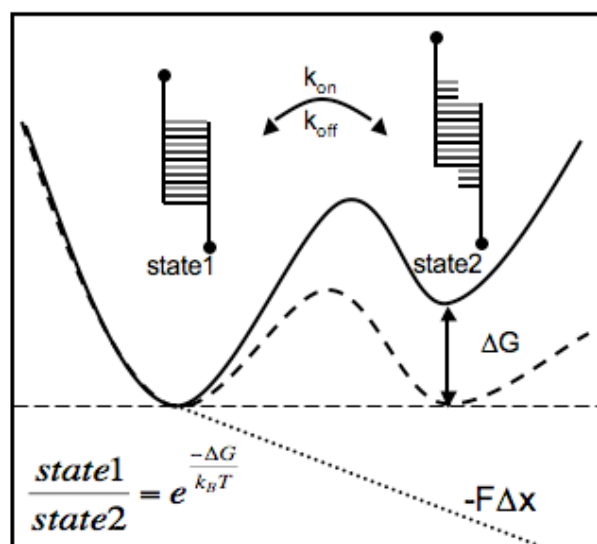


FIGURE 7. Gibbs free energy of a two state system under external force. The model describes the completely bound and the first lengthened state of a repetitive DNA duplex. The potential is tilted by an externally applied force. This results in an levelling of the energy of the two states, allowing the DNA duplex to fluctuate between the two states in equilibrium.

Having shown that all characteristic parameters describing the slipping process can be determined experimentally, we wanted to obtain more detailed information on how the system behaves near the critical force. The system for the native and elongated conformation of the DNA duplex can be described with a two state potential illustrated in figure 7. Application of an external force allows the tuning of the potential, so that the Gibbs free energy of these two states is the same as shown by the dashed line in figure 7. If this force equals the critical force f_c the system can fluctuate in equilibrium. This was achieved in the measurement shown in figure 8. Using the above mentioned measurement protocol a distance jump is performed and the force on the DNA duplex first increases over the critical force

limit f_c . As a result the DNA duplex elongates and the force drops to the critical force. At this force the system starts to perform multiple back and forward slipping events. An additional distance jump forces the DNA duplex in its elongated conformation until it finally ruptures completely. These fluctuations of the DNA duplex between the two states can be analyzed with random telegraph noise analysis similar to ion channel recordings (black curve in figure 8). The hidden Markovian process is characterized by the transition rates from one state to the other (32). The data trace shown in figure 8 exhibits mean lifetimes of 0.031 s for the elongated and 0.022 s for the shortened state. The energy difference of these two states is fluctuating between the binding energy of the DNA duplex and the bending energy of the cantilever. Although, the energy was found to be $\sim 7k_B T$, which is close to well-established values of about $\sim 8k_B T$ for a tri-nucleotide GTT repeat unit. The observed multiple forward and backward jumps in figure 8 could only be detected with short polymer spacers with lengths between 15 and 20 nm. A possible reason for this finding could be that the fluctuations of the cantilever allow the duplex to form a bulge loop at lower forces, which eventually diffuses to the other end. For longer spacers these fluctuations are averaged by the elasticity of the polymer (33). The alternative scenario, that the observed shortening is a simple transient bulge loop formation at the stretched end can be ruled out, since the lifetime of these bulge loops, even if they travel some steps into the molecule is orders of magnitude too small to explain the observed frequencies.

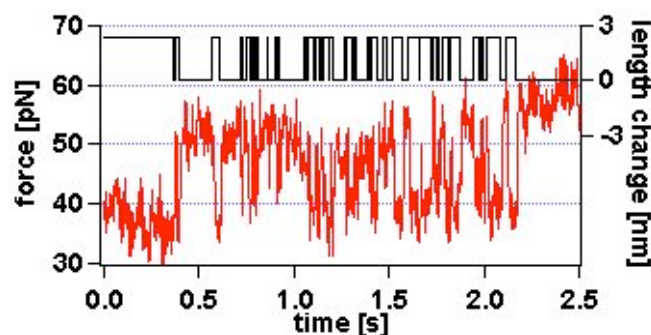


FIGURE 8. Example for the slipping of the DNA duplex between the elongated and the short state. A repetitive $(GTT)_{10}$ DNA duplex is held at a constant force analogous to figure 6. A distance jump drives the force over the critical force limit. This results in a lengthening of the DNA duplex and the force drops to the critical force. Consequently, the duplex lengthens and shortens by forward and backward slipping. The measured time trace (red) of the fluctuation process was analyzed with a telegraph noise algorithm to extract the dynamics of the length changes (black). The mean lifetimes were found to be 0.031 seconds for the fully hybridized state and 0.022 seconds for the lengthened state.

Discussion

The data presented here show that repetitive DNA duplexes elongate under an applied shear force and dissociate at forces of about 38 pN^2 , which is significantly lower than for heterogeneous DNA sequences. This is due to an additional unbinding path that allows the repetitive DNA du-

plex to increase its contour length without having to overcome a large free energy barrier. It should be pointed out that this unbinding path is energetically not favored over other paths but gets populated by force.

The theoretically predicted length increase takes place through discrete slipping steps. It could be shown that the resulting length increase of the whole DNA duplex is consistent with the length increase obtained by shifting both strands of di- and trinucleid sequences by one repeat unit. Slippage is faster, for shorter repeat units and smaller repeat numbers. This is consistent with the theory of bulge loop diffusion, since the expected slipping velocity decreases with the energy needed to produce a bulge loop. In addition, the diffusion of a bulge loop through the molecule is faster for shorter duplexes. The mechanism of relative strand motion caused by the creation, diffusion and absorption of bulge loop defects is similar to defect propagation in crystal lattices.

The critical slipping force determined in the measurements is larger than the theoretically predicted critical force f_c . This could be due to the small number of repeat units used in the experiments and to the simplistic model used for the theory. For instance, deformations and conformational changes in the backbone of the DNA duplex resulting from an externally applied force are not included in the model.

The slipping velocity is expected to scale inversely with the number of repeat units. This prediction could not be unambiguously confirmed, since only rather short sequences were available. Further experiments are necessary to quantify the dependence of slipping dynamics on the repeat number and flanking sequences. More detailed experiments will shed some light on the kinetics of the processes involved in expansion of microsatellites during replication. Because of its bi-directional property DNA slippage itself, is not the cause for the asymmetric increase effect of repeat units in the human genome.

Besides the biological importance of repetitive sequences, the remarkable properties of repetitive DNA might also be useful for different nano-mechanical applications (34-36). Since, the rupture force distribution for repetitive sequences is truncated sharply at forces close to 40 pN, repetitive DNA could serve as a programmable force sensor, with a threshold force that can be fine tuned by sequence composition. Adjustable viscoelastic buildingblocks in DNA self-assembly structures can be realized with repetitive sequences.

Furthermore, the relaxation of a large force to a critical force f_c with a time constant that can be chosen through length and sequence composition, could be used as a length independent force normal. Conversely, if extended, repetitive double stranded DNA contracts until the force f_c is built up, if the initial force is below f_c . Complementary repetitive single stranded DNA could therefore be applied for self-tightening connections in nanostructures. After initial hybridization, two single strands tend to maximize their overlap, i.e. the number of base pairs, until a tension of the order of the critical force f_c is built up. These adjustable induced force locations establish completely new features in nanoscale structures.

² Because of the possibility of fractional binding for repetitive sequences lower dissociation forces are possible in regular force distance curves (see figure 2).

We thank Ulrich Gerland and Stefan Thalhammer for helpful discussions and Steffen Mihatsch for help in data analysis. This study was supported by the German Science Foundation DFG and by the Fond der Chemischen Industrie.

MATERIALS AND METHODS

Oligonucleotides modified with a thiol-group at the 5'-terminus (for details see table 1; IBA GmbH, Göttingen, Germany; metabion GmbH, Martinsried, Germany) were immobilized on amino-functionalized surfaces using a hetero-bifunctional poly(ethylene glycol) (PEG) spacer. One oligonucleotide was immobilized on the cantilever and the complementary sequence was coupled to the surface. The cantilevers (Bio-lever, Olympus, Tokio, Japan) were cleaned and functionalized (37). Instead of epoxy-functionalized cantilevers, amino-modified surfaces on the cantilevers were prepared using 3-Aminopropyl-dimethylethoxysilane (ABCR GmbH, Karlsruhe, Germany). Commercially available amino functionalized slides (Slide A, Nexterion, Mainz, Germany) were used.

DNA duplex	sequence (cantilever)	sequence (slide)
(X) ₂₀	5'SH-TTTTTTTTTTTTTTTTTTTCG TTGGTGGCGGATACTCGGTAGTGGG ATACGACGATACCGAAGACAGCTCAT GTATAATATG-3'	5'SH-TTTTTTTTTTATCCCACTA CCGAGATATCCGCACCAACG-3'
(GT) ₁₀	5'SH-TTTTTTTTTTGTGTGTGTG TGTGTGTGTGT-3'	5'SH-TTTTTTTTTTACACACACAC ACACACACACA-3'
(GT) ₁₂	5'SH-TTTTTTTTTTGTGTGTGTG TGTGTGTGTGTGTGTGTGT-3'	5'SH-TTTTTTTTTTACACACACAC ACACACACACACACACAC-3'
(GGT) ₁₀	5'SH-TTTTTTTTTTGGTGGTGG TGGTGGTGGTGGTGGT-3'	5'SH-TTTTTTTTTTACCACCAAC ACCACCAACCACCAACC-3'

TABLE 1 DNA sequences

From this step on, the surfaces of cantilever and slide were treated in parallel as described in Blank et al. They were incubated in borate buffer pH 8.5 for one hour. This step was necessary to deprotonate the amino groups for coupling to the N-hydroxysuccinimide groups (NHS) of the heterobifunctional NHS-PEG-maleimide (MW 5000 g/mol; Nektar, Huntsville, Alabama). The PEG was dissolved in a concentration of 50 mM in borate buffer at pH 8.5 and incubated on the surfaces for one hour. In parallel, the oligonucleotides were reduced using TCEP beads (Perbio Science, Bonn, Germany) in order to generate free thiols. After washing with ultra pure water, a solution of the oligonucleotides (1,75 µM) was incubated on the surfaces for one hour. Finally, the surfaces were rinsed with PBS (phosphate buffered saline) to remove non-covalently bound oligonucleotides and stored in PBS until use.

REFERENCES

- Seeman, N. C. (2003) *Nature* **421**, 427-431.
- Schlotterer, C. & Tautz, D. (1992) *Nucl. Acids Res.* **20**, 211-215.
- Altan-Bonnet, G., Libchaber, A. & Krichevsky, O. (2003) *Physical Review Letters* **90**.
- Neher, R. A. & Gerland, U. (2006) *Physical Review E* **73**.
- Lyer, R. R., Pluciennik, A., Burdett, V. & Modrich, P. L. (2006) *Chemical Reviews* **106**, 302-323.
- Heidenfelder, B. L., Makhov, A. M. & Topal, M. D. (2003) *Journal of Biological Chemistry* **278**, 2425-2431.

- Karthikeyan, G., Chary, K. V. R. & Rao, B. J. (1999) *Nucleic Acids Research* **27**, 3851-3858.
- Levinson, G. & Gutman, G. A. (1987) *Molecular Biology and Evolution* **4**, 203-221.
- Trinh, T. Q. & Sinden, R. R. (1991) *Nature* **352**, 544-547.
- Li, Y. C., Korol, A. B., Fahima, T. & Nevo, E. (2004) *Molecular Biology and Evolution* **21**, 991-1007.
- Schlotterer, C. (2000) *Chromosoma* **109**, 365-371.
- Porschke, D. (1974) *Biophysical Chemistry* **2**, 83-96.
- Smith, S. B., Cui, Y. J. & Bustamante, C. (1996) *Science* **271**, 795-799.
- Perkins, T. T., Quake, S. R., Smith, D. E. & Chu, S. (1994) *Science* **264**, 822-826.
- Rief, M., Clausen-Schaumann, H. & Gaub, H. E. (1999) *Nature Structural Biology* **6**, 346-349.
- Cui, S., Albrecht, C., Kühner, F. & Gaub, H. E. (2006) *J. Am. Chem. Soc.* **128**, 6636-6639.
- EssevazRoulet, B., Bockelmann, U. & Heslot, F. (1997) *Proceedings of the National Academy of Sciences of the United States of America* **94**, 11935-11940.
- Lubensky, D. K. & Nelson, D. R. (2002) *Physical Review E* **65**.
- Friedsam, C., Wehle, A. K., Kühner, F. & Gaub, H. E. (2003) *Journal of Physics-Condensed Matter* **15**, S1709-S1723.
- Kühner, F., Costa, L. T., Bisch, P. M., Thalhammer, S., Heckl, W. M. & Gaub, H. E. (2004) *Biophysical Journal* **87**, 2683-2690.
- Krautbauer, R., Rief, M. & Gaub, H. E. (2003) *Nano Letters* **3**, 493-496.
- Strunz, T., Oroszlan, K., Schafer, R. & Güntherodt, H. J. (1999) *Proc Natl Acad Sci U S A* **96**, 11277-82.
- Neher, R. A. & Gerland, U. (2004) *Physical Review Letters* **93**, 8102-8102.
- Moiseev, L., Unlu, M. S., Swan, A. K., Goldberg, B. B. & Cantor, C. R. (2006) *Proceedings of the National Academy of Sciences of the United States of America* **103**, 2623-2628.
- Blank, K., Morfill, J. & Gaub, H. E. (2006) *ChemBioChem* published online **26 July 2006**.
- Oesterhelt, F., Rief, M. & Gaub, H. E. (1999) *New Journal of Physics*, 6-6.
- Evans, E. & Ritchie, K. (1997) *Biophys J* **72**, 1541-55.
- Friedsam, C., Wehle, A. K., Kühner, F. & Gaub, H. E. (2003) *Journal of Physics: Condensed Matter*, S1709-S1723.
- Evans, E. (2001) *Annu Rev Biophys Biomol Struct* **30**, 105-28.
- Heymann, B. & Grubmüller, H. (2000) *Physical Review Letters* **84**, 6126-6129.
- Oberhauser, A. F., Hansma, P. K., Carrion-Vazquez, M. & Fernandez, J. M. (2001) *Proc Natl Acad Sci U S A* **98**, 468-72.
- Venkataramanan, L. & Sigworth, F. J. (2002) *Biophysical Journal* **82**, 1930-1942.

33. Kühner, F. & Gaub, H. (2006) *Polymer* **47**, 2555-2563.
34. Neher, R. A. & Gerland, U. (2005) *Biophysical Journal* **89**, 3846-3855.
35. Albrecht, C., Blank, K., Lalic-Mülthaler, M., Hirler, S., Mai, T., Gilbert, I., Schiffmann, S., Bayer, T., Clausen-Schaumann, H. & Gaub, H. E. (2003) *Science* **301**, 367-370.
36. Simmel, F. C. & Dittmer, W. U. (2005) *Small* **1**, 284-299.
37. Neuert, G., Albrecht, C., Pamir, E. & Gaub, H. E. (2006) *Febs Letters* **580**, 505-509.

P3

Site-Specific Immobilization of Genetically Engineered Variants of *Candida antarctica* Lipase B

K. Blank, J. Morfill and H. E. Gaub

ChemBioChem, published online 26 July 2006

DOI: 10.1002/cbic.200600198

Site-Specific Immobilization of Genetically Engineered Variants of *Candida antarctica* Lipase B

Kerstin Blank, Julia Morfill, and Hermann E. Gaub^{*[a]}

The immobilization of proteins on solid surfaces has been a topic of intensive research for many years. Numerous methods have been developed to immobilize proteins for bioseparation, biosensors, diagnostic tests and single-molecule experiments.^[1] With the growing need for miniaturization and parallelization, new methods are needed for the immobilization of proteins with high functional density and specificity.^[2,3] Most of the methods used so far do not allow the covalent immobilization of a protein at a well-defined position. In this study, cysteines, introduced by genetic engineering, have been used for site-specific immobilization of a model enzyme to a glass surface by means of a heterobifunctional poly(ethylene glycol) (PEG) spacer.^[4] While PEG is used for a broad range of applications to render surfaces protein resistant,^[5–7] only a few reports describe its use as a linker for attaching proteins to surfaces.^[8–13] However, the use of a heterobifunctional PEG spacer would provide a protein-resistant surface displaying reactive groups for the covalent attachment of proteins in a controlled manner. In addition, the coupling of PEG to proteins has been shown to increase the stability of the protein and maintain it in an active conformation.^[14]

To evaluate the usefulness of this concept, *Candida antarctica* lipase B (CalB; EC 3.1.1.3) was used as a model enzyme.^[15] CalB is an industrially important lipase that is used for various applications in bioorganic synthesis.^[16] It is a 35 kDa monomer with three disulfide bridges. CalB has been immobilized on surfaces for various applications, but these methods are mainly based on the adsorption of hydrophobic or charged amino acids to supports.^[17] Site-specific immobilization of lipases would be advantageous because it has been shown that the properties of lipases depend on their orientation on a surface.^[18] In this study, mutants of CalB have been prepared that display a free cysteine at a defined position on the molecule

(Figure 1). Based on recent results obtained for the expression of CalB in *Escherichia coli*,^[19] one mutant has been produced that contains an additional cysteine at the C terminus of the protein after the His tag (CalB-HisGGC). The other mutant is based on the results of Velonia et al.^[20] who were able to selectively reduce one disulfide bond (Cys293–Cys311) on the surface of the protein. In the following step, the reduced cysteines were used to couple the protein to polystyrene. Since there is no way to control which cysteine is reacting with the maleimide-functionalized polystyrene, another approach was performed in this study here: Cys311 was replaced by alanine (CalB-C311A-His) to leave only one free cysteine for coupling. In addition, an N-terminal FLAG tag was attached to the lipase variants for detection purposes.

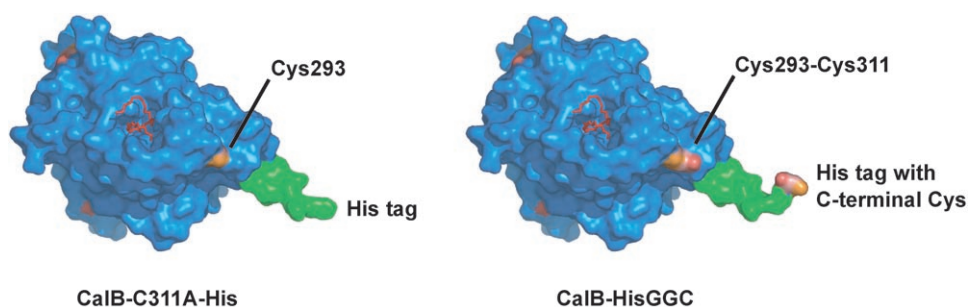


Figure 1. Mutants of the lipase CalB (PDB ID: 1LBT) possessing one free cysteine for the oriented coupling of the enzyme to surfaces. For CalB-C311A-His, one cysteine from a disulfide bridge on the surface of CalB was mutated to alanine. CalB-HisGGC contains an additional cysteine at the C terminus.

The mutants and an unmodified CalB containing a C-terminal His tag (CalB-His) were expressed in *E. coli* at 25 °C, as described previously.^[19] The expression levels of the mutants were compared with the unmodified enzyme by Western blot analysis by using two different antibodies (Figure S1). The free cysteines reduce the yield of the functionally expressed lipase by approximately a factor of 10. This effect is known for the expression of other proteins containing free cysteines in the periplasm of *E. coli*.^[21] The different lipase variants were purified from periplasmic extracts by using Ni²⁺-NTA columns. A washing step with 1 mM Tris(2-carboxyethyl)phosphine hydrochloride (TCEP) was included to remove all impurities that might have coupled to the free cysteine during expression and preparation of the cell extracts.^[22] The eluted fraction was dialyzed against coupling buffer (50 mM sodium phosphate, pH 7.2, 50 mM NaCl and 10 mM EDTA) and concentrated afterwards. The purity was analyzed by using reducing and nonreducing SDS-PAGE (Figure S2). Pure enzymes can be obtained after just one chromatography step. The purification procedure yields a certain amount of dimers, which is dependent on the position of the free cysteine on the molecule. Finally, the activity of the variants was measured by using the substrate *para*-nitrophenol butyrate. The tests showed that neither the additional cysteine at the C terminus nor the mutated disulfide bridge has any significant influence on the specific activity and the kinetic constants of CalB (Table S1).

Before the CalB variants were coupled to the surface, the proteins were reduced by using TCEP beads in order to gener-

[a] K. Blank, J. Morfill, Prof. Dr. H. E. Gaub
Lehrstuhl für Angewandte Physik and Center for Nanoscience
LMU München
Amalienstrasse 54, 80799 München (Germany)
Fax: (+49) 89-2180-2050
E-mail: hermann.gaub@physik.uni-muenchen.de

Supporting information for this article is available on the WWW under <http://www.chembiochem.org> or from the author.

ate free thiols. In parallel, amino-functionalized slides were incubated with borate buffer (pH 8.5). This step was necessary to deprotonate the amino groups for coupling to the *N*-hydroxy-succinimide groups (NHS) of the heterobifunctional NHS-PEG-maleimide ($M_w = 3400 \text{ g mol}^{-1}$), which was used as spacer for the immobilization of the CalB variants. The PEG was dissolved at a concentration of 50 mM in borate buffer and incubated on the surface for 1 hour. After the surfaces had been washed with ultrapure water, the CalB variants were spotted on them. A sample containing a 10000-fold excess of free cysteine was spotted as a negative control. In addition, these spotting solutions were prepared with nonreduced enzyme variants. After the spotted protein solutions had been incubated on the surface for 1 hour, the density of the immobilized CalB variants was detected by using an anti-FLAG antibody. The activity of the immobilized lipase variants was tested by using agar plates containing Tween 80 and CaCl_2 . The slide was put upside down on the agar plates and incubated on the plates overnight.

Both enzyme variants possessing the free cysteine could be immobilized to the maleimide-activated surfaces in an oriented and functional way (Figure 2). The binding of CalB-HisGGC and CalB-C311A-His is highly specific. No significant binding was detected for the negative controls: CalB-His without any free cysteine shows only very little binding to the surface, and the addition of free cysteine to the spotting solution blocks the binding of the enzyme variants very efficiently. The fact that only a very low signal is detected for CalB-His proves that the enzyme variants do not bind through the cysteines of the disulfide bridges, which might be reduced during incubation with the TCEP beads. The immobilization density of CalB-HisGGC is much higher than that of CalB-C311A-His. As the preparation of CalB-HisGGC contains a higher number of dimers, we conclude that the cysteine is much more accessible if it is located at the C terminus. In this case, the His tag serves as a spacer between the surface of the protein and the reactive cysteine. The image of the activity test with the Tween 80 plate shows an identical pattern. This corroborates the hypothesis that both enzyme variants are immobilized on a surface in an active conformation.

The use of PEG as a spacer for the oriented and covalent immobilization of proteins to surfaces yields very good ratios of specific to nonspecific binding. This method can be applied to every material for which amino groups can be generated by silanization or other procedures. Here, we have used a lipase as a model system to prove the applicability of this procedure. The site-specific immobilization of CalB represents a good basis for the optimization of reaction conditions. Because each enzyme is immobilized in the same orientation it should display identical characteristics. In addition, this method may be used for many other biomolecules such as oligonucleotides, peptides and other proteins. If the introduction of a cysteine is not possible by genetic engineering, then thiol groups can be introduced by chemical modification.^[23] However, the attachment of a cysteine to the C terminus of a protein is a very general strategy that can be employed for a variety of different proteins. An expression vector can be constructed that con-

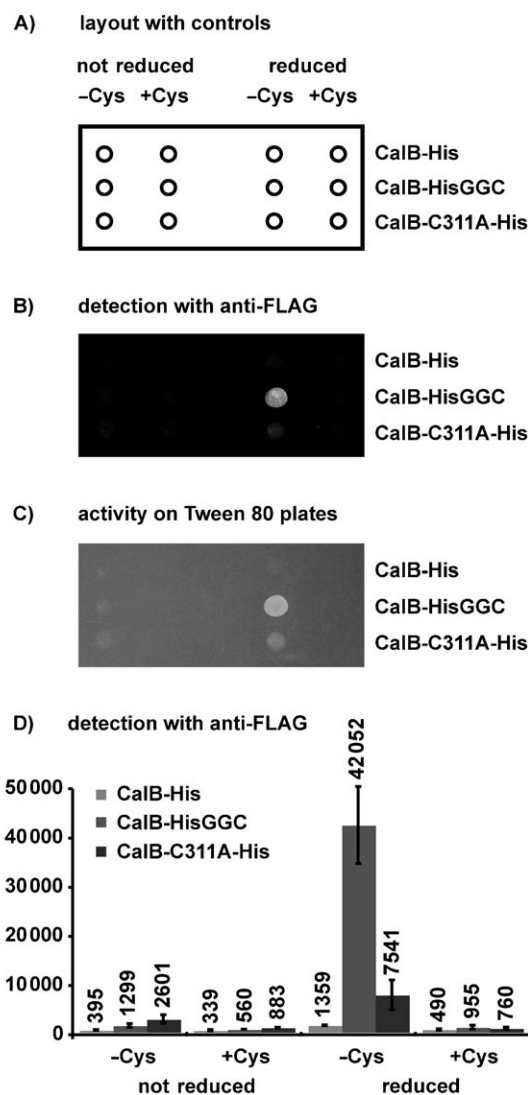


Figure 2. A) Schematic of the position of the different spots on the slide. Each enzyme variant was spotted with or without reduction and in a buffer with or without an excess of free cysteine. B) Fluorescence scan of the bound anti-FLAG antibody showing the density of the enzyme variants on the surface. C) Photograph of the Tween 80 agar plate showing the activity of the enzyme variants on the surface. D) Summary of the immobilization density detected with the anti-FLAG antibody (mean of three different slides).

tains the sequence of the His tag, the two glycines and the cysteine, thus allowing convenient cloning of the proteins of interest. Therefore, as no modification of the protein itself is necessary, the strategy is particularly useful if many different proteins need to be immobilized in parallel.

Acknowledgements

The authors thank Novozymes A/S for the gift of the calB gene, A. Plückthun for pAK400, K. Gottschalk for the help in preparing the figures and E. Puchner, H. Gump, T. Nicolaus, M. Skjot, A. Svendsen, N. Hatzakis and A. E. Rowan for helpful discussions.

This work was supported by the European Union and the Deutsche Forschungsgemeinschaft.

Keywords: CalB · immobilization · poly(ethylene glycol) · protein engineering · surface chemistry

- [1] L. Cao, *Carrier-Bound Immobilized Enzymes*, Wiley-VCH, Weinheim, **2005**.
- [2] K. Y. Tomizaki, K. Usui, H. Mihara, *ChemBioChem* **2005**, *6*, 782–799.
- [3] I. Sialaff, A. Arnold, G. Godin, S. Tugulu, H. A. Klok, K. Johnsson, *ChemBioChem* **2006**, *7*, 194–202.
- [4] M. J. Roberts, M. D. Bentley, J. M. Harris, *Adv. Drug Delivery Rev.* **2002**, *54*, 459–476.
- [5] S. I. Jeon, J. H. Lee, J. D. Andrade, P. G. Degennes, *J. Colloid Interface Sci.* **1991**, *142*, 149–158.
- [6] "Poly(ethylene glycol) Chemistry and Biological Applications", S. J. Sofia, E. W. Merrill, *ACS Symp. Ser.* **1997**, *680*, 342–360.
- [7] N. A. Alcantar, E. S. Aydil, J. N. Israelachvili, *J. Biomed. Mater. Res.* **2000**, *51*, 343–351.
- [8] J. Piehler, A. Brecht, R. Valiokas, B. Liedberg, G. Gauglitz, *Biosens. Bioelectron.* **2000**, *15*, 473–481.
- [9] C. D. Hodneland, Y. S. Lee, D. H. Min, M. Mrksich, *Proc. Natl. Acad. Sci. USA* **2002**, *99*, 5048–5052.
- [10] C. Albrecht, K. Blank, M. Lalic-Mülthaler, S. Hirler, T. Mai, I. Gilbert, S. Schiffmann, T. Bayer, H. Clausen-Schaumann, H. E. Gaub, *Science* **2003**, *301*, 367–370.
- [11] K. Blank, T. Mai, I. Gilbert, S. Schiffmann, J. Rankl, R. Zivin, C. Tackney, T. Nicolaus, K. Spinnler, F. Oesterhelt, M. Benoit, H. Clausen-Schaumann, H. E. Gaub, *Proc. Natl. Acad. Sci. USA* **2003**, *100*, 11 356–11 360.
- [12] G. L. Zhen, V. Eggli, J. Voros, P. Zammaretti, M. Textor, R. Glockshuber, E. Kuennemann, *Langmuir* **2004**, *20*, 10464–10473.
- [13] G. Neuert, C. Albrecht, E. Pamir, H. E. Gaub, *FEBS Lett.* **2006**, *580*, 505–509.
- [14] L. Cao, *Curr. Opin. Chem. Biol.* **2005**, *9*, 217–226.
- [15] J. Uppenberg, N. Ohrner, M. Norin, K. Hult, G. J. Kleywegt, S. Patkar, V. Waagen, T. Anthonsen, T. A. Jones, *Biochemistry* **1995**, *34*, 16838–16851.
- [16] E. M. Anderson, K. M. Larsson, O. Kirk, *Biocatal. Biotransform.* **1998**, *16*, 181–204.
- [17] T. Nakaoki, Y. Mei, L. M. Miller, A. Kumar, B. Kalra, M. E. Miller, O. Kirk, M. Christensen, R. A. Gross, *Ind. Biotechnol.* **2005**, *1*, 126–134.
- [18] J. M. Palomo, G. Muñoz, G. Fernández-Lorente, C. Mateo, M. Fuentes, J. M. Guisan, R. Fernández-Lafuente, *J. Mol. Catal. B* **2003**, *21*, 201–210.
- [19] K. Blank, J. Morfill, H. Gump, H. E. Gaub, *J. Biotechnol.* **2006**, published on-line 19th May 2006.
- [20] K. Velonia, A. E. Rowan, R. J. M. Nolte, *J. Am. Chem. Soc.* **2002**, *124*, 4224–4225.
- [21] K. Blank, P. Lindner, B. Diefenbach, A. Plückthun, *Protein Expression Purif.* **2002**, *24*, 313–322.
- [22] E. M. K. Hedin, S. A. Patkar, J. Vind, A. Svendsen, K. Hult, P. Berglund, *Can. J. Chem.* **2002**, *80*, 529–539.
- [23] V. Grazu, O. Abian, C. Mateo, F. Batista-Viera, R. Fernández-Lafuente, J. M. Guisan, *Biotechnol. Bioeng.* **2005**, *90*, 597–605.

Received: May 9, 2006

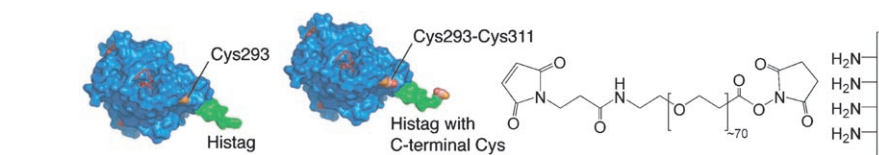
Published online on ■ ■ ■ ■, 2006

COMMUNICATIONS

K. Blank, J. Morfill, H. E. Gaub*



Site-Specific Immobilization of Genetically Engineered Variants of *Candida antarctica* Lipase B



 **Keep still!** A general strategy has been developed for the site-specific and covalent immobilization of biomolecules. The applicability of this protocol was demonstrated by using the industrially

important lipase CalB. Two mutants that possess a free cysteine (Cys293 or C-terminal) were prepared and immobilized in an active conformation at the desired position.

P4

Functional expression of *Candida antarctica* lipase B in *Escherichia coli*

K. Blank, J. Morfill, H. Gump and H. E. Gaub

Journal of Biotechnology, published online 17 May 2006



Functional expression of *Candida antarctica* lipase B in *Escherichia coli*

Kerstin Blank, Julia Morfill, Hermann Gumpp, Hermann E. Gaub*

Lehrstuhl für Angewandte Physik & Center for Nanoscience, LMU München, Amalienstrasse 54, 80799 München, Germany

Received 6 November 2005; received in revised form 24 March 2006; accepted 4 April 2006

Abstract

Candida antarctica lipase B (CalB) is an important catalyst in bio-organic synthesis. To optimize its performance, either the reaction medium is changed or the lipase itself is modified. In the latter case, mutants are generated in *Escherichia coli* and subsequently expressed in fungal hosts for their characterization. Here we present the functional expression of CalB in the periplasm of *E. coli*. By step-wise deletion of the CalB signal and propeptide we were able to express and purify two different variants of CalB (mature CalB and CalB with its propeptide). A N-terminal FLAG and a C-terminal His tag were used for the purification. For the substrates *para*-nitrophenol butyrate (*p*-NPB), *para*-nitrophenol laurate (*p*-NPL) and carboxyfluorescein diacetate (CFDA) the specific activity was shown to be similar to CalB expressed in *Aspergillus oryzae*. The kinetic constants k_M , v_{max} and k_{cat} were determined using the substrates *p*-NPB and *p*-NPL. Almost identical k_{cat}/k_M values ($0.423\text{--}0.466\text{ min}^{-1}\text{ }\mu\text{M}^{-1}$ for *p*-NPB and $0.068\text{--}0.071\text{ min}^{-1}\text{ }\mu\text{M}^{-1}$ for *p*-NPL) were obtained for the CalB variants from *E. coli* and *A. oryzae*. The results clearly show that CalB can be functionally expressed in *E. coli* and that the attachment of tags does not alter the properties of the lipase.

© 2006 Elsevier B.V. All rights reserved.

Keywords: CalB; *Candida antarctica*; Lipase activity; Periplasmic expression; Propeptide

1. Introduction

Lipases (EC 3.1.1.3) are enzymes that catalyze the hydrolysis of neutral lipids in biological systems. However many lipases have been found to catalyze a variety

of reactions, which can be very different from the reaction for which the enzyme has evolved to in nature. As these enzymes are naturally acting at an oil–water interface they are, generally, very compatible with organic solvents. Their ability to accept a wide range of substrates (lipids, sugars, alcohols, acids and esters) and their capability to maintain activity and selectivity in organic solvents has enabled their wide use as biocatalysts in industrial applications: In aqueous solvents lipases are used for hydrolyzing esters and in

* Corresponding author. Tel.: +49 89 21803172;
fax: +49 89 21802050.

E-mail address: Hermann.Gaub@physik.uni-muenchen.de
(H.E. Gaub).

organic solvents they are catalyzing the reverse reaction achieving esterification, transesterification, aminolysis or thioesterification (Anderson et al., 1998; Schmid and Verger, 1998).

Lipase B from *Candida antarctica* (CalB) (Patkar et al., 1992) is one of the most widely used biocatalysts (Anderson et al., 1998). Its structure has been resolved 1994 (Uppenberg et al., 1994, 1995). As many other lipases CalB shows the typical α/β hydrolase fold. Its active site is composed of a Ser-His-Asp catalytic triad. The active site pocket is composed of two channels. The structure of these channels is responsible for the high regio- and stereo-selectivity of CalB towards secondary alcohols (Magnusson et al., 2005). In contrast to other lipases CalB displays no interfacial activation (Overbeeke et al., 2000; Rotticci et al., 2000) and does not possess a typical lid domain (Martinelle et al., 1995; Rotticci et al., 2000).

Because of the importance of CalB in organic synthesis, especially for the kinetic resolution of racemates, numerous approaches have been used to optimize the activity, specificity, selectivity and stability of CalB. This has been achieved either by changing the microenvironment of the enzyme or by optimizing the enzyme itself using random or site-directed mutagenesis. Factors influencing the microenvironment are, for example, supports for immobilization (Fernandez-Lafuente et al., 1998), the content of water in an organic solvent (Piyatheerawong et al., 2004) or the nature of the organic solvent itself (Wescott and Klibanov, 1994; Ottosson et al., 2002). CalB mutants have been generated using site-directed mutagenesis (Patkar et al., 1997; Rotticci et al., 2001; Magnusson et al., 2005), circular permutation (Qian and Lutz, 2005) or directed evolution (Zhang et al., 2003; Suen et al., 2004; Chodorge et al., 2005).

While all cloning steps are always carried out in *Escherichia coli* screening for the desired mutants, in most cases, involves expression in the fungal hosts *Aspergillus oryzae* (Hoegh et al., 1995), *Pichia pastoris* (Rotticci-Mulder et al., 2001) or *Saccharomyces cerevisiae* (Zhang et al., 2003; Suen et al., 2004). In all cases CalB is expressed together with its own (Hoegh et al., 1995) or a host specific signal peptide (Rotticci-Mulder et al., 2001), which directs the lipase to the medium. Following the expression, the supernatant containing the lipase is analyzed for enzymatic activity. The fact that different fungal hosts are used suggests that there

have been problems in expressing CalB in *E. coli*. Only one recent report (Chodorge et al., 2005) describes the use of *E. coli* expressed CalB for a screening assay. However, the improved mutants are not purified and characterized in vitro. The possibility of using *E. coli* expressed CalB directly for screening of the mutants would greatly simplify the process of generating optimized variants. Especially the time span to get from the cloned construct to the functional test of the desired mutant would be much shorter if CalB could be expressed in a functional form in *E. coli*.

Here, we report the soluble expression of CalB in the periplasm of *E. coli*. The influence of the signal and propeptide of CalB was analyzed by sequentially removing these peptides. The possibility of attaching a N-terminal FLAG tag and a C-terminal His tag to allow the use of well-established protocols for purification and detection was investigated. Finally, the specific activity and the kinetic constants of the purified enzymes were compared with a reference sample of CalB expressed in *A. oryzae*.

2. Materials and methods

2.1. Cloning of expression plasmids

The plasmids for the periplasmic expression of CalB (Fig. 1) are based on the pAK series (Krebber et al., 1997). The plasmid pAK400, which contains a strong RBS, a pelB signal sequence and a His tag, was used. The *NcoI* site in the *cat* gene was removed and an *EcoRI* site was introduced in front of the His tag using site directed mutagenesis. Based on this plasmid (pKB3) three different constructs of CalB were cloned. The *calB* gene was amplified from a plasmid obtained from Novozymes using the following primers: For CalBSP-His the forward primer was chosen such that the signal and propeptide of CalB remain attached to the *calB* gene. For CalBP-His the primer included the sequence of the propeptide. And for CalB-His the sequence of mature CalB was amplified. All forward primers contained the sequence of a short FLAG tag (Knappik and Plückthun, 1994) and a *NcoI* site as in the original pAK400 plasmid. The forward primers had the following sequences: CalBSP_forw 5'-CATGCCATGGCGGACTACAAAGATATGAAGC TACTCTCTGACCGG-3', CalBP_forw 5'-CATG

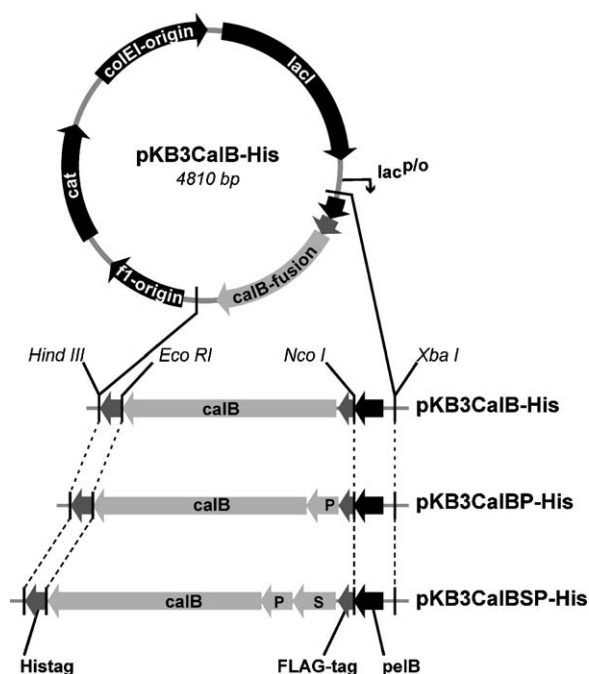


Fig. 1. Plasmids for the periplasmic expression of the different CalB variants. The plasmid is a derivative of the pAK series. It contains a *lac* promoter, the strong RBS T7G10 and the signal peptide *pelB*. After cleavage of the signal peptide the CalB variants possess a N-terminal FLAG tag in front of the respective *calB* sequence. To obtain the construct pKB3CalBSP-His the *calB* sequence was cloned together with its signal and propeptide. The construct pKB3CalBP-His only contains the propeptide in front of the *calB* sequence. For the construct pKB3CalB-His the sequence of mature CalB was cloned after the FLAG tag. All constructs contain a C-terminal His tag.

CCATGGCGGACTAGAAAGATGCCACTCCTTTG
GTGAAGC-3', CalB_forw 5'-CATGCCATGGCGG
 ACTACAAACATCTACCTTCCGGTTCCGGACC-3'
 (The *Nco*I site is underlined, the sequence of the *calB* gene is written in italics.) An identical reverse primer introducing an *Eco*RI site after the *calB* gene was used for all constructs: CalB_*Eco*RI_rev 5'-CCGGAATTCGGGGGTGACGATGCCG-3'. The PCR fragments were purified, cut with *Nco*I and *Eco*RI and cloned into the pKB3 plasmid resulting in the plasmids pKB3CalBSP-His, pKB3CalBP-His and pKB3CalB-His.

2.2. Expression of CalB variants

The plasmids encoding the three different variants of CalB were transformed in the *E. coli* K12

strain TB1 (New England Biolabs, Frankfurt, Germany). Small scale expressions for Western blot analysis were performed at 37 or 25 °C and 250 rpm using 50 ml of SB medium (20 g l⁻¹ tryptone, 10 g l⁻¹ yeast extract, 5 g l⁻¹ NaCl, 50 mM K₂HPO₄) containing 30 μg ml⁻¹ chloramphenicol. The cultures for the purification of the lipase variants were grown in 200 ml of SB medium at 25 °C and 250 rpm. These cultures were inoculated from a 20 ml preculture to OD₆₀₀ = 0.1. Expression was induced with 1 mM isopropyl-β-D-thiogalactopyranosid (IPTG) at an OD₆₀₀ between 1.0 and 1.5. The cells were harvested 3 h after induction by centrifugation at 5000 × g and 4 °C for 10 min.

2.3. Western blot analysis

The obtained cell pellets were resuspended in loading buffer (50 mM sodium phosphate pH 8.0, 300 mM NaCl, 10 mM imidazole), normalized to their end OD₆₀₀ using 2.5 ml buffer per 1 unit OD₆₀₀. Whole cell extracts were prepared by French Press lysis at 10,000 psi and 1 ml of the crude extract was centrifuged for 60 min at 16,000 × g and 4 °C. The supernatants containing the soluble proteins were transferred to a new vessel and the pellet was resuspended in 1 ml of buffer. These samples were analyzed using anti-FLAG antibody M1 (Sigma, Taufkirchen, Germany) and anti-His antibody Penta-His (Qiagen, Hilden, Germany): SDS-PAGE was carried out under reducing conditions according to standard protocols using 15% polyacrylamide gels. The proteins were transferred to a PVDF membrane (Millipore, Eschborn, Germany). For the detection with the anti-FLAG antibody the membrane was blocked with 5% bovine serum albumin (BSA) in FLAG-Ca²⁺ buffer (50 mM Tris/HCl pH 8.0, 10 mM NaCl, 1 mM CaCl₂) for 30 min. The anti-FLAG M1 antibody was diluted by a factor of 4000 in FLAG-Ca²⁺ buffer containing 0.5% BSA and 0.05% Tween 20. The membrane was incubated in this solution for 60 min followed by washing the membrane 3 × 5 min in FLAG-Ca²⁺ buffer with 0.05% Tween 20. For detection purposes the secondary rabbit anti-mouse antibody carrying a fluorescence label (Alexa Fluor 647; Invitrogen, Karlsruhe, Germany) was diluted 1:2000 in FLAG-Ca²⁺ buffer containing 0.5% BSA and 0.05% Tween 20. After shaking the membrane with this solution for 30 min, the membrane

was again washed three times with buffer. Western blots with the anti-His antibody were carried out using an Alexa Fluor 647 labeled antibody according to the manufacturer's instructions. Fluorescence images were taken using a LS300 scanner (Tecan, Crailsheim, Germany).

2.4. Two-step purification

Cell pellets were resuspended in loading buffer. After adding DNase I (Roche Diagnostics, Mannheim, Germany), cell disruption was achieved by French Press lysis. The suspension was clarified by centrifugation at maximum speed for 60 min at 4 °C and filtration through a 0.22 µm filter. This crude extract was loaded onto a Ni²⁺-NTA column (Qiagen, Hilden, Germany) equilibrated with loading buffer. The column was washed with 30 column volumes of loading buffer and 5 column volumes of a washing buffer (50 mM sodium phosphate pH 8.0, 300 mM NaCl, 30 mM imidazole). Elution was achieved by adding five column volumes of elution buffer (50 mM sodium phosphate pH 8.0, 300 mM NaCl, 200 mM imidazole). The eluted fraction was dialyzed against FLAG-Ca²⁺ buffer and loaded onto an anti-FLAG affinity column (M1 antibody; Sigma, Taufkirchen, Germany) equilibrated with the same buffer. The column was washed with 30 column volumes of FLAG-Ca²⁺ buffer. The protein was eluted by adding 10 times 2 ml of FLAG-EDTA buffer (50 mM Tris/HCl pH 8.0, 10 mM NaCl, 10 mM EDTA). Finally, the fractions containing the pure enzyme were dialyzed against assay buffer (50 mM sodium phosphate pH 7.0, 150 mM NaCl) and concentrated using Centricon YM-10 (Millipore) to a final concentration of approximately 1 mg ml⁻¹. Samples from each step were analyzed by reducing SDS-PAGE using 15% polyacrylamide gels. The actual concentration of the purified lipases was determined by measuring the absorbance at 280 nm. The extinction coefficients of the different CalB variants have been calculated using the program Vector NTI (Invitrogen). Finally, identical amounts of the lipase variants were compared to a glycosylated and deglycosylated sample of CalB from *A. oryzae* using reducing SDS-PAGE. Deglycosylation was carried out using PNGase F (New England Biolabs, Frankfurt, Germany) using the protocol supplied by the manufacturer.

2.5. Activity measurements

To compare the activity of the different CalB variants three different substrates were used: *para*-nitrophenol butyrate (*p*-NPB; Sigma, Taufkirchen, Germany), *para*-nitrophenol laurate (*p*-NPL; Sigma) and carboxyfluorescein diacetate (CFDA; Invitrogen). Before the measurements could take place, calibration curves were determined to correlate the absorbance at 405 nm (*p*-NPB and *p*-NPL) or fluorescence at 517 nm (CFDA) with the concentration of the generated product. The extinction coefficient for *para*-nitrophenol determined for the buffer used was 9100 (1 mol⁻¹ cm⁻¹). For the measurements with *p*-NPB and *p*-NPL stock solutions of the substrates were prepared with a concentration of 20 mM in isopropanol. The assay mixture contained 50 mM sodium phosphate pH 7.0, 150 mM NaCl, 0.5% Triton X-100, 5% isopropanol. The following substrate concentrations were used: 1000, 200, 80 and 50 µM. The reaction was started by adding the respective lipase to a final concentration of 100 nM. The temperature was kept constant at 25 °C. The generation of the product could be followed by measuring the increase in absorbance every 10 s for a total time of 300 s. For the CFDA measurements a 25 mM stock solution was prepared in DMSO. The assay mixture contained 50 mM sodium phosphate pH 7.0, 150 mM NaCl, 10% DMSO and 100 nM lipase. The reaction was started by adding CFDA to a final concentration of 1000 µM. Again the temperature was kept constant at 25 °C and the increase in fluorescence was measured for 300 s in time intervals of 10 s. All measurements were carried out in triplicate. Assay mixtures containing BSA instead of lipase were used as reference samples. The increase in absorbance or fluorescence of the BSA samples was subtracted from the values obtained from the lipase samples. These corrected curves were used to calculate the reaction velocity *v*, which describes the concentration of the generated product per minute.

3. Results

CalB is an extracellular protein, which contains three disulfide bonds. To allow the correct formation of these disulfide bonds in *E. coli* it is necessary to target the protein to the periplasmic space. Therefore, the *calB*

gene was cloned into an expression plasmid containing a pelB signal sequence, which is recognized from the *E. coli* transport machinery. In its natural host *Candida antarctica* CalB is expressed in form of a preproprotein. Its 18 amino acid long signal peptide targets the protein to the secretory pathway. The function of the seven amino acid long propeptide is not known yet (Hoegh et al., 1995). As nothing is known about the processing of fungal preproproteins in *E. coli* three different constructs were cloned as described before (Fig. 1): One construct contains the complete sequence of the preproprotein (CalBSP-His), the second construct misses the signal peptide (CalBP-His) and the third construct represents the sequence of the mature protein (CalB-His). In order to check if the respective peptides are still present at the N-terminus of the expressed protein the sequence of a FLAG tag was attached in front of the respective lipase sequence. In addition, the FLAG tag can be used to investigate if the protein is transported to the periplasmic space correctly (Knappik and Plückthun, 1994): Since the anti-FLAG antibody M1 only binds to the tag if the tag is located at the N-terminus, the protein can be recognized only if the pelB signal peptide is processed during transport to the periplasm. All constructs were cloned with a C-terminal His tag to allow purification and detection of the proteins.

The expression was carried out at 37 and 25 °C. At 37 °C precultures could be grown to a high density over night and the expression cultures reached an OD₆₀₀ of 1.0 after 4 h (starting at OD₆₀₀ = 0.1). At 25 °C the growth rate was much slower. The precultures needed 48 h and the expression culture had to grow over night before the culture could be induced (data not shown). In both cases the cells grew for another 3 h after the induction took place. The cells were normalized to their end OD₆₀₀ and lysed. The soluble and the insoluble fractions were analyzed on Western blots using both anti-FLAG (Fig. 2) and anti-His antibodies (data not shown). Both blots are almost identical and show one strong band of the same size indicating that the three different variants are full-length protein and that the CalB signal and propeptides are not cleaved in *E. coli*. Comparing the amount of soluble and insoluble protein at the different expression temperatures, no protein can be detected in the soluble fractions at 37 °C. In contrast, at 25 °C the soluble fractions of CalB-His and CalBP-His contain a certain amount of soluble protein, which

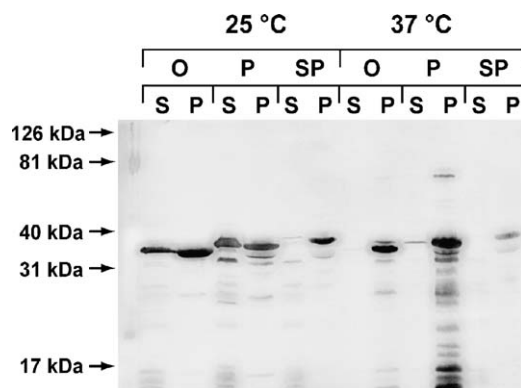


Fig. 2. Anti-FLAG blot showing the expression levels of the CalB variants at 25 and 37 °C. *E. coli* cells expressing the different CalB variants were grown at 25 and 37 °C. The cells were normalized to their end OD₆₀₀ and lysed. Soluble proteins (S) were separated from the insoluble fraction (P) by centrifugation. The insoluble fraction was resuspended in the original volume. The same volume of the soluble and the insoluble fraction was loaded onto the gel. The CalB variants contain a N-terminal FLAG tag. The blot shows one major band proving that all variants are translocated to the periplasmic space and that the CalB signal peptide and propeptide are not cleaved by the *E. coli* transport machinery. Except for CalBP-His only little degradation of the proteins occurs. For CalB-His (O) and for CalBP-His (P) soluble protein is detected at 25 °C. CalBSP-His (SP) does not show any soluble expression at this temperature. At 37 °C no soluble expression can be seen for all three variants.

equals the amount of insoluble protein. No expression can be detected for CalBSP-His.

Since CalB-His and CalBP-His are expressed as soluble proteins at 25 °C the next step was to grow larger cultures and purify these two variants of CalB. The most convenient way to purify these proteins was to make use of their His tag and FLAG tag (Fig. 3A and B). The crude extract was loaded onto a Ni²⁺-NTA column to remove most of the contaminants. After dialysis against a buffer containing Ca²⁺ the eluted fractions from the Ni²⁺-NTA column were loaded onto the anti-FLAG column. Due to the Ca²⁺ dependent binding of the M1 antibody, the protein could be eluted under mild conditions with a buffer containing EDTA. The eluted fractions contain one single band with a size of approximately 35 kDa, which refers to the size of the cloned CalB variants with the two tags. After concentrating the protein preparations, the concentrations were determined by measuring the absorbance at 280 nm. To analyze the purity of these two CalB variants, the same amount of protein was analyzed

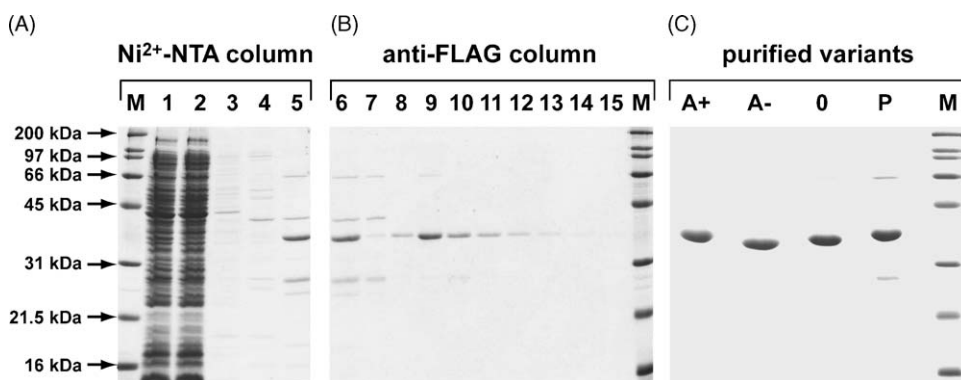


Fig. 3. SDS-PAGE showing the fractions of the two-step purification procedure for CalB-His and the purified lipase variants. (A) For the first step a Ni^{2+} -NTA column was used: 1—crude extract, 2—flow through, 3—washing with 10 mM imidazole, 4—washing with 30 mM imidazole, 5—elution with 200 mM imidazole. (B) Fraction 5 was dialyzed against FLAG- Ca^{2+} buffer, Fraction 6 shows the sample after dialysis. Fraction 6 is loaded onto an anti-FLAG affinity column in the next step. Fraction 7 represents the flow trough, fraction 8 a washing step with FLAG- Ca^{2+} buffer. Fractions 9–15 represent the eluted fractions using FLAG-EDTA buffer. Fractions 10–15 were pooled for further analysis. (C) The purity of the enzyme variants used for the activity tests (A+: CalB from *A. oryzae*, 0: CalB-His and P: CalBP-His) and of a deglycosylated sample of CalB from *A. oryzae* (A–) was compared using SDS-PAGE. The references from *A. oryzae* (A+ and A–) show only one single band. CalB-His (0) contains a very little amount of other proteins. In the preparation of CalBP-His (P) two other bands are present. The different bands show slight differences in the size of the proteins. It can be clearly seen that P is larger than the version without the propeptide (0). Comparing the size of the variants from *E. coli* (0) and *A. oryzae* (A–), CalB from *E. coli* has a higher molecular weight than the deglycosylated enzyme from *A. oryzae* since it contains a FLAG and a His tag.

by SDS-PAGE. In addition, the size was compared to glycosylated and deglycosylated CalB expressed in *A. oryzae* (Hoegh et al., 1995) without any tags (Fig. 3C). Whereas the preparation of CalB-His is almost pure, the preparation of CalBP-His contains two additional bands. As expected the variants with the attached tags expressed in *E. coli* are bigger than the deglycosylated CalB from *A. oryzae*. CalBP-His is larger than the construct without the propeptide (CalB-His) again proving that the propeptide is still attached to CalBP-His.

Using the preparations previously analyzed by SDS-PAGE the specific activities of the enzymes were determined for three different substrates (Table 1). For CalB from *A. oryzae* the glycosylated enzyme was used. To determine the specific activities the reaction velocities v at the highest substrate concentration (1000 μM) were

divided by the amount of enzyme in the reaction mixtures. For all three substrates similar specific activities were obtained for CalB-His and CalB from *A. oryzae*. The specific activity of CalBP-His is a factor of 1.2 lower for all three substrates. This might refer to this particular preparation, which contains a few contaminating proteins. The specific activities for *p*-NPB and *p*-NPL have an error of approximately 10% of the measured value. The error for CFDA is much higher. This is due to the fast auto-hydrolysis of the substrate, which competes with the enzyme-catalyzed reaction.

Therefore, the kinetic constants for the different enzyme variants have been measured only for *p*-NPB and *p*-NPL (Fig. 4). Here the reaction velocity was plotted against the substrate concentration. The data was fitted with the Michaelis-Menten equation to obtain

Table 1
Specific activities of the different CalB variants

	Specific activity <i>p</i> -NPB ($\mu\text{mol min}^{-1} \text{mg}^{-1}$)	Specific activity <i>p</i> -NPL ($\mu\text{mol min}^{-1} \text{mg}^{-1}$)	Specific activity CFDA ($\text{nmol min}^{-1} \text{mg}^{-1}$)
<i>Aspergillus</i>	10.52 ± 1.07	0.936 ± 0.136	1.69 ± 0.37
<i>E. coli</i> CalB	10.57 ± 0.28	0.941 ± 0.075	1.58 ± 0.85
<i>E. coli</i> CalBP	8.75 ± 0.24	0.746 ± 0.048	1.30 ± 0.73

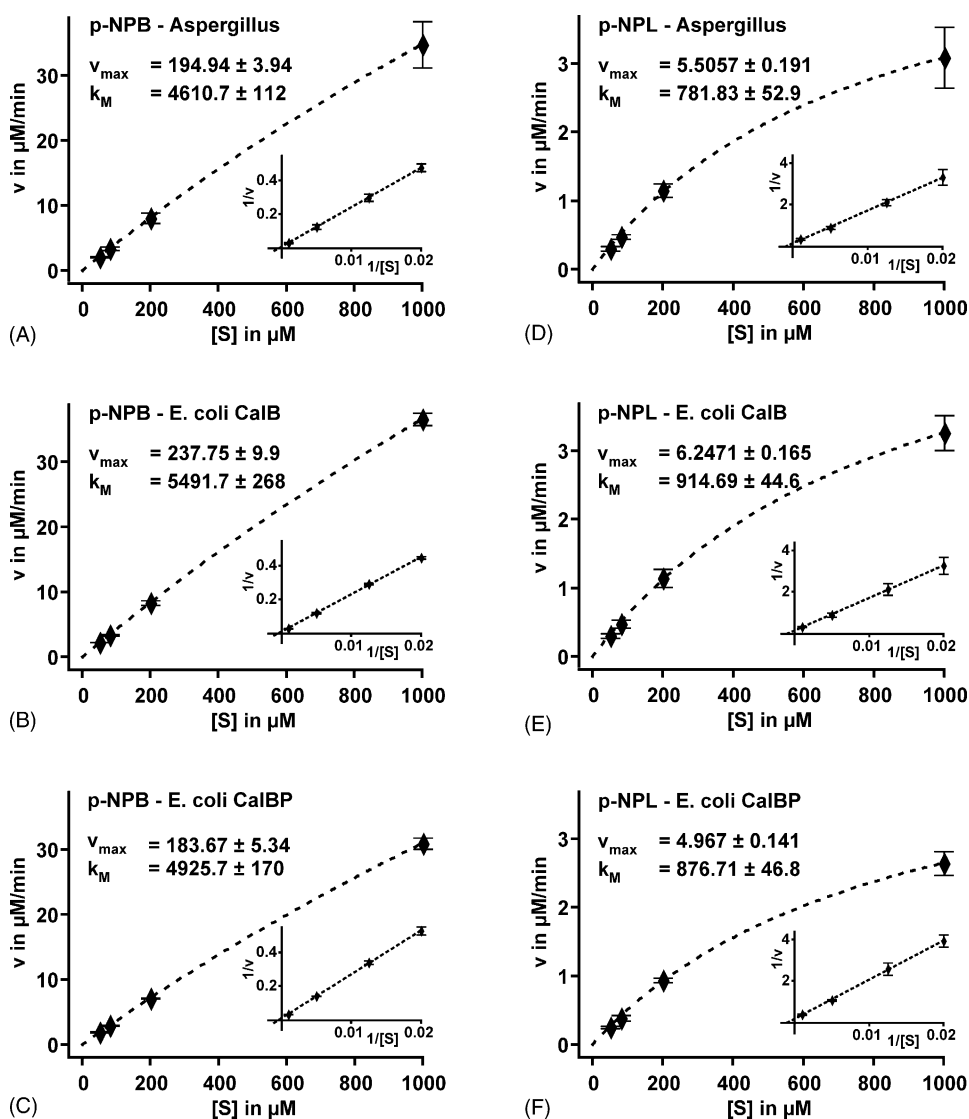


Fig. 4. Michaelis–Menten and Lineweaver–Burk plots for the *p*-NPB and *p*-NPL substrates. The big plots show the Michaelis–Menten plots for the different substrates and enzyme variants. The points (◆) show the measured values with their standard deviation. The dashed line (---) represents the fit using the Michaelis–Menten equation. The small plots show the corresponding Lineweaver–Burk plots. The linearity of the Lineweaver–Burk plots proves that the hydrolysis of the substrates is a first order reaction and therefore the data can be fitted with the Michaelis–Menten equation to obtain the values for v_{\max} and k_M . For *p*-NPB (A, B, C) as a substrate the values for v_{\max} and k_M differ only slightly for the different enzyme variants. This also applies for the substrate *p*-NPL (D, E, F).

the Michaelis–Menten constant k_M and v_{\max} . To determine whether the enzymatic hydrolysis of the different substrates is a first order reaction, the data was analyzed with the Lineweaver–Burk plot. For both substrates, the three different enzyme variants show a straight line in the Lineweaver–Burk plot proving that the reaction is a

first order reaction and therefore the achieved data can be fitted with the Michaelis–Menten equation. Other lipases, which are interfacially activated, do not follow a first order reaction with the *p*-NPL substrate under similar reaction conditions (Redondo et al., 1995). k_{cat} and the specificity constant k_{cat}/k_M were calculated

Table 2
Summary of kinetic constants of the different CalB variants

Substrate	Enzyme	v_{\max} ($\mu\text{M min}^{-1}$)	k_M (μM)	k_{cat} (min^{-1})	k_{cat}/k_M ($\text{min}^{-1} \mu\text{M}^{-1}$)
<i>p</i> -NPB	<i>Aspergillus</i>	194	4612	1949	0.423
	<i>E. coli</i> CalB	237	5492	2378	0.433
	<i>E. coli</i> CalBP	183	4930	2298	0.466
<i>p</i> -NPL	<i>Aspergillus</i>	5.51	781	55.1	0.070
	<i>E. coli</i> CalB	6.25	915	62.5	0.068
	<i>E. coli</i> CalBP	4.97	877	62.1	0.071

based on the obtained values for k_M and v_{\max} (Table 2). Having a more detailed look at the data one can see that all constants are in the same range for the different enzyme variants. The specificity constant is the same for all three different enzymes.

4. Discussion

The data clearly shows that CalB can be functionally expressed in *E. coli*. The strategy of lowering the expression temperature from 37 to 25 °C (Baneyx and Mujacic, 2004) yields soluble and functional protein for CalB with or without the propeptide. These variants of CalB from *E. coli* show identical catalytic activity compared with the enzyme from *A. oryzae*. This indicates that the structures of their active sites are the same. In addition, tags can be attached to the N-terminus and to the C-terminus without changing the properties of the enzyme. These tags can be used for detection and purification of the enzyme.

Although CalB has been the subject of intensive research, the function of some important structural features is still not known. The propeptide, as has been shown for proteases (Wiederanders et al., 2003) and the lipase of *Rhizopus oryzae* (Beer et al., 1998), can act as an inhibitor or assist in folding of the protein into its native state. The experiments, which are presented here, could not detect a difference between the variants with and without the propeptide. This data and the fact that propeptides involved in folding are normally much larger (Beer et al., 1998; Wiederanders et al., 2003) lead to the conclusion that the propeptide is not involved in folding. The construct lacking the propeptide can also fold into a native and active conformation. However, for the lipase from *R. oryzae* it has been shown that the enzyme with the propeptide has improved fold-

ing kinetics and a higher stability. We cannot eliminate the possibility of similar contributions of the propeptide since in vitro unfolding and refolding experiments would be necessary to obtain more detailed information. Furthermore, an inhibitory effect of the propeptide principally cannot be excluded since the construct used in this study does not possess the original propeptide because of the presence of the FLAG tag. Based on the data presented here, no conclusion can be drawn about the function of the propeptide. This also applies to the glycosylation. CalB from *E. coli* lacks the glycosylation. However, no difference in the enzymatic activity can be seen compared to the glycosylated enzyme from *A. oryzae*.

Further on it also remains unclear if the enzyme is active within *E. coli*. In the other expression systems used CalB is secreted to the culture medium. In *E. coli* the lipase remains inside the cell and could in principle degrade lipids in *E. coli*. This does not seem to be the case since no difference in growth can be seen when the lipase is expressed in soluble or insoluble form (data not shown). Other lipases possess a lid, which shields the active site from the solvent in an aqueous environment. During contact with a hydrophobic interface, the lipase undergoes a conformational change and the active site becomes accessible. In contrast, CalB does not have a typical lid domain and does not show interfacial activation (Overbeeke et al., 2000; Rotticci et al., 2000). However, Velonia et al. (2005) could show that one enzyme can exist in catalytically active and catalytically inactive conformations. The question if CalB only exists in an inactive conformation in *E. coli* and if this is actively regulated is going beyond the scope of this study.

Having a more detailed look at the kinetic constants for the different substrates, one can see that CalB has a higher specificity constant for *p*-NPB, a short fatty

acid chain. This result is in contrast to other reports in the literature. A similar specificity for C₄ (*p*-NPB) and C₁₂ (*p*-NPL) fatty acid chains was observed in cyclohexane (Garcia-Alles and Gotor, 1998). Another report describes a preference for fatty acid chains longer than 10 carbon atoms in hexane (Kirk et al., 1992). Since the specificity of the enzyme is dependent on the solvent no conclusion can be drawn from these findings. Probably, the reaction rates for different substrates are not only a matter of specificity of the enzyme but also depend on the solubility of the substrate in the respective solvent. The solubility of the substrate is a critical point for the activity tests, which were performed. The range of concentrations is limited by the detection limit of the generated product and by the solubility of the substrate in the reaction buffer.

The possibility of expressing CalB in *E. coli* opens up new ways for screening and rational design of improved variants. For example, by using phage display (Danielsen et al., 2001; Fernandez-Gacio et al., 2003) a higher number of mutants can be screened in order to obtain the desired molecule. The use of phage display would in addition circumvent the drawback that CalB is expressed intracellularly in *E. coli*. Furthermore, the possibility to make fusion proteins will allow numerous new options for the immobilization of the enzyme. Especially methods for directed immobilization will make the optimization of reaction conditions more reliable since the enzyme will always be immobilized in the same orientation with the active site pointing away from the immobilization matrix. Directed immobilization will also be an important tool for single molecule studies of the enzyme, which can gain further insights of the mechanism how CalB switches between the active and inactive conformations.

Acknowledgements

The authors thank Novozymes A/S for the gift of the *calB* gene and purified CalB from *Aspergillus*, Andreas Plückthun for the gift of pAK400, Angelika Kardinal for dedicated initial work to this project, Elias Punchner, Michael Skjot, Allan Svendsen, Nikos Hatzakis and Alan Rowan for helpful discussions as well as Gregor Neuert for critically reading the manuscript. This work was supported by the European Union and the Deutsche Forschungsgemeinschaft.

References

- Anderson, E.M., Larsson, K.M., Kirk, O., 1998. One biocatalyst—many applications: The use of *Candida antarctica* B-Lipase in organic synthesis. *Biocatal. Biotransform.* 16, 181–204.
- Baneyx, F., Mujacic, M., 2004. Recombinant protein folding and misfolding in *Escherichia coli*. *Nat. Biotechnol.* 22, 1399–1408.
- Beer, H.D., McCarthy, J.E.G., Bornscheuer, U.T., Schmid, R.D., 1998. Cloning, expression, characterization and role of the leader sequence of a lipase from *Rhizopus oryzae*. *Biochim. Biophys. Acta* 1399, 173–180.
- Chodorge, M., Fourage, L., Ullmann, C., Duvivier, V., Masson, J.M., Lefevre, F., 2005. Rational strategies for directed evolution of biocatalysts—Application to *Candida antarctica* lipase B (CALB). *Adv. Synth. Catal.* 347, 1022–1026.
- Danielsen, S., Eklund, M., Deussen, H.J., Graslund, T., Nygren, P.A., Borchert, T.V., 2001. In vitro selection of enzymatically active lipase variants from phage libraries using a mechanism-based inhibitor. *Gene* 272, 267–274.
- Fernandez-Gacio, A., Uguen, M., Fastrez, J., 2003. Phage display as a tool for the directed evolution of enzymes. *Trends Biotechnol.* 21, 408–414.
- Fernandez-Lafuente, R., Armisen, P., Sabuquillo, P., Fernandez-Lorente, G., Guisan, J.M., 1998. Immobilization of lipases by selective adsorption on hydrophobic supports. *Chem. Phys. Lipids* 93, 185–197.
- Garcia-Alles, L.F., Gotor, V.V., 1998. Alcohol inhibition and specificity studies of lipase B from *Candida antarctica* in organic solvents. *Biotechnol. Bioeng.* 59, 163–170.
- Hoegh, I., Patkar, S., Halkier, T., Hansen, M.T., 1995. 2 Lipases from *Candida antarctica*—cloning and expression in *Aspergillus oryzae*. *Can. J. Bot.* 73, S869–S875.
- Kirk, O., Björkling, F., Godtfredsen, S.E., Larsen, T.O., 1992. Fatty acid specificity in lipase-catalyzed synthesis of glucoside esters. *Biocatalysis* 6, 127–134.
- Knappik, A., Plückthun, A., 1994. An improved affinity tag based on the FLAG peptide for the detection and purification of recombinant antibody fragments. *Biotechniques* 17, 754–761.
- Krebber, A., Bornhauser, S., Burmester, J., Honegger, A., Willuda, J., Bosshard, H.R., Plückthun, A., 1997. Reliable cloning of functional antibody variable domains from hybridomas and spleen cell repertoires employing a reengineered phage display system. *J. Immunol. Meth.* 201, 35–55.
- Magnusson, A.O., Rotticci-Mulder, J.C., Santagostino, A., Hult, K., 2005. Creating space for large secondary alcohols by rational redesign of *Candida antarctica* lipase B. *ChemBiochem* 6, 1051–1056.
- Martinelle, M., Holmquist, M., Hult, K., 1995. On the interfacial activation of *Candida antarctica* lipase-a and lipase-b as compared with humicola-lanuginosa lipase. *Biochim. Biophys. Acta* 1258, 272–276.
- Ottosson, J., Fransson, L., King, J.W., Hult, K., 2002. Size as a parameter for solvent effects on *Candida antarctica* lipase B enantioselectivity. *Biochim. Biophys. Acta* 1594, 325–334.
- Overbeeke, P.L.A., Govardhan, C., Khalaf, N., Jongejan, J.A., Heijnen, J.J., 2000. Influence of lid conformation on lipase enantioselectivity. *J. Mol. Catal. B: Enzym.* 10, 385–393.

- Patkar, S., Bjorkling, F., Zundell, M., Schulein, M., Svendsen, A., Hansen, H.H., Gormsen, E., 1992. Purification of two lipases from *Candida antarctica* and their inhibition by various inhibitors. *Indian J. Chem.* 32B, 76–80.
- Patkar, S.A., Svendsen, A., Kirk, O., Clausen, I.G., Borch, K., 1997. Effect of mutation in non-consensus sequence Thr-X-Ser-X-Gly of *Candida antarctica* lipase B on lipase specificity, specific activity and thermostability. *J. Mol. Catal. B: Enzym.* 3, 51–54.
- Piyatheerawong, W., Iwasaki, Y., Xu, X.B., Yamane, T., 2004. Dependency of water concentration on ethanolysis of trioleoylglycerol by lipases. *J. Mol. Catal. B: Enzym.* 28, 19–24.
- Qian, Z., Lutz, S., 2005. Improving the catalytic activity of *Candida antarctica* lipase B by circular permutation. *J. Am. Chem. Soc.* 127, 13466–13467.
- Redondo, O., Herrero, A., Bello, J.F., Roig, M.G., Calvo, M.V., Plou, F.J., Burguillo, F.J., 1995. Comparative kinetic-study of lipase-a and lipase-b from *candida-rugosa* in the hydrolysis of lipid *p*-nitrophenyl esters in mixed micelles with triton-X-100. *Biochim. Biophys. Acta* 1243, 15–24.
- Rotticci, D., Norin, T., Hult, K., Martinelle, M., 2000. An active-site titration method for lipases. *Biochim. Biophys. Acta* 1483, 132–140.
- Rotticci, D., Rotticci-Mulder, J.C., Denman, S., Norin, T., Hult, K., 2001. Improved enantioselectivity of a lipase by rational protein engineering. *Chembiochem* 2, 766–770.
- Rotticci-Mulder, J.C., Gustavsson, M., Holmquist, M., Hult, K., Martinelle, M., 2001. Expression in *Pichia pastoris* of *Candida antarctica* lipase B and lipase B fused to a cellulose-binding domain. *Prot. Express. Purif.* 21, 386–392.
- Schmid, R.D., Verger, R., 1998. Lipases: Interfacial enzymes with attractive applications. *Angew. Chem. Int. Ed.* 37, 1609–1633.
- Suen, W.C., Zhang, N.Y., Xiao, L., Madison, V., Zaks, A., 2004. Improved activity and thermostability of *Candida antarctica* lipase B by DNA family shuffling. *Protein Eng. Des. Sel.* 17, 133–140.
- Uppenberg, J., Hansen, M.T., Patkar, S., Jones, T.A., 1994. Sequence, crystal-structure determination and refinement of 2 crystal forms of lipase-b from *Candida antarctica*. *Structure* 2, 293–308.
- Uppenberg, J., Ohrner, N., Norin, M., Hult, K., Kleywegt, G.J., Patkar, S., Waagen, V., Anthonsen, T., Jones, T.A., 1995. Crystallographic and molecular-modeling studies of lipase B from *Candida antarctica* reveal a stereospecificity pocket for secondary alcohols. *Biochemistry* 34, 16838–16851.
- Velonia, K., Flomenbom, O., Loos, D., Masuo, S., Cotlet, M., Engelborghs, Y., Hofkens, J., Rowan, A.E., Klafter, J., Nolte, R.J., de Schryver, F.C., 2005. Single-enzyme kinetics of CALB-catalyzed hydrolysis. *Angew. Chem. Int. Ed.* 44, 560–564.
- Wescott, C.R., Klibanov, A.M., 1994. The solvent dependence of enzyme specificity. *Biochim. Biophys. Acta* 1206, 1–9.
- Wiederanders, B., Kaulmann, G., Schilling, K., 2003. Functions of propeptide parts in cysteine proteases. *Curr. Prot. Pept. Sci.* 4, 309–326.
- Zhang, N.Y., Suen, W.C., Windsor, W., Xiao, L., Madison, V., Zaks, A., 2003. Improving tolerance of *Candida antarctica* lipase B towards irreversible thermal inactivation through directed evolution. *Prot. Eng.* 16, 599–605.

P5

Covalent immobilization of recombinant fusion proteins with hAGT for single molecule force spectroscopy

S. Kufer, H. Dietz, C. Albrecht, K. Blank, A. Kardinal, M. Rief and H. E. Gaub

European Biophysics Journal (2005) 35: 72-78

Stefan K. Kufer · Hendrik Dietz · Christian Albrecht
Kerstin Blank · Angelika Kardinal
Matthias Rief · Hermann E. Gaub

Covalent immobilization of recombinant fusion proteins with hAGT for single molecule force spectroscopy

Received: 1 April 2005 / Revised: 5 July 2005 / Accepted: 18 July 2005 / Published online: 14 September 2005
© EBSA 2005

Abstract A genetically modified form of the human DNA repair protein O⁶-alkylguanine-DNA-alkyltransferase (hAGT) was used to immobilize different recombinant hAGT fusion proteins covalently and selectively on gold and glass surfaces. Fusion proteins of hAGT with Glutathione S-Transferase and with tandem repeats of Titin Ig-domains, were produced and anchored via amino-polyethylene glycol benzylguanine. Anchoring was characterized and quantified with surface plasmon resonance, atomic force microscope and fluorescence measurements. Individual fusion proteins were unfolded by single molecule force spectroscopy corroborating the selectivity of the covalent attachment.

Keywords Molecular recognition · SPR · AFM · Suicide coupler · hAGT · SNAP-tag

Abbreviations hAGT: O⁶-alkylguanine-DNA-alkyltransferase · GST: Glutathione S-Transferase · PEG: Polyethylene glycol · BG: Benzylguanine · SPR: Surface plasmon resonance · AFM: Atomic force microscope · EDC: 1-ethyl-3-(3-diaminopropyl) carbodiimide hydrochloride · NHS: *N*-hydroxy succinimide · GST: Glutathione S-transferase · CMC: Carboxymethylcellulose

Introduction

Various areas of modern biotechnology are in great demand for strategies and protocols to attach recombinant proteins permanently, selectively and in a defined manner to solid surfaces. Especially in the field of single molecule biophysics the need for such techniques is emerging. For a broad range of conventional binding studies at surfaces, physisorption of, e.g. a capture antibody in an ELISA, is sufficient as long as the spontaneous off-rate is slower than the one of the target molecule, a covalent attachment is essential for the rapidly growing number of experiments, where forces are measured between molecules. In such experiments the weakest of the bonds in series ruptures first and it must not be the attachment. However, since the force required to rupture a bio-molecular complex is not directly correlated to the binding energy, physisorption, although thermally stable is in many cases insufficient. Various strategies for a covalent attachment have therefore been investigated and established, most of them based on covalently binding the protein of choice either via amines or the thiol group of a cysteine. Besides the limited lifetime due to hydrolysis, the low selectivity and the limited yield of these coupling reactions motivate the search for alternative strategies. Here, we investigated the possibility of using fusion proteins with a mutant of O⁶-alkylguanine-DNA-alkyltransferase (hAGT) also known as SNAP-tag in combination with its substrate polyethylene glycol (PEG)-benzylguanine (BG) as a promising strategy for the covalent and directed attachment of proteins for single molecule force spectroscopy.

The natural role of hAGT is the repair of alkylation damage of the DNA at the O⁶-position of guanine in a unique, stoichiometric reaction (Daniels and Tainer 2000). Since hAGT also accepts free O⁶-benzylguanine as a substrate it is possible to inactivate hAGT irreversibly with this small molecule (Pegg et al. 1993). Interestingly, oligonucleotides containing derivatives of O⁶-benzylguanine with substituted benzyl rings are also accepted as

S. K. Kufer · C. Albrecht · K. Blank · A. Kardinal
H. E. Gaub (✉)
Lehrstuhl für Angewandte Physik, Sektion Physik,
Ludwig-Maximilians-Universität München
and Center for NanoScience, Amalienstrasse 54,
80799 Munich, Germany
E-mail: Hermann.Gaub@physik.uni-muenchen.de
Fax: +49-89-21802050

H. Dietz · M. Rief
Physik-Department E22, Technische Universität München,
James-Franck-Strasse, 85747 Garching, Germany

substrates of hAGT (Damoiseaux et al. 2001). As a consequence, various derivatives of BG were used to label hAGT fusion proteins with small molecules in vivo (Keppler et al. 2003). A BG-PEG-amino derivative, covalently attached to carboxy dextran gold surfaces (Biacore) via EDC/NHS chemistry, was used in a previous study to immobilize GST-hAGT fusion proteins on these BG activated slides (Kindermann et al. 2003).

Here we used the same BG-PEG-amino derivative as an anchor (Fig. 1) and verified the immobilization of Gluthathione S-Transferase (GST)-hAGT fusion proteins on gold surfaces. In the next step, Titin-GFP-hAGT fusion proteins (Fig. 2) were anchored on gold and glass surfaces and were investigated with surface plasmon resonance (SPR), fluorescence and single molecule measurements.

Materials and methods

If not stated otherwise, all chemicals used for the functionalization of surfaces were of analytical standard and

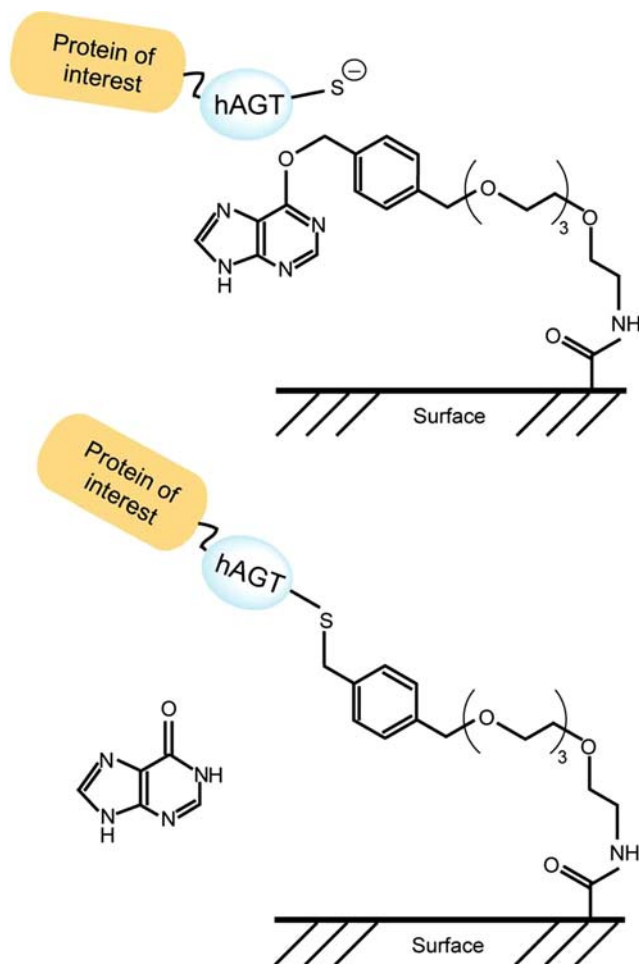


Fig. 1 Immobilization principle of hAGT fusion proteins. The BG-PEG-amino derivative is attached to carboxylized gold and glass surfaces via EDC/NHS chemistry. The hAGT protein accepts BG as a substrate and connects itself to the surface

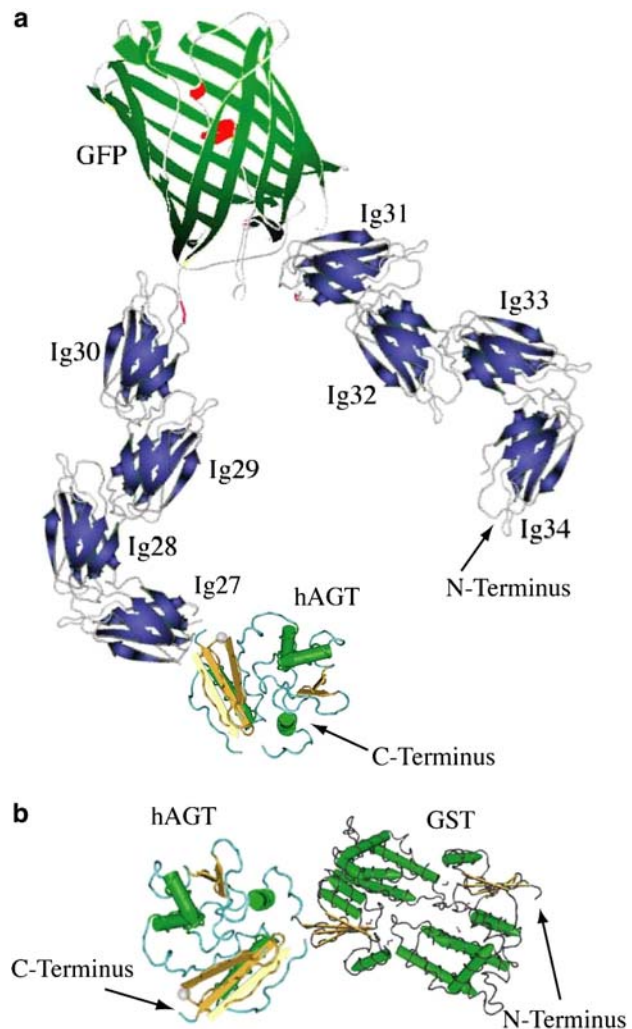


Fig. 2 O⁶-alkylguanine-DNA-alkyltransferase fusion proteins used for the immobilization experiments. **a** Titin-GFP-hAGT fusion protein. Molecular weight about 100 kDa. GFP serves as a fluorescence marker, the eight Ig-domains as molecular rulers for unfolding forces and segment lengths. **b** GST-hAGT fusion protein. Molecular weight about 45 kDa

purchased by Sigma (Taufkirchen, Germany). PBS (10 mM PBS, 150 mM NaCl, pH 7.4) and MES (10 mM MES, 150 mM NaCl, pH 6.3) were used as buffer solutions. For the hAGT fusion proteins, we used a genetically modified form of the wild type form of hAGT, that has a 20-fold increased activity against BG (Juillerat et al. 2003). In addition, the DNA binding site was mutated (Gendreizig et al. 2003) and cysteine 62 was exchanged to alanine (unpublished data). The DNA sequence of this hAGT mutant was C-terminally fused to the sequences of GST and Titin-GFP using standard molecular biology protocols. The recombinant proteins were expressed in *E. coli*. The GST-hAGT fusion protein was expressed following the protocol in Kindermann et al. (2003) and purified with a GST affinity column following the instructions of the affinity medium (Amersham Biosciences, Freiburg, Germany). Purified GST-hAGT fusion proteins were stored in PBS or MES

at 4°C. The Titin-GFP-hAGT fusion protein was expressed exactly as described for Titin-GFP fusion proteins (Dietz and Rief 2004b). The Titin-GFP-hAGT fusion proteins were immobilized without prior purification. Therefore BG functionalized slides were incubated directly with crude extracts of *E. coli* cells expressing this fusion protein.

Surface plasmon resonance measurements

To investigate the binding of hAGT fusion proteins on gold-slides, we used a homebuilt multi-channel SPR device that consists of several commercially available SPR-sensor chips (Neuert et al. 2004). Spreeta Evaluation Module software (version 5.21) was used to analyse the SPR curves. All SPR experiments were performed at constant room temperature with thoroughly degassed PBS or MES buffer solutions at a constant flow-rate of 0.03 ml/min.

Cover slides were evaporated at a pressure of $1-2 \times 10^{-6}$ mbar with 1 nm chrome/nickel (GoodFellow, GB) as adhesive layer and 50 nm high-purity gold (purity degree: 99.99%, Leybold Optics, Germany). Afterwards, the slides were incubated with cysteamine (20 mM) for 12 h to obtain a cysteamine monolayer. Carboxymethylcellulose (CMC) was bound to these amino groups using standard EDC protocols to obtain carboxylized gold surfaces. In addition to CMC surfaces, sulphur-PEG-COOH ($M=20$ kd) (Rapp Polymere GmbH, Tübingen, Germany) gold coated surfaces were prepared. For this purpose S-PEG-COOH molecules were solved in H₂O (3 mM). The COOH groups of that polymers were activated in solution with EDC (100 mM) and *N*-hydroxysuccinimide (NHS) (50 mM). Those activated polymers were incubated with BG (5 mM) for 12 h. All non-reacted COOH groups were quenched with ethanolamine (1 M) for 30 min. Gold coated cover slides were incubated with the BG activated PEG for 4 h. The control sample was treated identically except for the BG activation, which was omitted.

These gold slides were optically coupled to the SPR sensors using index matching oil (518 C, Zeiss, Germany).

Fluorescence binding measurements

To verify the specific anchoring of Titin-GFP-hAGT fusion proteins using the auto-fluorescence properties of GFP, Titin-GFP-hAGT proteins were immobilised on aldehyde-functionalised glass slides (Quantifoil Micro Tools GmbH, Germany). The aldehyde groups were oxidised with potassium permanganate to carboxyl groups. After that, spots of BG (3 mM) were attached to these groups using standard EDC/NHS protocols. All non-reacted NHS groups were blocked with 1 M ethanolamine. Following this, the Titin-GFP-hAGT fusion proteins were coupled to this surface by incubating the whole slide with the crude extract of hAGT-expressing *E. coli* cells. After an incubation time of 45 min all un-

bound proteins from the cell extract were removed by extensive washing with PBS.

A fluorescence-scanner (LS100, Tecan, Austria) was used to determine the amount of bound fusion proteins. GFP was excited with a 488 nm laser and the emitted light was filtered with a 500–570 nm band-pass filter. The spatial resolution was 20 μ m. Mean fluorescence as well as background intensity was determined by using NIH IMAGE software (National Institutes of Health, Bethesda).

Single molecule force spectroscopy

All single molecule force measurements were performed with a custom-built atomic force microscope (AFM) (Oesterhelt et al. 1999). Cantilevers were calibrated in solution using the equipartition theorem (Butt and Jaschke 1995; Florin et al. 1995). This method provides a resolution, in force, of roughly 10%. Two types of gold-coated cantilevers (Bio-Levers, Olympus, Japan) with spring constants and resonance frequencies of 30 pN/nm and 8.5 kHz or 6 pN/nm and 1.5 kHz, respectively, were used. The force curves of the Titin-GFP-hAGT construct were collected at pulling speeds ranging around 300 nm/s. All experiments were conducted at room temperature in PBS buffer.

Titin-GFP-hAGT fusion proteins were immobilised on BG activated aldehyde-functionalised glass slides as described before (see fluorescence binding measurements).

Results and discussion

Binding studies with surface plasmon resonance

In the beginning we describe an experiment on CMC functionalized cover slides. The CMC layer in channel 1 was activated with BG (Covalys Biosciences AG, Switzerland) using standard EDC/NHS protocols. As a control for specific immobilisation of the fusion proteins in channel 2 no BG, but also EDC/NHS was added. The attachment of the BG-PEG-amino derivative causes an increase of layer thickness of about 6 Å in channel 1 (Fig. 3). After blocking all non-reacted NHS groups from both channels with 1 M ethanolamine, each channel was incubated with GST-hAGT fusion protein. The sensor response of channel 1 (BG activated) was about four times higher than the response of channel 2 (non-activated with BG) (Fig. 4).

The SPR measurements show that a protein layer of the same thickness as a GST-hAGT monolayer is bound only to the BG activated surface. The result of this immobilisation experiment is in good accordance with literature values (Kindermann et al. 2003).

With the anchoring protocol established for GST, in the second experiment we now immobilised a Titin-GFP-hAGT fusion protein on a S-PEG-COOH coated

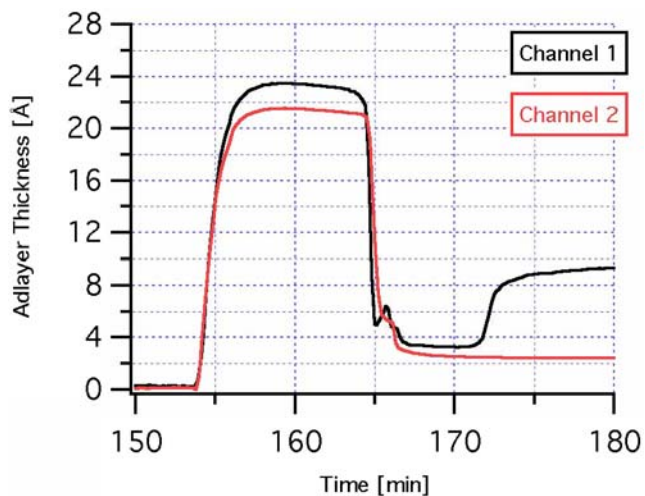


Fig. 3 Surface plasmon resonance signal of the BG-PEG-amino anchor. Carboxylized gold surfaces were activated with EDC/NHS ($t=154$ min). After a short washing step with H_2O (Millipore, Germany) ($t=164$ min) the BG-PEG-amino derivative was anchored to the surface of channel 1. The immobilization of the BG anchor causes an increase in layer thickness of about 6 Å

gold surface. The PEG of channel 1 was activated with BG and the PEG of channel 2 was not. First the surfaces were equilibrated in MES buffer. After 10 min the surfaces of both channels were incubated with crude cell extract of Titin-GFP-hAGT expressing bacteria resuspended in MES buffer. We observed a sizable increase (about 12 Å) in the measured adlayer thickness, which we attribute to the high density of the cell content (Fig. 5). The thickness of the surface in channel 2 slightly decreased in time to drop to nearly zero after

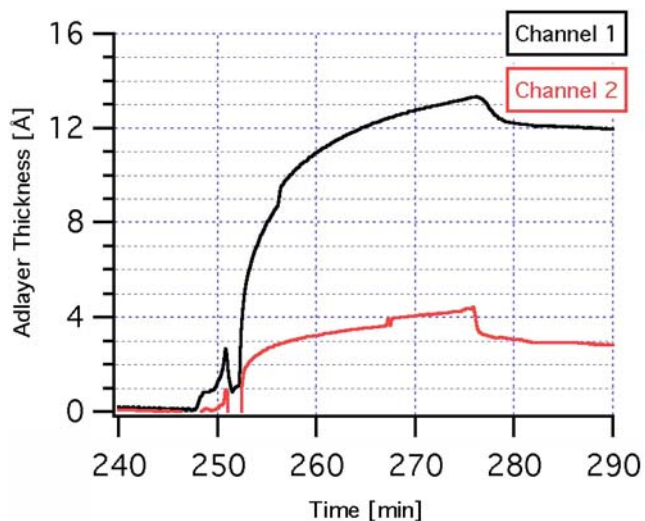


Fig. 4 Surface plasmon resonance signal of GST-hAGT fusions proteins. Surface of channel 1 was activated with BG. Surface of channel 2 was not activated with BG. At time $t=248$ min the surfaces of both channels were incubated with GST-hAGT fusion proteins. After an incubation time of about 30 min all unbound proteins were washed away with PBS buffer ($t=276$ min). The SPR response of channel 1 was about four times higher than that of channel 2

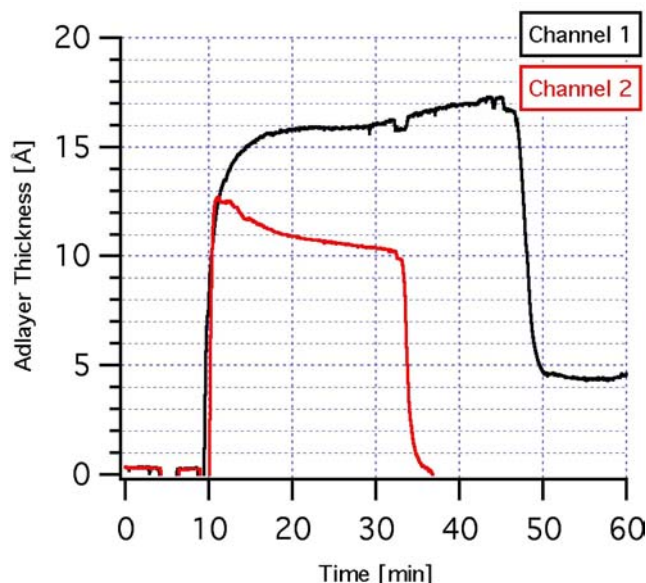


Fig. 5 Surface plasmon resonance signal of Titin-GFP-hAGT fusion proteins. The surface of channel 1 was activated with BG. The surface of channel 2; A was not activated with BG. At time $t=10$ min the surfaces of both channels were incubated with crude cell extract of Titin-GFP-hAGT expression bacteria. After an incubation time of about 35 min all unbound proteins were washed away with MES buffer ($t=45$ min, channel 1; $t=35$ min channel 2). On the surface of channel 2 no protein was bound whereas in channel 1 a film thickness of 4.5 Å remained

extensive rinsing with MES buffer. The thickness in channel 1, however, slightly increased with time. After rinsing, a final thickness increase of 4.5 Å remained.

Verification of anchoring with fluorescence measurements

The specific binding of Titin-GFP-hAGT fusion proteins on BG coated surfaces was verified by spotting BG on EDC/NHS activated slides. Titin-GFP-hAGT fusion proteins were anchored to these slides as described above. The amount of bound fusion proteins was detected by fluorescence measurements. The result is shown in Fig. 6.

The result of the fluorescence-binding assay clearly shows that Titin-GFP-hAGT fusion proteins are only bound to BG activated spots of the glass slide. It also proves the high selectivity of this immobilisation technique since the anchoring was carried out with crude cell lysate.

Single molecule force spectroscopy on anchored proteins

The selectivity of the attachment of hAGT fusion proteins was also investigated by single molecule force spectroscopy. This method is complementary to SPR and fluorescence measurements. Single proteins anchored between surface and AFM cantilever tip can be

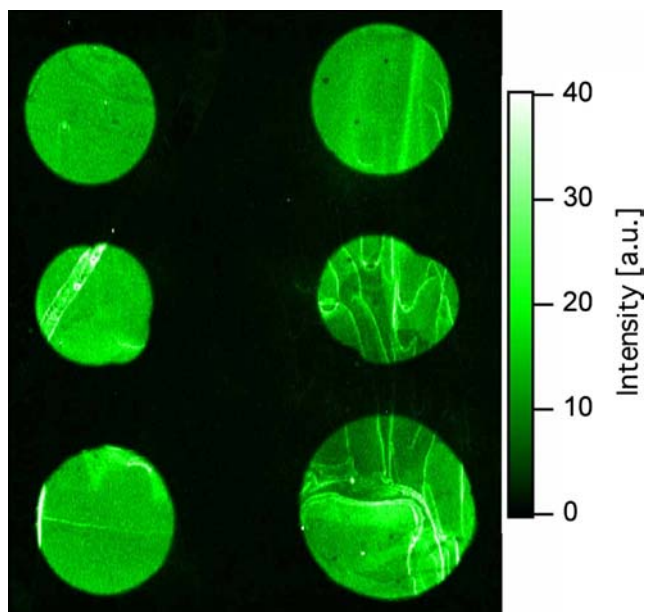


Fig. 6 Fluorescence signal of immobilized Titin-GFP-hAGT fusion proteins. The whole area was activated with EDC/NHS and six spots of BG were coupled to this surface. After blocking all non-reacted NHS groups with 1 M ethanolamine the whole area was incubated with Titin-GFP-hAGT fusion proteins. The fluorescence signal between BG activated areas to non-activated areas was typically 17:1

identified via their specific mechanical unfolding pattern (Rief et al. 1997). Recently, the mechanical unfolding of single Titin-GFP proteins (lacking the hAGT domain) has been investigated and their specific mechanical unfolding pattern has been identified (Dietz and Rief 2004b). Those experiments were performed with unspecific adsorbed proteins. Here we anchored hAGT-Titin-GFP fusion proteins with BG on a glass slide in a site-directed manner. For this purpose, one spot (upper spot Fig. 7b) on the glass slide was activated with BG while the other spot was not activated. Both spots were incubated for 45 min with *E. coli* crude extract and afterwards extensively rinsed with PBS buffer to remove all unbound molecules.

Figure 7a shows typical force-extension traces collected at the BG activated spot. They exhibit the typical saw-tooth pattern due to sequential domain unfolding in single Titin and Titin-GFP molecules as described before (Dietz and Rief 2004b; Rief et al. 1997). At extensions below 100 nm all traces exhibit complicated force patterns, which are most probably due to multiple molecule interactions. Then, at higher extensions the force gradually increases according to polypeptide elasticity until one of the contained Titin domains unfolds. This leads to a quasi-instantaneous increase in the contour length of the polypeptide and the force drops rapidly. Then, subsequent stretching of the lengthened molecule takes place until the next Titin domain unfolds. These unfolding events are equidistant since the Titin domains are identical in size. Then ultimately, the whole

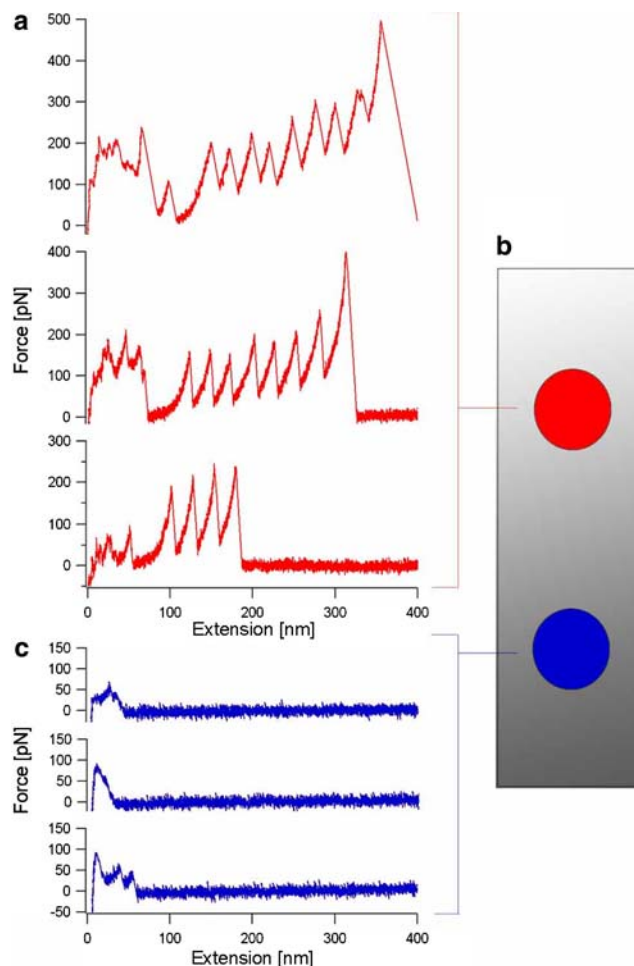
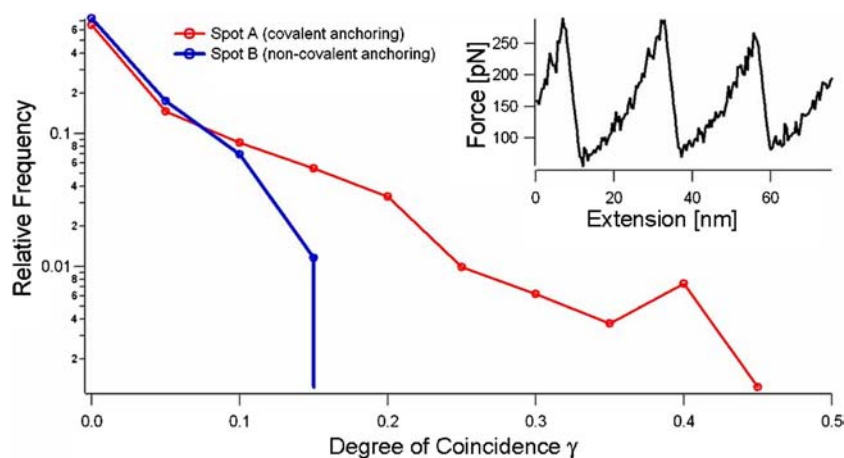


Fig. 7 Atomic force microscope experiments on immobilized hAGT-Titin fusion proteins. The upper spot of the slide was activated with the BG anchor while the lower spot was not activated (b). Both spots were incubated with Titin-GFP-hAGT fusion proteins. Before the AFM experiments, all unbound proteins were washed away with PBS buffer. a Typical force-extension traces collected at the BG activated spot. c Typical force-extension traces collected at the non-activated spot

molecule ruptures from the cantilever (reflected by the last force peak in each trace) and the force drops to zero.

Titin domains exhibit a much higher unfolding force than GFP and thus GFP unfolding always occurs in small extensions. Therefore, this unfolding event will be often masked by non-specific interactions (Dietz and Rief 2004a). This can also be seen in our data—especially in the two topmost traces in Fig. 7a. There we note at least seven Titin domain unfolding events and therefore, also expect a detected GFP unfolding event. However, this event is obviously masked by the multiple molecule interactions below 100 nm extension. The same will most probably be true for the hAGT domain contained in the investigated molecules. In our data we could not find clear indication for an additional event reflecting the unfolding of the hAGT domain. This also supports the notion that hAGT loses partly its structural integrity when it binds to its target BG (Daniels et al.

Fig. 8 Results of the search for Titin domain unfolding events on the activated and on the non-activated spot with a pattern recognition algorithm. We searched all force-distance curves from both areas for the typical Titin fingerprint (inset). It is clearly visible that at the BG activated spot the frequency of partial ($\gamma > 0.2$) and good matching ($\gamma > 0.35$) with the three Titin domain-unfolding pattern is by far higher than at the non-activated spot



2000). The mechanical contribution of the amino-polyethylene glycol linker to the force-extension curves should be negligible, since the PEG linker consists of only three monomers. It will be an important task for the future to further characterise the mechanical properties of this enzyme.

However, the traces in Fig. 7a clearly demonstrate on the single molecule level the successful anchoring of the Titin-GFP-hAGT molecules. In contrast, the traces collected at spot B (Fig. 7c) exhibit only unspecific low-force interaction patterns, which cannot be attributed to the unfolding of modules contained in the Titin-GFP-hAGT molecule.

To compare quantitatively the yield of force-extension traces exhibiting Titin unfolding patterns collected on both spots, we performed an analysis based on pattern recognition techniques as described in Dietz and Rief (2004a). This method involves first definition of a test pattern, then identification of the best matching section with the test pattern in each force trace and finally calculation of a degree of coincidence γ with the pattern as defined in equation 10 in Dietz and Rief (2004a). As a test pattern we chose a section of a measured single molecule force-extension trace exhibiting three Titin domain-unfolding events (Fig. 8, inset). The graph shows the distribution of the degrees of coincidence with the given pattern as they have been assigned to each force trace contained in the data sets collected at the BG activated spot and at the non-activated spot. It is clearly visible that at the BG activated spot the frequency of partial ($\gamma > 0.2$) and good matching ($\gamma > 0.35$) with the three Titin domain-unfolding pattern is by far higher than at the non-activated spot. This testifies again that proteins containing Titin domains are selectively immobilised only on the BG activated spot.

We therefore conclude that the anchoring is indeed performed via the hAGT-BG coupling mechanism. However, from our single molecule experiments we cannot infer directly if the binding is covalent since the forces at which the molecules rupture from the cantilever are compromised by the fact that the connection

between the stretched molecules and the cantilever was still unspecific. It will be necessary to anchor single proteins selectively and specifically on both the substrate and cantilever. Then, from the rupture forces one would be able to infer if the nature of the binding is covalent, since rupture forces should then reach into the nN regime (Grandbois et al. 1999).

Conclusion

Our study clearly shows that anchoring of fusion proteins via hAGT to BG activated surfaces is a suitable technique for single molecule force spectroscopy. The results show that the hAGT in the fusion acts as an anchor for the coupling and that it does not influence the unfolding behaviour of the molecule of interest. This technique offers several advantages: the first one lies in the gentle coupling procedure (in particular no drying required). There is no need for any (chemical) modification on the protein of interest making it possible to investigate the protein under native conditions. The possibility to use different functionalized surfaces (here CMC and S-PEG-COOH coated surfaces) is another advantage especially in terms of investigations with the AFM. The highly specific, self-searching coupling mechanism, which relies on biological recognition, allows the implementation of patterning experiments; hAGT will direct the protein of interest to the desired positions and anchor it on the surface covalently. Furthermore, time-consuming purification steps could be avoided and proteins can be coupled directly from crude cell extract onto the BG coated surfaces. Due to the high fidelity of this coupling method, covalent attachment of recombinant proteins out of single cells expressing hAGT fusion proteins should be possible.

Acknowledgements We thank Martin Benoit for advise and help. Special thank also to Jan Barnikow and Kai Johnsson from Cov-lys Switzerland who provided the BG-anchor and the hAGT vector. This work was supported by the DFG.

References

- Butt HJ, Jaschke M (1995) Calculation of thermal noise in atomic force microscopy. *Nanotechnology* 6:1–7
- Damoiseaux R, Keppler A, Johnsson K (2001) Synthesis and applications of chemical probes for human O6-alkylguanine-DNA alkyltransferase. *ChemBiochem* 2:285–287
- Daniels DS, Tainer JA (2000) Conserved structural motifs governing the stoichiometric repair of alkylated DNA by O(6)-alkylguanine-DNA alkyltransferase. *Mutat Res* 460:151–163
- Daniels DS, Mol CD, Arvai AS, Kanugula S, Pegg AE, Tainer JA (2000) Active and alkylated human AGT structures: a novel zinc site, inhibitor and extrahelical base binding. *Embo J* 19:1719–1730
- Dietz H, Rief M (2004a) Single molecule force spectroscopy of proteins. In: Proceedings of NATO ASI and SUSSP 59th. *Soft condens Matter Phys Mol cell Biol* (in press)
- Dietz H, Rief M (2004b) Exploring the energy landscape of green fluorescent protein by single molecule mechanical experiments. *PNAS* 101:16192–16197
- Florin E-L, Rief M, Lehmann M, Ludwig M, Dornmair C, Moy T, Gaub HE (1995) Sensing specific molecular interactions with the atomic force microscope. *Biosensors Bioelectronics* 10:895–901
- Gendreizig S, Kindermann M, Johnsson K (2003) Induced protein dimerization in vivo through covalent labeling. *J Am Chem Soc* 125:14970–14971
- Grandbois M, Beyer M, Rief M, Clausen-Schaumann H, Gaub HE (1999) How strong is a covalent bond?. *Science* 283:1727–1730
- Juillerat A, Gronemeyer T, Keppler A, Gendreizig S, Pick H, Vogel H, Johnsson K (2003) Directed evolution of O6-alkylguanine-DNA alkyltransferase for efficient labeling of fusion proteins with small molecules in vivo. *Chem Biol* 10:313–317
- Keppler A, Gendreizig S, Gronemeyer T, Pick H, Vogel H, Johnsson K (2003) A general method for the covalent labeling of fusion proteins with small molecules in vivo. *Nat Biotechnol* 21:86–89
- Kindermann M, George N, Johnsson N, Johnsson K (2003) Covalent and selective immobilization of fusion proteins. *J Am Chem Soc* 125:7810–7811
- Neuert G, Kufer SK, Benoit M, Gaub HE (2004) Modular multichannel surface plasmon spectrometer. *Review of Scientific Instruments* (in press)
- Oesterhelt F, Rief M, Gaub HE (1999) Single molecule force spectroscopy by AFM indicates helical structure of poly(ethylene-glycol) in water. *New J Phys*, pp 6.1–6.11
- Pegg AE, Boosalis M, Samson L, Moschel RC, Byers TL, Swenn K, Dolan ME (1993) Mechanism of inactivation of human O6-alkylguanine-DNA alkyltransferase by O6-benzylguanine. *Biochemistry* 32:11998–12006
- Rief M, Gautel M, Oesterhelt F, Fernandez JM, Gaub HE (1997) Reversible unfolding of individual titin immunoglobulin domains by AFM. *Science* 276:1109–1112

P6

Double chip protein arrays using recombinant single-chain Fv antibody fragments

I. Gilbert, S. Schiffmann, S. Rubenwolf, K. Jensen, T. Mai, C. Albrecht,
A. Lankenau, G. Beste, K. Blank, H. E. Gaub and H. Clausen-Schaumann

Proteomics (2004) 4: 1417-1420

Double chip protein arrays using recombinant single-chain Fv antibody fragments

Ilka Gilbert¹, Susanne Schiffmann¹, Susanne Rubenwolf², Kristian Jensen²,
Thao Mai¹, Christian Albrecht^{1,3}, Andreas Lankenau¹, Gerald Beste², Kerstin Blank^{1,3},
Hermann E. Gaub³ and Hauke Clausen-Schaumann^{1*}

¹nanotype, Gräfelfing, Germany

²Xerion Pharmaceuticals, Martinsried, Germany

³Lehrstuhl für Angewandte Physik and Center for NanoScience, LMV, München, Germany

Protein arrays permit the parallel analysis of many different markers in a small sample volume. However, the problem of cross-reactivity limits the degree of multiplexing in parallel sandwich immunoassays (using monoclonal antibodies (mAbs)), meaning antibodies must be pre-screened in order to reduce false positives. In contrast, we use a second chip surface for the local application of detection antibodies, thereby efficiently eliminating antibody cross-reactions. Here, we illustrate the potential advantages of using single-chain Fv fragments rather than mAbs as capture and detection molecules with this double chip technology.

Keywords: Multiplexing / Protein array / Recombinant antibody / Sandwich immunoassay

Received	10/10/03
Revised	22/12/03
Accepted	29/12/03

1 Introduction

Chip-based protein assays facilitate parallel measurements with large numbers of different diagnostic markers in small sample volumes. With the increasing focus on the proteomic state of the cell, robust antibody arrays are becoming one of the most popular analytic tools. Currently, mAbs are the molecules of choice, but other molecules such as recombinant antibodies offer many significant advantages [1, 2]. Recombinant antibodies have already been used in various protein detection applications, e.g. sandwich immunoassays (IAs) [3–5] or functional protein analysis, such as chromophore-assisted laser inactivation (Xerion Pharmaceuticals, Martinsried, Germany; unpublished data). Similarly, they have recently shown promise as capture molecules for antibody arrays [6, 7]. One critical aspect concerning antibody arrays is their lack of specificity [8]. Generally, for single marker assays a sandwich format increases the specificity [1], but in multiplexed sandwich IA systems antibodies must be pre-screened for cross-reactivity [9, 10]. We recently introduced a double chip format (Fig. 1A), which provides

a different solution [11, 12]. This format consists of a capture array containing spots of different capture antibodies (capAbs) and a reference array. Fluorescently labeled detection antibodies (detAbs) are coupled to this reference array *via* DNA duplexes and are applied locally onto their corresponding spots on the capture array. Since this format reduces the complexity of a multimarker assay to the simplicity of a single marker sandwich ELISA, antibody cross-reactions are effectively eliminated and time-consuming antibody prescreening is not necessary. Here, we show that single-chain Fv fragments (scFvs) can be used instead of mAbs in multiplexed sandwich IAs using this double chip format. We could demonstrate this with three different scFvs randomly chosen from a pool of twenty.

2 Materials and methods

β -Galactosidase mAbs were purchased from Roche Diagnostics (Mannheim, Germany; capAb) and Dunn Labor-technik (Asbach, Germany; detAb). β -Galactosidase was purchased from Roche Diagnostics. Recombinant scFv antibody fragments were made by phage display [13]. For purification, they were expressed with a His-Tag. The scFvs were biotinylated using the FluoReporter Biotin/DNP Protein Labeling Kit (Molecular Probes, Leiden,

Correspondence: Dr. Hauke Clausen-Schaumann, Fraunhofer Institute, Biomedical Technology, Invalidenstrasse 42, 10115 Berlin, Germany
E-mail: Hauke.Clausen-Schaumann@ibmt.fhg.de
Fax: +49-30-2093-8635

Abbreviations: CapAb, capture antibodies; DetAb, detection antibodies; IA, immunoassay; ScFv, single-chain Fv fragment

* Current address: Fraunhofer Institute, Biomedical Technology, Berlin, Germany

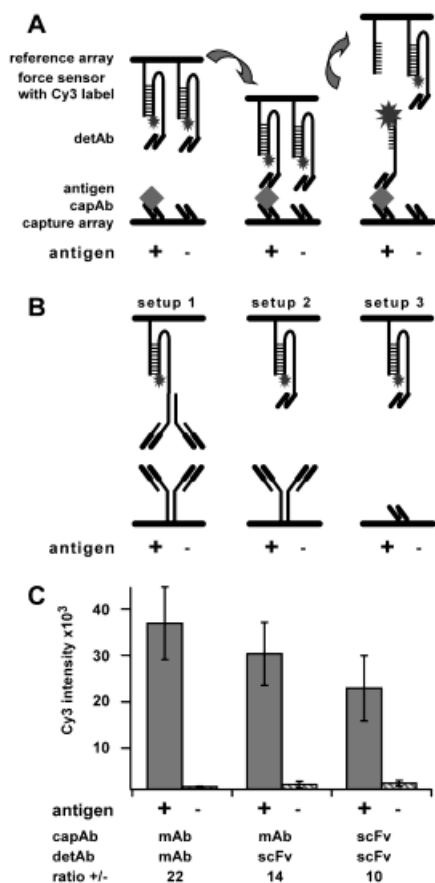


Figure 1. Substituting mAbs by scFv fragments. A) Assay setup: CapAbs were immobilized on the capture array by random coupling *via* their amino groups. On the reference array, the labeled detAbs were immobilized *via* DNA duplexes in unzipping geometry. The two arrays were brought into contact to allow binding of the detAbs to the antigens. Whenever a detAb could bind to its antigen, the DNA duplex opened and the detAb was transferred onto the capture array, together with the Cy3 labeled oligo. B) Stepwise replacement of mAbs by scFvs. In setup 1 mAbs were used as capAb and detAb; for setup 2, a mAb was used as capAb and scFv clone 3A6 ($K_D = 5.5$ nM) was used as detAb; and for setup 3 scFv clone 3A6 was used as capAb and detAb. Each setup was tested with and without incubation of antigen on the capture array. C) Fluorescence intensities of different combinations of mAbs and scFv fragments. The gray bars show the Cy3 intensities measured when antigen was incubated on the capture array, and the striped bars show the intensities without antigen. The mean values and SD (error bars) were calculated from at least 6 independent experiments, all carried out on different slides. The highest Cy3 intensity was measured when mAbs were used as capAb and detAb, with a +/- antigen ratio of 22. When the detAb was a scFv both the Cy3 intensity and the +/- antigen ratio decreased. Substituting both antibodies by scFvs resulted in a further decrease of Cy3 intensity and the +/- antigen ratio. But a ratio of 10 still shows highly efficient specific transfer.

The Netherlands). Excess biotin was removed by gel filtration and dialysis. An amino-reactive surface for the capture array was prepared by oxidizing QMT aldehyde slides (Quantifoil Microtools, Jena, Germany) and activating the resulting COOH-groups with 1-ethyl-3-(3-dimethylamino-propyl) carbodiimide and *N*-hydroxysuccinimide. Antibodies (mAb and scFvs) were spotted onto the activated surface in a concentration of 200 $\mu\text{g/mL}$. After 1 h of incubation, the slides were washed with PBS + 0.05% Tween 20 (PBST) and PBS. Free reactive groups were blocked with a solution of 150 mM Tris, 1 M ethanolamine and 2% BSA for 1 h followed by incubation with PBS + 1% BSA overnight. A solution of β -galactosidase (1 $\mu\text{g/mL}$ in PBS + 0.4% BSA or 20% fetal calf serum in PBS) was incubated for 1 h, followed by a wash with PBST and PBS. The reference array was prepared using a support of polydimethylsiloxane exactly as described [12]. For the conjugation of detAbs and DNA oligonucleotides, NeutrAvidin (Perbio Science, Bonn, Germany) was used instead of streptavidin. The biotinylated mAb was diluted to a final concentration of 2 $\mu\text{g/mL}$ and the biotinylated scFvs were used at a concentration of 10 $\mu\text{g/mL}$. The contact process of the reference and the capture array was carried out as described [12].

3 Results and discussion

We have recently shown that our double chip format enhances the specificity of multiplexed IAs using mAb sandwiches [11, 12]. In the present study, we established a model system using recombinant scFvs in place of mAbs in the double chip format to detect β -galactosidase (Figs. 1A and B). We started by replacing the monoclonal detAb by an scFv detAb, to investigate whether biotinylation of the scFv alters its functionality. In the next step we also replaced the mAb on the capture array to obtain an scFv sandwich. Each setup included a negative control where no antigen was incubated on the capture array. The fluorescence intensities measured on the capture array, as well as the calculated ratios for specific/nonspecific transfer (+/- antigen) for the three different setups are shown in Fig. 1C. Each setup showed a high specific/nonspecific ratio. Both the biotinylated and the immobilized scFvs maintained their functionality. However, the fluorescence intensity for the sandwich containing scFvs as capAb and detAb reached only 62% of the intensity obtained with the mAb sandwich. This may be due to the fact that scFvs are smaller in size resulting in a higher chance of binding sites being inactivated during random coupling or immobilization procedures [5]. However, this problem can be easily solved by expressing fusion proteins where the tag can be utilized for directed immobilization [4, 5].

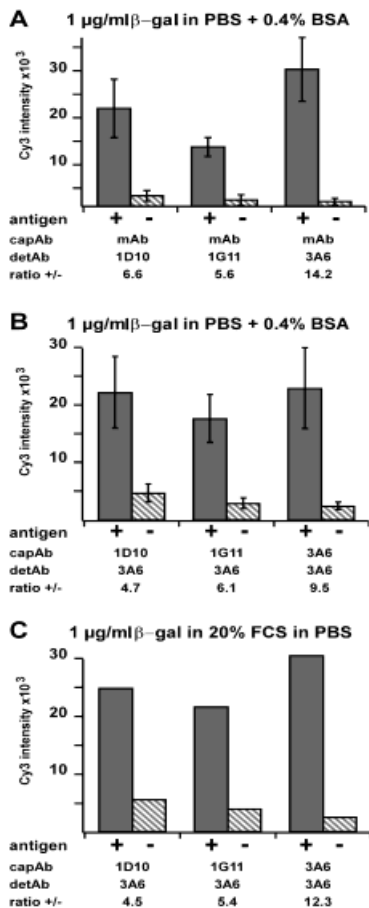


Figure 2. Fluorescence intensities for different combinations of antibodies. A) Combination of different scFVs as detAbs with a monoclonal capAb. The values represent the mean of at least 6 independent experiments. The error bars represent inter-slide SD. Using the scFv clone 3A6 as detAb resulted in the highest absolute Cy3 intensity and the highest +/- antigen ratio (right). Both additional scFVs tested showed less specific transfer (+ antigen; gray bars) and also higher nonspecific transfer (- antigen; striped bars). However, the specific transfer is still significantly higher than the nonspecific transfer (ratios of 6.6 for clone 1D10 and 5.6 for clone 1G11). B) Different sandwiches of scFVs (6 independent experiments, inter-slide SD). The best clone (3A6) from experiment A) was used as detAb in combination with different scFv clones as capAbs. Again clone 3A6 showed the highest absolute intensity and the best +/- antigen ratio (14.2). The absolute intensities for clones 1D10 and 1G11 show the same pattern as measured in experiment A). However, since the nonspecific transfer for clone 1D11 is extremely high, this clone gives the lowest +/- antigen ratio (4.7). Nevertheless, the specific transfer is still significantly higher than the nonspecific transfer for all combinations. C) Assay performance in complex biological fluids: The same sets of scFVs as used in B), were used to detect antigen diluted in 20% fetal calf serum. The results (mean values of 2 experiments) are comparable to the results obtained in PBS + BSA.

Finally, we investigated the performance of three different randomly chosen scFVs in the sandwich setup (clones 1D10, 1G11 and 3A6). For these scFVs, BIAcore measurements yielded K_D s of 558 nM for 1D10, 7.3 nM for 1G11 and 5.5 nM for 3A6. Again, the monoclonal detAb was replaced first by the different scFVs. All scFVs showed high specific/nonspecific ratios when used as the detAb (Fig. 2A). Subsequently, the same three scFVs were tested as capAbs in combination with clone 3A6 as the detAb (Fig. 2B). The comparison of the intensities obtained with the scFv sandwiches, now using different capAbs, resembled the data in Fig. 2A, although the specific/nonspecific ratios differ slightly. Again, similar results were obtained, when the antigen was diluted in 20% fetal calf serum (diluted with PBS) instead of PBS + 0.4% BSA (Fig. 2C), showing that the antigen can be detected in complex biological mixtures with the same intensity as the purified antigen.

The specific to nonspecific ratios of the scFVs perfectly match the ratios these fragments showed in direct binding assays with fluorescently labeled β -galactosidase (data not shown). Comparison to BIAcore data indicates, however, that although clone 1G11 has a K_D similar to that of clone 3A6, it is not as efficient in binding in our experiments, as well as in the direct binding assay. This might be the result of activity losses of the antibodies after chemical modification and immobilization. In contrast to the protein array setup, where the antibodies are either immobilized or biotinylated, in the BIAcore measurements, the antigen is immobilized and the antibodies are used without chemical modification.

4 Concluding remarks

We could clearly show that scFVs specifically and efficiently function as capAbs and detAbs in combination with our double chip technology, even with random coupling and immobilization chemistries. In the above experiments the performance of each scFv is a product of the affinity, stability and percentage of functional molecules after chemical modification. Consequently, several strategies exist to enhance the overall performance of the assay: high affinity scFVs can be generated using standard procedures [13]. The use of a single, stability optimized framework [6] should reduce nonspecific binding to hydrophobic antibody residues. Finally, fusion proteins enable directed immobilization resulting in a high percentage of functional scFVs [4, 5]. The use of scFVs with the double chip format ideally combines the specificity of a sandwich ELISA with the advantages of recombinant antibody technologies, namely, high-throughput production and affinity optimization. In particular, the ability to gener-

ate binders with different affinities is of great value for antibody-based arrays. As protein concentrations in the proteome vary over a broad range the use of recombinant antibodies with different affinities will considerably extend the dynamic range of such an assay [2, 8]. In summary, the double chip assay based on recombinant antibodies can provide high specificity and a high dynamic range for the detection of diagnostically relevant markers in a multiplexed format.

The authors would like to acknowledge support from G. Brink, F. Oesterheld, B. Steipe, M. Benoit, R. Zivin, M. Olive, and A. A. Göttig, as well as financial support from the Bundesministerium für Bildung und Forschung and the Deutsche Forschungsgemeinschaft.

5 References

- [1] Borrebaeck, C. A., *Immunol. Today* 2000, 21, 379–382.
- [2] Kusnezow, W., Hoheisel, J. D., *Biotechniques* 2002, Suppl., 14–23.
- [3] Kerschbaumer, R. J., Hirschl, S., Kaufmann, A., Ibl, M., *et al.*, *Anal. Biochem.* 1997, 249, 219–227.
- [4] Härmä, H., Tarkkinen, P., Soukka, T., Lovgren, T., *Clin. Chem.* 2000, 46, 1755–1761.
- [5] König, T., Skerra, A., *J. Immunol. Methods* 1998, 218, 73–83.
- [6] Steinhauer, C., Wingren, C., Hager, A. C., Borrebaeck, C. A., *Biotechniques* 2002, Suppl., 38–45.
- [7] Pavlickova, P., Knappik, A., Kambhampati, D., Ortigao, F. *et al.*, *Biotechniques* 2003, 34, 124–130.
- [8] Mitchell, P., *Nat. Biotechnol.* 2002, 20, 225–229.
- [9] Mendoza, L. G., McQuary, P., Mongan, A., Gangadharan, R. *et al.*, *Biotechniques* 1999, 27, 778–788.
- [10] Schweitzer, B., Roberts, S., Grimwade, B., Shao, W. *et al.*, *Nat. Biotechnol.* 2002, 20, 359–365.
- [11] Albrecht, C., Blank, K., Lalic-Mühlthaler, M., Hirler, S. *et al.*, *Science* 2003, 301, 367–370.
- [12] Blank, K., Mai, T., Gilbert, I., Schiffmann, S. *et al.*, *Proc. Natl. Acad. Sci. USA* 2003, 100, 11356–11360.
- [13] Hoogenboom, H. R., Chames, P., *Immunol. Today* 2000, 21, 371–378.

P7

Double-chip protein arrays: force-based multiplex sandwich immunoassays with increased specificity

K. Blank, A. Lankenau, T. Mai, S. Schiffmann, I. Gilbert, S. Hirler, C. Albrecht,
M. Benoit, H. E. Gaub and H. Clausen-Schaumann

Analytical and Bioanalytical Chemistry (2004) 379:974-981

Kerstin Blank · Andreas Lankenau · Thao Mai
Susanne Schiffmann · Ilka Gilbert · Siegfried Hirler
Christian Albrecht · Martin Benoit · Hermann E. Gaub
Hauke Clausen-Schaumann

Double-chip protein arrays: force-based multiplex sandwich immunoassays with increased specificity

Received: 20 January 2004 / Revised: 17 March 2004 / Accepted: 18 March 2004 / Published online: 21 April 2004

© Springer-Verlag 2004

Abstract Protein assays provide direct access to biologically and pharmacologically relevant information. To obtain a maximum of information from the very smallest amounts of complex biological samples, highly multiplexed protein assays are needed. However, at present, cross-reactions of binding reagents restrict the use of such assays to selected cases and severely limit the potential for up-scaling the technology. Here we describe a double-chip format, which can effectively overcome this specificity problem for sandwich immunoassays. This format consists of a capture array and a reference array with fluorescent labeled detection antibodies coupled to the reference array via DNA duplexes. This format allows for the local application of the labeled detection antibodies onto their corresponding specific spots on the capture array. Here we show that this double-chip format allows for the use of cross-reactive antibodies without generating false positive signals, and an assay for the parallel detection of seven different cytokines was set up. Even without further optimization, the dynamic range and the limit of detection for interleukin 8 were found to be comparable to those obtained with other types of multiplexed sandwich immunoassays.

Keywords Sandwich immunoassay · Protein array · Cytokine · Specificity · Cross-reactivity · Multi-analyte

Introduction

Today, it is widely accepted that the parallel analysis of proteins, their abundance, their modifications, and their

interactions, reveal unique insights into complex biological systems, such as immunology and cell signaling [1, 2]. An ideal assay to answer both the questions posed in the drug development process and those posed in diagnosing disease should be able to measure many proteins in a small amount of sample with high specificity and sensitivity. Two formats are typically used: microarrays and sandwich immunoassays. Microarray formats are employed for the parallel measurement of proteins [3, 4, 5, 6, 7], and are well suited for the analysis of small sample volumes, whereas sandwich immunoassays have the potential for the specific detection of proteins [8], even at low concentrations. Both technologies are well established, and different groups have shown encouraging proof of principle experiments, which combine the two formats [9, 10, 11, 12, 13, 14, 15, 16].

One of the most serious drawbacks of multiplexed sandwich immunoassays is lack of specificity caused by antibody cross-reactions. In conventional sandwich-ELISAs the secondary detection antibody (detAb) improves the specificity of the assay [17]. However, in a multiplexed microarray format the use of a detAb is actually an additional source of false positive signals. When a cocktail of detAb is incubated on the array, each detAb can interact with any antigen bound somewhere on the surface of the array [9, 10, 13, 18]. As a result, the chance of false positives increases geometrically with the number of spots on a protein array [19]. For this reason it is no coincidence that all published capture array formats that employ a sandwich format measure cytokines [9, 10, 11, 12, 13, 14, 15, 16]. Cytokines are the only group of molecules for which sets of cross-reactivity optimized antibodies are commercially available from different suppliers [4, 8].

A common strategy to overcome this specificity problem is prescreening of antibodies for cross-reactivity [9, 10, 13, 14, 15, 16]. Alternatively, one can optimize assay conditions (e.g., buffers, blocking, use of detergents, and concentrations of detection molecules). These approaches can improve the specificity of the assay; however, they are time-consuming and expensive. Another approach is the use of more specific capture reagents [20], such as re-

K. Blank · A. Lankenau · T. Mai · S. Schiffmann · I. Gilbert
S. Hirler · C. Albrecht · H. Clausen-Schaumann (✉)
nanotype GmbH,
Lochhamer Schlag 12, 82166 Gräfelfing, Germany
Tel.: +49-89-21803132, Fax: +49-89-21802050,
e-mail: Hauke.Clausen-Schaumann@physik.uni-muenchen.de

M. Benoit · H. E. Gaub
Lehrstuhl für Angewandte Physik & Center for NanoScience,
Amalienstrasse 54, 80799 München, Germany

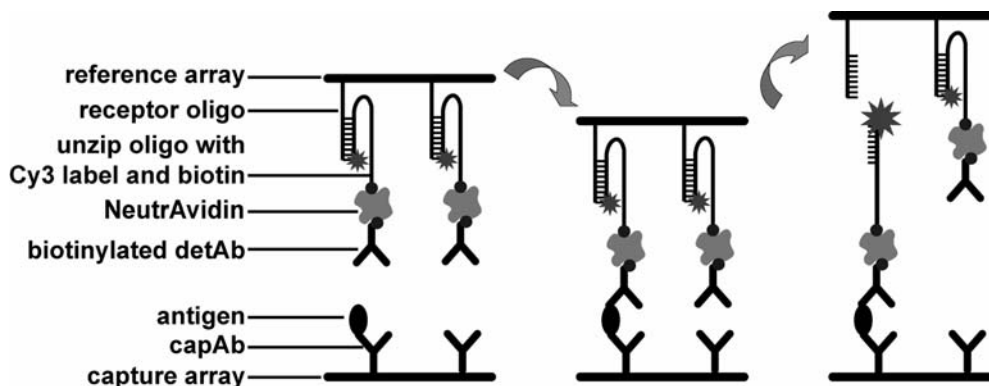


Fig. 1 Principle of a double-chip assay. CapAbs are immobilized on the capture array by random coupling via their amino groups. The detAbs are immobilized on the reference array via DNA force sensors hybridized in unzipping geometry and carrying a Cy3 label. NeutrAvidin is used to connect the biotinylated detAb to the DNA force sensor. The assembly of the DNA force sensor NeutrAvidin and the biotinylated detAb results in the force sensor complex. The two arrays are brought into contact to allow binding of the detAb to the antigen. If the antigen is present and the detAb can bind this antigen, the DNA duplex opens, and the detAb and the unzipping oligo (including the Cy3 label) are transferred onto the capture array

combinant antibodies [21, 22], affibodies [23], or photo aptamers [24]. But in this approach, too, the entire process of prescreening the capture reagents and optimizing assay conditions has to be carried out for each new capture reagent.

Here, we employ a double-chip format [25, 26], which can effectively overcome the specificity problems of multiplexed sandwich immunoassays. The concept relies on using a conventional capture array coupled with a reference array, which is used to locally apply the detAbs. The detAbs are coupled to the reference array via DNA duplexes which serve as molecular force sensors. After the antigens are bound to the capture array, the reference array (with the detAbs arranged such that each detAb is right opposite the corresponding capAb) is brought into contact with the capture array. If the specific antigen is present, the detAb will bind, and the DNA duplex will open when the two chip surfaces are separated. As the detAb carries a fluorescence label, the transfer of this label onto the capture array is finally measured.

By using this format, we demonstrate that cross-reactive capAbs do not lead to false positive results and that commercially available antibody sandwiches can be used for a multiplex assay without any previous antibody testing. Finally, we give an example which demonstrates that both the dynamic range and the limit of detection (LOD) of this new format are comparable to that obtained by other sandwich immunoassays. For better comparison of the data with other types of assays, all experiments were carried out with cytokine antibodies.

Experimental

Three different series of double-chip experiments have been carried out using the same assay principle, which is illustrated in Fig. 1. The preparation of capture and reference arrays follows the same procedure for the different experiments. Briefly, the capture array was prepared by spotting solutions of capture antibodies onto a glass microarray slide. After blocking, the slide was incubated with a sample containing the antigens. The reference array was prepared in a two-step procedure. First, the components of the force sensor complex (including the detAbs) were bound sequentially to 10 mm×10 mm pads of poly(dimethylsiloxane) (PDMS), covering the whole surface homogenously. Second, disks were punched out of the different PDMS pads (each containing one of the detAbs) and assembled as an array such that the detAbs were right opposite to their corresponding capAbs during the contact process. Both arrays were aligned and brought into contact using the contact device shown in Fig. 2A. Finally, the fluorescence on the slide was measured using a microarray scanner. In the following sections the description of one series of experiments (cross-reactive model system) is given in detail. For the other series only the differences are described.

Materials

All monoclonal antibodies used as capAbs as well as the biotinylated monoclonal antibodies used as detAbs were commercially available (see Table 1 for details). Purified human cytokines were purchased from the following suppliers: interleukin 2 (IL-2), interleukin 12 (IL-12), and monocyte chemoattractant protein-1 (MCP-1) from BD Biosciences Pharmingen (Heidelberg, Germany); tumor necrosis factor α (TNF- α), interferon γ (IFN- γ), and interleukin 8 (IL-8) from Perbio Science (Bonn, Germany); and interleukin 5 (IL-5; human and mouse) from R&D Systems (Wiesbaden, Germany). β -Galactosidase (β -gal) was purchased from Roche Diagnostics (Mannheim, Germany). Lyophilized antibodies and antigens were reconstituted as recommended by the supplier. Antibody solutions were divided into aliquots and stored as recommended by the supplier. Bovine serum albumin (BSA) was purchased from Roth (Karlsruhe, Germany), Perfect-Block from MoBiTec (Göttingen, Germany), and fetal calf serum (FCS) from Biochrom (Berlin, Germany). Unless stated otherwise, chemicals for the modification of the surfaces were purchased from Sigma (Taufkirchen, Germany).

Preparation of antibody spotting solutions

Most capAbs were supplied in phosphate-buffered saline (PBS) without any additives (see Table 1 for details). These antibody stock solutions were diluted to a concentration of 200 $\mu\text{g mL}^{-1}$ in 10% glycerol to obtain the spotting solution. The anti-MCP-1 and anti-IFN- γ antibodies were purified by using magnetic protein G Beads (Dynabeads; Dynal Biotech, Hamburg, Germany), as they

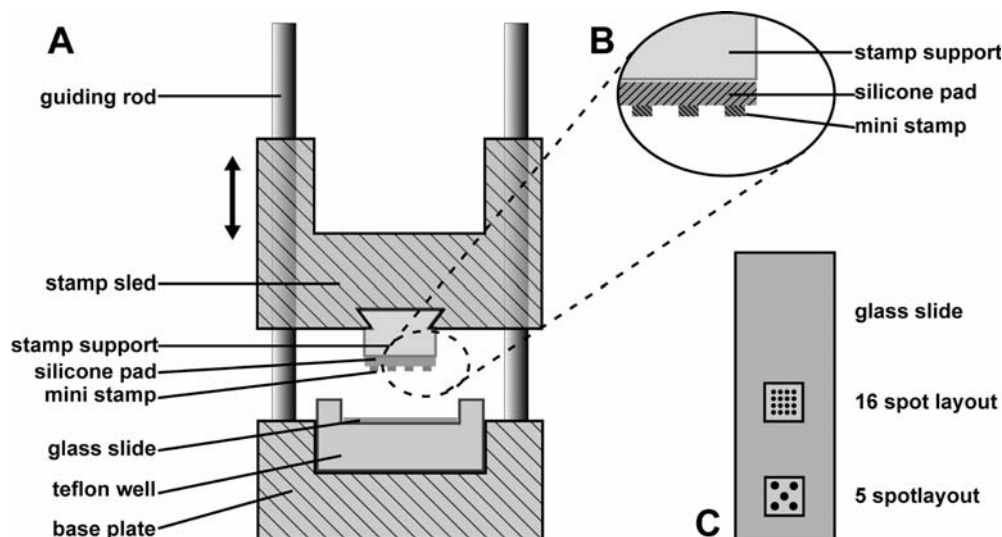


Fig. 2A–C Schematic of the contact device and the array layout. **A** The contact device consists of an element to position a glass slide (containing the capture arrays) and a unit, which holds the reference array and allows for the contact of the arrays. A Teflon well, which can be filled with buffer solution, containing the glass slide is adjusted on the base plate. The reference array is put onto the stamp sled, which runs on two guiding rods. The contact device has two stamp sleds, which can be used in parallel. **B** Detailed view of the reference array. The reference array consists of 5 or 16 individual mini stamps, which are assembled on a plain silicone pad in a pre-defined layout. To maintain an appropriate pressure, the diameter of one mini stamp is 2 mm for the 16-spot layout and 3.2 mm for the 5-spot layout. These mini stamps are manually positioned on the stamp support. The silicone pad between the mini stamps and the stamp support is necessary to compensate for local unevenness. **C** Layout of capture and reference array. One glass slide contains two capture arrays, which are either spotted with 16 or 5 spots. The reference array uses exactly the same layout to ensure an overlap of the corresponding spots during the contact process

were supplied in Tris or BSA, which can react with an amino-reactive surface and influence the coupling efficiency. Binding and washing steps were carried out as recommended by the supplier.

Bound antibodies were eluted with 10 mM citrate buffer, pH 2.5, and neutralized to pH 7 with NaOH. Finally, the antibody was diluted to 200 $\mu\text{g mL}^{-1}$ in an aqueous solution of 10% glycerol.

Preparation of capture arrays

For the cross-reactive model system CSS aldehyde slides (Genetix, Hampshire, UK) were incubated with 6 mM HCl-NH₂-PEG-COOH (3,400 g mol⁻¹; Shearwater Polymers, Huntsville, AL) for 1 h under a 24 mm×60 mm cover slip (300 μL) and rinsed with ddH₂O. The Schiff bases were reduced in 1% aqueous NaBH₄ for 30 min and again rinsed with ddH₂O. For the activation of the carboxy groups, the slides were treated with 50 mM each of 1-ethyl-3-(3-dimethylaminopropyl)carbodiimide (EDC) and *N*-hydroxysuccinimide (NHS) for 30 min under a 24 mm×60 mm cover slip in a humid atmosphere at room temperature (RT). The slides were rinsed with ddH₂O and dried. The freshly prepared antibody spotting solution of the anti-IL-5 capAb was manually spotted (1 $\mu\text{L spot}^{-1}$) onto the slides using a standard 10- μL pipette. The 5-spot layout of Fig. 2C was used. After 1 h incubation in a humid atmosphere at RT the spots were removed by aspiration, and the slides were washed in PBS+0.05% Tween 20 (PBST)+1% PerfectBlock for 3 min. Finally, the slides were blocked in PBS+3% PerfectBlock+1% BSA at 4°C overnight.

Table 1 Capture and detection antibodies used for the protein array experiments^a

Sandwich	Capture				Detection		
	Supplier	Conc. (mg ml ⁻¹)	Buffer	Purified	Supplier	Conc. (mg ml ⁻¹)	Buffer
Interferon γ	Calbiochem	5.06	PBS+BSA	Protein G	BD	0.5	PBS
Interleukin 2	BD	0.5	PBS	No	BD	0.5	PBS
Interleukin 5 (hu)	R&D	1.0	PBS	No	R&D	0.5	TBS+BSA
Interleukin 5 (mu)					R&D	0.5	TBS+BSA
Interleukin 8	Perbio	1.0	PBS	No	Perbio	0.21	PBS+BSA
Interleukin 12	BD	1.0	PBS	No	BD	0.5	PBS
TNF- α	Perbio	1.0	PBS	No	Perbio	0.5	PBS+BSA
MCP-1	BD	0.5	TBS	Protein G	BD	0.5	PBS
β -Galactosidase	Biotrend	10	PBS	No	Dunn	0.2	PBS+BSA

All capture antibodies listed are specific for human cytokines, except the anti-IL5 capture antibody, which is specific for human and mouse IL-5. All detection antibodies are specific for human cytokines, except one IL-5 antibody, which is specific for the murine

antigen. *R&D* R&D Systems; *BD* BD Biosciences Pharmingen; *Perbio* Perbio Science; *Dunn* Dunn Labortechnik, Asbach, Germany; *Biotrend* Biotrend, Köln, Germany

Immobilization of the force sensor complex on the PDMS pads

PDMS (poly(dimethylsiloxane), Sylgard 184, Dow Corning, Wiesbaden, Germany) was prepared according to the manufacturer's instructions. For casting, a 4" microstructured silicone wafer glued to a glass plate (NMI Natural and Medical Sciences Institute, Reutlingen, Germany), a 1-mm spacer ring with a casting gap, and a plain glass plate were clamped together to form a mold. This mold was placed vertically, filled with the degassed elastomer/curing agent mixture (10:1), and left at RT for 24 h. The resulting PDMS slab was transferred to a plastic dish and allowed to terminate polymerization for 24 h at 50°C. Pads of 10 mm×10 mm, a suitable size for efficient binding and hybridization processes, were cut out manually. The PDMS surface microstructure was composed of 150- μ m squares separated by channels of 50- μ m width and 5- μ m depth. These 10 mm×10 mm PDMS pads were cleaned ultrasonically in 50% abs. ethanol for 3 min, and rinsed with ethanol and ddH₂O. Surface activation was carried out by water plasma treatment. The pads were put into a plasma cleaner (Harrick Scientific Corporation, Ossining, NY) together with a glass petridish filled with ice. The chamber was evacuated until constant pressure was obtained. The plasma was applied at "low" for 60 s. The pads were immediately transferred to an ethanolic solution of 2% 3-aminopropyltrimethoxysilane (ABC, Karlsruhe, Germany)+10% ddH₂O. After 30 min incubation at RT, the pads were rinsed with ethanol and ddH₂O and dried under N₂. An aqueous solution (25 μ L) of 18 mM NHS-PEG-NHS (MW=3,000 g mol⁻¹; Rapp Polymere, Tübingen, Germany) was incubated for 1 h on the pads under a cover slip in humid atmosphere at RT, rinsed with ddH₂O, and dried. The amino-labeled receptor oligonucleotide (5'-NH₂-AAA AAA AAA AAT CTG TCT CCG GCT TTA CGG CGT AT-3'; metabion, Martinsried, Germany, 1.5 μ M) and 50 mM EDC were bound to the PEG surface under a cover slip in humid atmosphere at RT for 1 h. The pads were washed (2×15 min) with saline-sodium citrate buffer (1×SSC) containing 0.5% sodium dodecyl sulfate (SDS). The pads were blocked in an aqueous solution of 2% BSA for 1 h at RT to reduce non-specific binding. Cy3-labeled unzip oligonucleotides (5'-Cy3-ATA CGC CGT AAA GCC GGA GAC AGA TAA GAC GCT ACA TGA AAA AAA AAA AA-biotin-3') were diluted to 0.5 μ M in 5×SSC and hybridized under a cover slip (15 μ L) in humid atmosphere at 4°C overnight. The pads were washed (3×5 min) in 1×SSC+0.1% SDS, and rinsed with PBS. NeutrAvidin (Perbio Science) was used as linker between the 3'-biotinylated unzip oligonucleotide and the biotinylated detection antibody. The pads with the attached DNA were incubated in 4 mL of 2 μ g mL⁻¹ NeutrAvidin in PBS containing 0.4% BSA (PBS-BSA) for 1 h at RT and washed with PBST and PBS. The biotinylated detAbs against human IL-5 (huIL-5) or murine IL-5 (muIL-5) were diluted to a concentration of 2 μ g mL⁻¹ in PBS-BSA. Each PDMS was incubated with 150 μ L of one of the detAb solutions, rinsed with PBST, PBS, and dried.

Sample incubation and reference experiment

The capture array was either incubated with a solution of 10 nM huIL-5, 10 nM muIL-5, or a mixture of both in PBS-BSA (10 nM of each antigen). Each slide was gently shaken with 4 mL of one of the sample solutions for 1 h at RT and washed with PBST and PBS immediately before the contact process.

For the reference experiment using a conventional sandwich setup the capture arrays were prepared, and the incubation of the antigens was carried out exactly as described above. A cocktail of detection antibodies (2 μ g mL⁻¹ of each biotinylated anti-IL-5 antibody) in PBS-BSA was applied to the capture arrays. This step was followed by incubation with Cy3-streptavidin.

Assembly of the reference arrays and contact process

Since conventional spotting was found to be poorly reliable on the PDMS surface, an alternative method was employed. After the force sensor complexes had been immobilized on pads of PDMS homo-

genously, as described above, disks were cut out of these 10 mm×10 mm pads and reassembled in the desired order (see Figs. 2B and C). For this process, the shaft of a disposable surgical biopsy punch (Stiefel Laboratorium GmbH, Offenbach, Germany) was hollowed out with a drill, and its back end was attached to a conventional disposable 5-mL syringe. With mild pressure, disks (mini stamps) of 3.2-mm diameter were punched out of one freshly coated 10 mm×10 mm PDMS pad. Deposition onto plain silicone pads was effected by an air pressure pulse (i.e., by pressing the syringe).

Two pre-assembled reference arrays (each consisting of 5 mini stamps) were then positioned on the two stamp supports of the contact device (see Fig. 2A). For each of the two reference arrays, two mini stamps containing the anti-muIL-5 and two mini stamps containing the anti-huIL-5 antibody were used. The fifth mini stamp in the middle contained either anti-muIL-5 or anti-huIL-5. The slide containing the two capture arrays was positioned in the Teflon well under pre-cooled PBS. The stamp sled was cranked down slowly onto the slide until its weight resulted in a pressure of 1.6 N cm⁻² in the contact areas. After 10 min the arrays were separated carefully, and the slide was rinsed with ddH₂O and dried.

Multiplexing experiment (7 cytokines)

For the multiplexing experiment a different protocol was used to prepare an amino-reactive surface for the spotting of the capAbs. QMT aldehyde slides (Quantifoil Microtools GmbH, Jena, Germany) were oxidized in a 0.5% solution of KMnO₄ in 150 mM Na₂HPO₄, pH 9.1 at 70°C for 20 min and dried. The generated carboxy groups were activated with EDC/NHS and used for spotting immediately. In a 16-spot layout the spotting solutions of 8 different capAbs were applied (0.3 μ L spot⁻¹) as shown in Fig. 4A. The reference arrays were prepared as described using the 16-spot layout. The diameter of individual mini disks was reduced to 2 mm to maintain the pressure in the contact area in the appropriate range.

FCS was used as a matrix for three different "sample solutions". A single, partial, or complete mixture of all 7 antigens was prepared by diluting the stock solutions in 20% heat-inactivated FCS in PBS (20% FCS) to a final concentration of 10 ng mL⁻¹. The complete mixture contained all 7 cytokines, namely, IFN- γ , IL-2, IL-5, IL-8, IL-12, TNF- α , and MCP-1. (The β -gal antibody sandwich served as a negative control.) The partial mixture contained IL-8, TNF- α , and MCP-1, the "single mixture" only IL-8.

Dilution series of interleukin 8

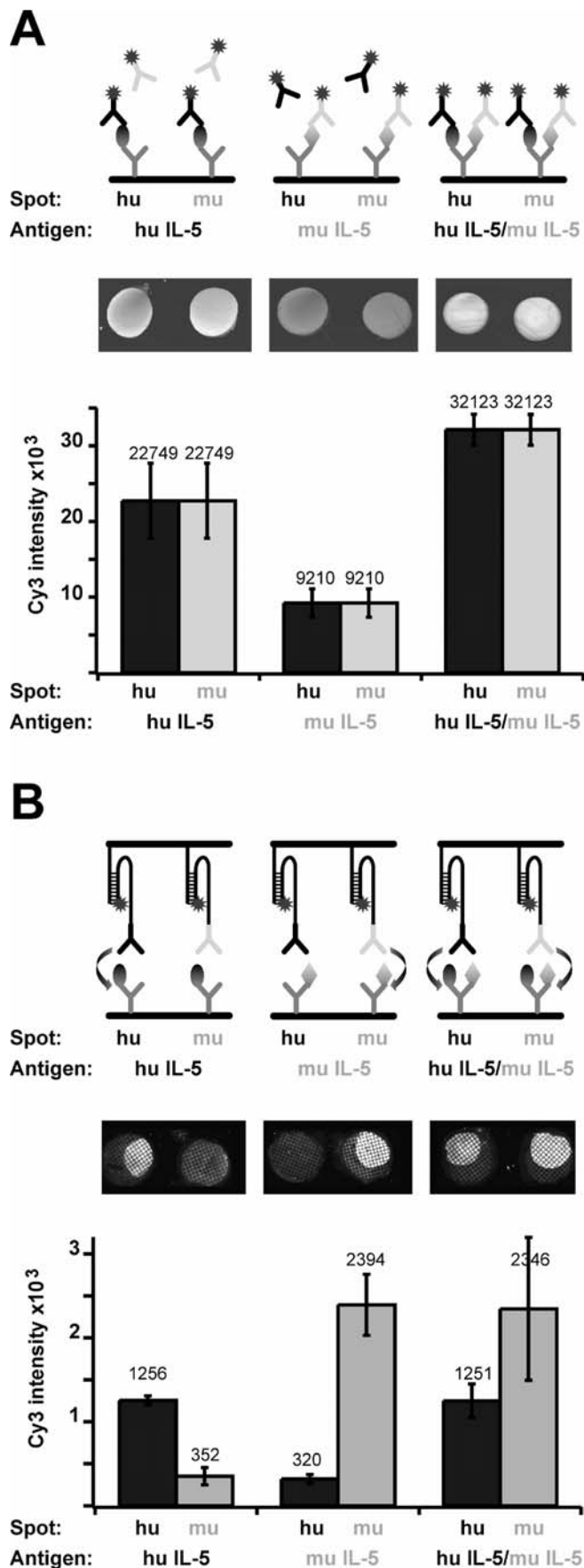
Dynamic range and limit of detection were determined for one of the cytokine sandwiches (IL-8) in the 5-spot layout. On the capture array (based on QMT slides), 4 identical spots (1 μ L) of the capAb were applied in the corner positions, and the center was left empty. The reference arrays were prepared with 5 mini stamps, as described above using only anti-IL-8 detAbs.

Seven identical capture arrays were incubated in 4 mL IL-8 solution of 0, 0.1, 1, 10, 100, 1,000, or 10,000 pg mL⁻¹ (diluted in PBS-BSA) at RT for 1 h. The slides were stored at 4°C and washed with PBST and PBS one by one immediately before the contact process.

A reference experiment was carried out as described for the cross-reactive model system using the biotinylated anti-IL-8 antibody and Cy3-streptavidin.

Fluorescence measurement and data evaluation

The capture array slide was transferred to a GenePix 4000B microarray reader (Axon Instruments, Foster City, CA, USA) and measured in the Cy3 channel. Mean fluorescence transfer was determined with the NIH Image (NIH Bethesda, MD, USA) analysis software. Mean background fluorescence, measured in the grid between the printed microstructure squares, was subtracted from the mean value of the squares to obtain the mean fluorescence transfer.



Results

Cross-reactive model system

The following system was chosen to investigate and compare the effects of a cross-reactive capAb in a conventional protein array experiment and in a double-chip assay. An antibody binding both murine (mu) and human (hu) IL-5 was used as capAb. While this antibody was 100% cross-reactive for both antigens, the detAbs were specific for either muIL-5 or huIL-5. The specificity was tested in simple binding experiments (data not shown). Spots for the detection of either huIL-5 or muIL-5 were defined by their x,y position on the capture array. Two spots were defined as anti-mu and two spots were defined to be anti-hu. The capture array was incubated with a solution of muIL-5, huIL-5, or a mixture of both in a concentration tested to be below saturation of the IL-5 capAb. Bound antigens were detected using a cocktail of both detAbs. The results are shown in Fig. 3A. If only muIL-5 was incubated on the array, it could be detected on the anti-mu and on the anti-hu spots with the same intensity. This was also true if only huIL-5 was used. For the mixture of the antigens, again the same signal was measured on the anti-mu and on the anti-hu spots. Here, the signal was the sum of the signals generated when only one antigen was present. With this setup, it was not possible to discriminate between the two antigens resulting in false positive signals. In addition, the signal of one particular spot was not correlated to the concentration of the antigen to be measured on this spot, but to the total amount of all antigens bound to this spot, making a precise quantification of the different antigens impossible.

By using the double-chip format to detect the antigens, each capture spot was brought into contact with only one sort of detAb. The anti-mu capture spot was opposite to an anti-mu detAb, and similarly, the anti-hu spot was

Fig. 3 Cross-reactive model system. Spots for the detection of either huIL-5 or muIL-5 were defined by their x,y position on the capture array. The capAb at the different positions was cross-reactive between the human and the murine antigen. **A** If this capture array is incubated with huIL-5 (*left*), muIL-5 (*middle*), or a mixture of both antigens (*right*) and a cocktail of detAbs is used as in a traditional format, a signal is measured on the anti-hu and anti-mu spots. The scan shows that discrimination between the two antigens is not possible, as each detAb will interact with its antigen, regardless of where it is bound. The resulting signal is not dependent on the species and amount of antigen in the sample. Mean fluorescence intensities of 4 spots for each antigen are summarized in the diagram. **B** If the double-chip format is used, where the detAbs are immobilized at defined positions on the reference array, labeling of the antigen will only take place at the allocated spot on the capture array. The measured signals where detAb and capAb do not form a specific sandwich (intensity of 352 or 320) represent non-specific transfer which is also measured when a detAb is brought into contact with the blocked capture array containing no antigen (data not shown). In addition, precise quantification of antigen is now possible. Both antigens are measured independently when the second chip is used for specific encoding. The diagram shows the mean fluorescence intensities of four spots

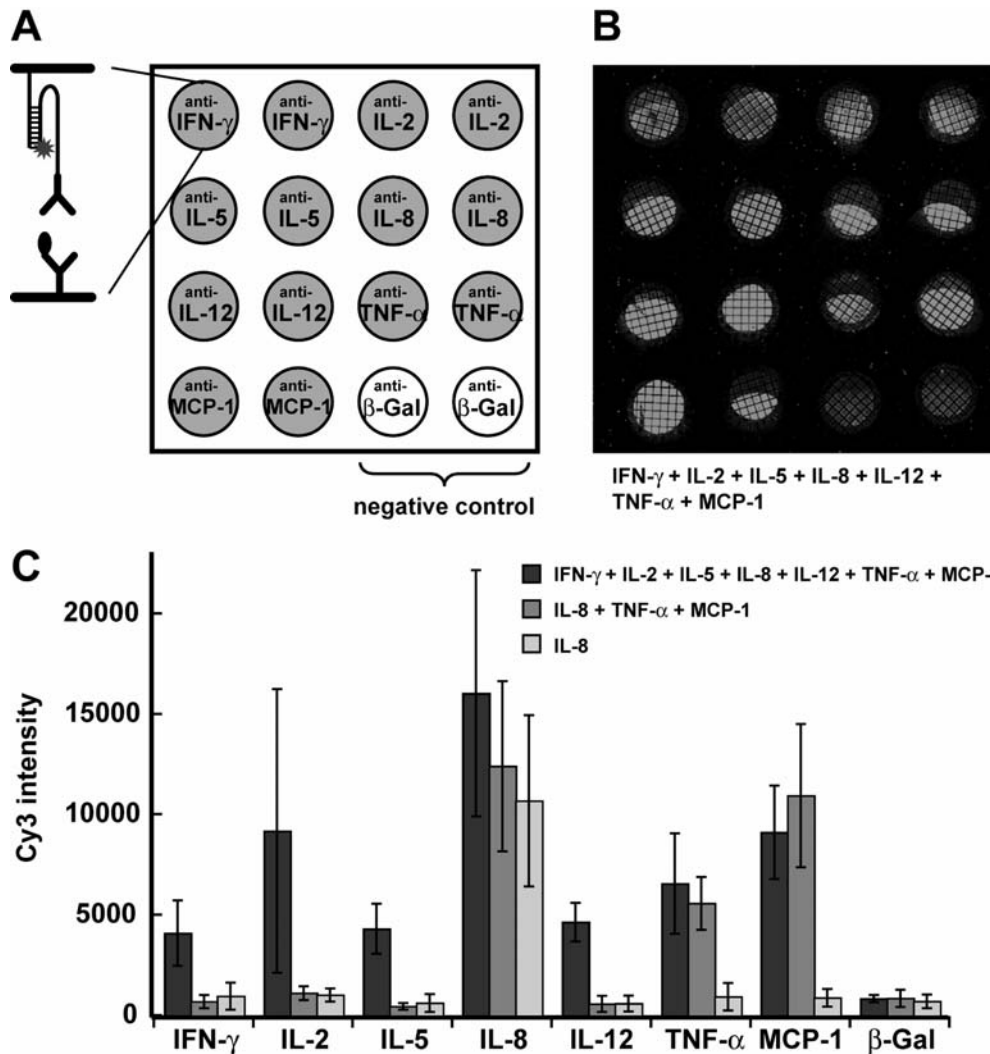


Fig. 4A–C Detection of 7 different cytokines with a 4 \times 4 array. **A** Layout of one capture array. The capAbs against 7 different cytokines (IFN- γ , IL-2, IL-5, IL-8, IL-12, TNF- α , and MCP-1) were spotted in duplicate. The anti- β -gal antibody (*bottom right*) was used as a negative control. After the incubation of this capture array with a mixture of different cytokines, it was brought into contact with the reference array. The reference array contained detAbs for the respective antigens, which were assembled in a way such that each capture and detection antibody formed a specific antibody sandwich. **B** Fluorescence scan of one capture array. On this array a complete mixture of all 7 cytokines was incubated. All positions containing an anti-cytokine antibody are brightly illuminated (intensities between 16,052 for IL-8 and 4,106 for IFN- γ). Only a faint signal (max. intensity 860) is measured on the two negative control spots. **C** Diagram showing the fluorescence intensities determined for 3 different mixtures of cytokines. The mean values and standard deviations for each mixture were calculated from 12 spots (3 independent experiments with 2 identical capture arrays containing duplicates). The *black bars* show the intensities determined for a complete mixture of all 7 cytokines, the *dark gray bars* show a partial mixture with only IL-8, TNF- α , and MCP-1 and the *light gray bars* show the intensities when only IL-8 was incubated on the array

anti-hu spots, it was only detected if it was bound to the anti-mu spot. Similarly, the human antigen was only detected on the anti-hu spot. If both antigens were present, both types of capture spots were labeled; however, in this case, the signal on the anti-mu spot, for example, was not influenced by the presence of the human antigen, and vice versa.

Multiplexing experiment

Six antibody pairs, which were optimized for sandwich ELISAs (IL-2, IL-5, IL-8, IL-12, TNF- α , and MCP-1) and one non-optimized pair (IFN- γ ; capAb and detAb from different suppliers, see Table 1) were arbitrarily chosen from different suppliers, without considering possible cross-reactivities. All seven sandwiches were functional in our assay format and could directly be used for a multiplexing assay for the detection of 7 different cytokines in parallel. To investigate interferences of the cytokines with other proteins, the cytokines were used in a rather high concentration (10 ng mL⁻¹) and in a complex biological sample (20% FCS). The capAbs were spotted in duplicate, and an antibody directed against β -gal was used as a

probed only with an anti-hu detAb. The results of this local application of detAbs are shown in Fig. 3B. Although it was possible for muIL-5 to bind to the anti-mu and the

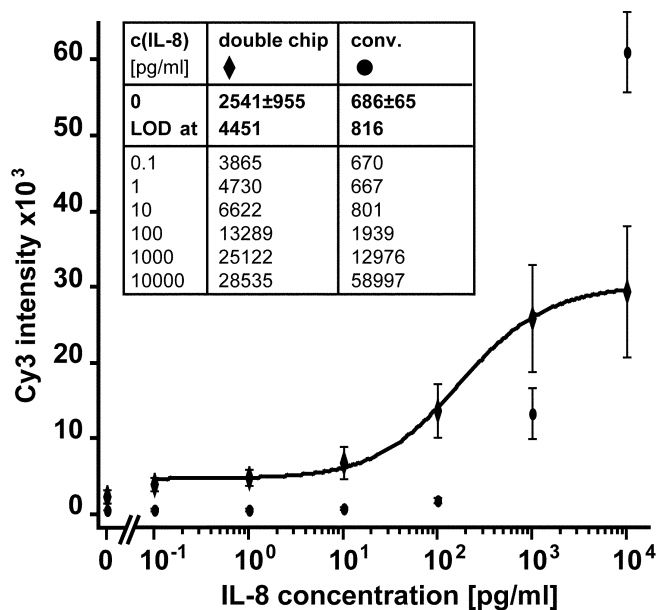


Fig. 5 Standard curves for the IL-8 sandwich. The *table* summarizes the mean values of 16 spots for each concentration (2 independent experiments with 2 identical capture arrays containing 4 capture antibody spots). The limit of detection (LOD) was determined from the experimental data using the signal at zero analyte concentration incremented by two-fold standard deviation of this signal. For the double-chip experiment, the LOD is below 1 pg mL⁻¹ and for the conventional setup (conv.), the LOD is little above 10 pg mL⁻¹. The mean values and the standard deviations of the measured data (◆ double chip and ● conv.) were plotted and the double-chip data were fitted using 5PL logistic regression (—)

negative control. For each spot on the capture array, there was a corresponding detAb spot on the reference array. For a detailed layout of the assay see Fig. 4A. The capture arrays were incubated with 3 different mixtures of cytokines, brought into contact with the reference arrays, separated, and fluorescence intensities were recorded. The results are summarized in Figs. 4B and C. Figure 4B shows a fluorescence scan of a capture array where the complete mixture of all 7 cytokines was used. All spots show a signal significantly higher than the negative control (bottom right). In the diagram of Fig. 4C, the average fluorescence intensities of the three different mixtures are quantified. The black bars represent the complete mixture and again show that a signal significantly above the negative control is measured for all 7 cytokines. If only one (light gray) or three (dark gray) cytokines were present, only the corresponding capture spot(s) show(s) a high signal, while the other signals are in the same range as the negative control. For IL-8 in the different mixtures, the differences in fluorescence intensity are well within the respective error bars. The same is the case for MCP-1 and TNF- α . The results demonstrate that the presence of other proteins in the mixture does not interfere with the measurement of one of the cytokines and that all 7 cytokines can be detected specifically.

Dilution series of IL-8

The results from the previous experiments demonstrate that the specific detection of antigens is possible with this new assay format. However, in most protein assays a reliable measurement of different concentrations of an antigen is also important. Therefore, for one of the cytokine sandwiches (IL-8), the dynamic range and LOD were determined and compared to a conventional protein array setup. Figure 5 shows the measured data points for the double-chip and the conventional setup, where a biotinylated detAb and Cy3-streptavidin was incubated on the array. The LOD determined from the experimental data is below 1 pg mL⁻¹ (125 fM) for the double-chip assay and above 10 pg mL⁻¹ for the conventional setup.

The double-chip standard curve can be fitted by using logistic regression (5PL fit function), which is a standard curve-fitting algorithm for ELISA data [27, 28]. A dynamic range over 4 orders of magnitude (from 1 pg mL⁻¹ to 10,000 pg mL⁻¹) could be determined. Unfortunately, the standard curve for the conventional setup does not reach saturation and cannot be fitted with the above equation. Nevertheless, the measured data points clearly show that the performance of the double-chip assay is comparable to standard ELISA formats or conventional protein arrays, especially for low analyte concentrations.

Discussion

Both the cross-reactive model system and the multiplexing experiment show that a multiplex sandwich immunoassay in the double-chip format can be easily set up without time-consuming prescreening of antibodies for cross-reactions and optimization of assay conditions. The problem of cross-reactive antibodies can be overcome by the local application of detAbs, which is achieved by the attachment of the detAbs in a complementary pattern on the reference array. In this format, the second chip surface provides a second dimension of specific encoding.

The detAbs are bound to the reference array via molecular force sensors consisting of DNA duplexes in unzipping geometry. Since the unzipping force is independent of the length of the duplex, the latter may be chosen such that the spontaneous off-rate of the duplex by far exceeds the time required for the assay [29]. In our assay, the unzipping force of this duplex serves as a reference for the discrimination between specific and non-specific binding [26]. This force threshold establishes stringent assay conditions, which are difficult to obtain using standard protocols, as only little modifications in wash stringencies can be applied for protein interactions [30].

Both experiments clearly demonstrate that commercially available antibody sandwiches can be easily integrated in a double-chip assay. If a desired antibody sandwich cannot be obtained from commercial sources and a new sandwich pair is needed, testing for an appropriate pair is necessary. However, it is only necessary to screen for a pair which performs well in a standard sandwich

ELISA format, meaning that both antibodies bind different epitopes with appropriate affinity constants for the analyte concentration of interest. Still, no screening for potential cross-reactions is necessary, which is otherwise most time-consuming and costly.

Not only could we demonstrate that our new assay format is highly specific, we could also provide an example which demonstrates that the LOD of the double-chip assay is at least comparable to a conventional protein array setup using the same capture array. In addition, the LOD and the dynamic range are comparable to those obtained in other cytokine assays [9, 11, 12, 13, 14, 15, 16, 31]. While many other assays use procedures for signal amplification, such as chemiluminescence [9, 11], RCA [15], or TSA [31], or complicated instrumentation [16], here the LOD is a direct consequence of the double-chip format itself. First, the detAbs are applied in a very high local concentration. Therefore, hindered diffusion and depletion of antibodies near the chip surface do not limit the sensitivity. Second, as the contact is made immediately after incubating the sample, there is no loss of bound antigen during further incubation steps (e.g., of the secondary antibody). Third, the concentration of the detAb, applied to the surface, is independent of the number of analytes to be detected. In a conventional assay, the total concentration of detAbs is increased with the number of analytes [19] resulting in an increase of the background signal. Here, the local application provides a constant amount of detAb, which can interact with the capture surface. As mentioned earlier, neither the spotting of the antibodies onto the arrays nor the contact process was done in an automated way. We believe that improvements in this field will greatly reduce the variability of the assay in the future and that even better values for the LOD or the limit of quantification (LOQ) can be obtained.

Conclusions

In summary, specific and sensitive detection of different analytes is possible in a multiplexing format with this new double-chip assay. As a result of the local application of detAbs, cross-talk between the different spots is effectively eliminated and the complexity of a multi-analyte protein assay is reduced to the simplicity of single analyte ELISAs, where extensive screening for cross-reactivities is usually not necessary. Here, the performance of the assay is independent of the degree of multiplexing. One of the most promising applications of this new format will be protein arrays for the detection of structurally related proteins or disease markers, where multiple sets of optimized antibody sandwiches are not commercially available. Therefore, this new format will be extremely useful in all areas in which the analysis of patterns of markers creates additional information [32, 33, 34] for the drug development process and for biomedical diagnostics (e.g., cell signaling, early prediction of cancer, and differential cancer diagnostics).

Acknowledgements We thank Danielle Mendik, Gunnar Brink, Robert Zivin, Michael Olive, and Horst Domdey for their support. The authors would like to acknowledge financial support from the Bundesministerium für Bildung und Forschung and the Deutsche Forschungsgemeinschaft.

References

1. Kusnezow W, Hoheisel JD (2002) *Biotechniques Suppl*:14–23
2. Hanash S (2003) *Nature* 422:226–232
3. Haab BB, Dunham MJ, Brown PO (2001) *Genome Biol* 2: RESEARCH0004.0001–0004.0013
4. Cutler P (2003) *Proteomics* 3:3–18
5. Ekins RP, Chu F (1994) *Trends Biotechnol* 12:89–94
6. Cahill DJ (2001) *J Immunol Methods* 250:81–91
7. MacBeath G, Schreiber SL (2000) *Science* 289:1760–1763
8. MacBeath G (2002) *Nat Genet* 32 Suppl:526–532
9. Huang RP, Huang R, Fan Y, Lin Y (2001) *Anal Biochem* 294: 55–62
10. Mendoza LG, McQuary P, Mongan A, Gangadharan R, Brignac S, Eggers M (1999) *Biotechniques* 27:778–788
11. Moody MD, Van Arsdell SW, Murphy KP, Orencole SF, Burns C (2001) *Biotechniques* 31:186–194
12. Carson RT, Vignali DA (1999) *J Immunol Methods* 227:41–52
13. Tam SW, Wiese R, Lee S, Gilmore J, Kumble KD (2002) *J Immunol Methods* 261:157–165
14. Wang CC, Huang RP, Sommer M, Lisoukov H, Huang R, Lin Y, Miller T, Burke J (2002) *J Proteome Res* 1:337–343
15. Schweitzer B, Roberts S, Grimwade B, Shao W, Wang M, Fu Q, Shu Q, Laroche I, Zhou Z, Tchernev VT, Christiansen J, Velleca M, Kingsmore SF (2002) *Nat Biotechnol* 20:359–365
16. Pawlak M, Schick E, Bopp MA, Schneider MJ, Oroszlan P, Ehrat M (2002) *Proteomics* 2:383–393
17. Borrebaeck CA (2000) *Immunol Today* 21:379–382
18. Mitchell P (2002) *Nat Biotechnol* 20:225–229
19. Abbott A (2002) *Nature* 415:112–114
20. Templin MF, Stoll D, Schrenk M, Traub PC, Vohringer CF, Joos TO (2002) *Trends Biotechnol* 20:160–166
21. Holt LJ, Enever C, de Wildt RM, Tomlinson IM (2000) *Curr Opin Biotechnol* 11:445–449
22. Steinhauer C, Wingren C, Hager AC, Borrebaeck CA (2002) *Biotechniques Suppl*:38–45
23. Nord K, Gunneriusson E, Ringdahl J, Stahl S, Uhlen M, Nygren PA (1997) *Nat Biotechnol* 15:772–777
24. Petach H, Gold L (2002) *Curr Opin Biotechnol* 13:309–314
25. Albrecht C, Blank K, Lalic-Mülthaler M, Hirler S, Mai T, Gilbert I, Schiffmann S, Bayer T, Clausen-Schaumann H, Gaub HE (2003) *Science* 301:367–370
26. Blank K, Mai T, Gilbert I, Schiffmann S, Rankl J, Zivin R, Tackney C, Nicolaus T, Spinnler K, Oesterhelt F, Benoit M, Clausen-Schaumann H, Gaub HE (2003) *Proc Natl Acad Sci USA* 100:11356–11360
27. Findlay JW, Smith WC, Lee JW, Nordblom GD, Das I, De-Silva BS, Khan MN, Bowsher RR (2000) *J Pharm Biomed Anal* 21:1249–1273
28. Baud M (1993) In: Masseyeff RF (ed) *Methods of immunological analysis vol 1: fundamentals*. VCH, New York, pp 656–671
29. Rief M, Clausen-Schaumann H, Gaub HE (1999) *Nat Struct Biol* 6:346–349
30. Kumble KD (2003) *Anal Bioanal Chem* 377:812–819
31. Woodbury RL, Varnum SM, Zangar RC (2002) *J Proteome Res* 1:233–237
32. Miller JC, Butler EB, Teh BS, Haab BB (2001) *Dis Markers* 17:225–234
33. Petricoin EF, Zoon KC, Kohn EC, Barrett JC, Liotta LA (2002) *Nat Rev Drug Discov* 1:683–695
34. Gander TR, Brody EN, Mehler RE, Heilig JS, Singer BS, Gold L (2003) *Med Lab Observer* 51:11–20

P8

A force-based protein biochip

K. Blank, T. Mai, I. Gilbert, S. Schiffmann, J. Rankl, R. Zivin, C. Tackney,
T. Nicolaus, K. Spinnler, F. Oesterhelt, M. Benoit, H. Clausen-Schaumann
and H. E. Gaub

Proceedings of the National Academy of Sciences USA (2003) 100:11356-11360

A force-based protein biochip

K. Blank*, T. Mai*, I. Gilbert*, S. Schiffmann*, J. Rankl*, R. Zivin†, C. Tackney‡, T. Nicolaus*, K. Spinnler*, F. Oesterheld*, M. Benoit§, H. Clausen-Schaumann*, and H. E. Gaub§¶

*nanotype, Lochhamer Schlag 12, 82166 Gräfelfing, Germany; †Drug Discovery, Johnson & Johnson Pharmaceutical Research & Development, Raritan, NJ 08869; ‡Ortho-Clinical Diagnostics, Raritan, NJ 08869; and §Lehrstuhl für Angewandte Physik and Center for NanoScience, Amalienstrasse 54, 80799 Munich, Germany

Communicated by Heinrich Rohrer, IBM Zurich Research Laboratory, Wollerau, Switzerland, August 4, 2003 (received for review June 1, 2003)

A parallel assay for the quantification of single-molecule binding forces was developed based on differential unbinding force measurements where ligand–receptor interactions are compared with the unzipping forces of DNA hybrids. Using the DNA zippers as molecular force sensors, the efficient discrimination between specific and nonspecific interactions was demonstrated for small molecules binding to specific receptors, as well as for protein–protein interactions on protein arrays. Finally, an antibody sandwich assay with different capture antibodies on one chip surface and with the detection antibodies linked to a congruent surface via the DNA zippers was used to capture and quantify a recombinant hepatitis C antigen from solution. In this case, the DNA zippers enable not only discrimination between specific and nonspecific binding, but also allow for the local application of detection antibodies, thereby eliminating false-positive results caused by cross-reactive antibodies and nonspecific binding.

Previous studies have shown that unbinding forces between molecular interaction partners provide novel and extremely valuable information on the nature of this interaction: specific versus nonspecific interactions and differences in binding modes can be resolved, and even energetically equivalent interactions can be discriminated by forced unbinding (1–5). Moreover, because the binding partners are forced apart, the kinetics of the experiment can be chosen according to assay requirements, and even strong binders, where the spontaneous off-reaction takes weeks or more, may be separated in fractions of seconds (6, 7). Nevertheless, the widespread use of force-based discrimination in bioanalytical applications has been hindered by the limited throughput of these techniques and the high experimental burden imposed by complicated and expensive instrumentation like atomic force microscopes (AFM), optical traps, or the like (8–12). Highly parallel micrometer and submicrometer cantilever arrays, which are currently being developed, might increase the throughput of AFM-based force spectroscopy in the future (13–15). In this study, however, we used a format that not only measures unbinding forces on the single-molecule level in a parallel format, but that is also compatible with standard chip based assays. Here we briefly describe the assay. A more detailed description of the assay is given elsewhere (16).

In standard single-molecule force spectroscopy assays, one of the binding partners is linked to an actuator and the other to a force sensor. The molecules are brought into contact to allow for binding, and on separation the force is recorded as a function of the separation of actuator and force sensor until the bond ruptures (17). In all technical realizations of this principle, the force resolution is limited by thermal fluctuations, which couple into the system via the force sensors (18, 19). We have shown in the past that miniaturization of the force sensors increases their sensitivity (20). Consequently, we employ a single molecule as force sensor in the new format, which is described here. To further improve the force resolution, we implemented a differential measurement format, where the unbinding force of the measured molecular bond is directly compared with the unbinding force of a known reference bond. Both improvements are merged in our Congruent Force Intermolecular Test (C-FIT) format: a molecular chain consisting of the sample bond, a

known reference bond, which serves as force sensor, and a reporter molecule, e.g., a fluorescence label, is formed. The ends of this chain are covalently grafted to two surfaces via polymer spacers. During separation of the two surfaces, the force along the chain increases and the bonds are increasingly loaded with the same force until the weaker of the two bonds ruptures. As a result, after separation of the surfaces the reporter molecule is found at the side of the ruptured chain, containing the stronger bond. Thermal fluctuations broaden this yes/no discrimination by force differences on the order of $k_B T/l$, where l is the characteristic width of the binding potential: the separation between potential minimum and barrier (21).

Obviously, such experiments are primed to be carried out in parallel by using a chip format, with identical molecular chains within each spot and different types of molecules in different spots of the chip. Counting the reporters on either surface, e.g., by counting fluorophores or alternatively measuring fluorescence intensities, then provides a measure for the relative unbinding forces. Analogous to previous studies, bond rupture probabilities may then be calculated taking into account molecular details like spacer lengths and separation rates to correlate the measured unbinding ratios to thermodynamically defined properties such as equilibrium constants and off-rates (7, 21–23).

Methods

Immobilization of Proteins on Slides (Bottom Surface). Proteins and antibodies were purchased from Roche Diagnostics, Biotrend (Cologne, Germany), Calbiochem, Pierce, Biomol (Hamburg, Germany), and pab productions (Hebertshausen, Germany). Hepatitis C virus (HCV) antibodies and the corresponding antigen were provided by Johnson & Johnson. CSS Aldehyde slides (Genetix, Hampshire, U.K.) were incubated with 6 mM HCl-NH₂-PEG-COOH (3,400 g/mol; Shearwater Polymers, Huntsville, AL; PEG, polyethylene glycol). The resulting Schiff bases were then reduced by using 1% aqueous NaBH₄ (VWR Scientific). Alternatively, epoxy slides (Quantifoil Micro Tools, Jena, Germany) were treated with pure diamino PEG (2,000 g/mol; Rapp Polymere, Tübingen, Germany) by melting the diamino PEG and incubating it onto the surface at 75°C for 24 h. The remaining amino groups were then converted into carboxy groups by incubating the slides in a solution of 5 M glutaric anhydride in dry DMF overnight (24). For both types of slides the carboxy groups of the PEG were then activated with a solution containing 50 mM 1-ethyl-3-(3-dimethylaminopropyl)-carbodiimide hydrochloride (EDC; Sigma) and 50 mM *N*-hydroxysuccinimide (NHS; Sigma). The proteins were spotted immediately onto the activated surface. Antibodies were spotted in a concentration of 200 μ g/ml. The antigens were spotted in concentrations between 20 and 100 μ g/ml. After 1 h of incubation, the slides were washed with PBS (Roche Diagnostics)

Abbreviations: HCV, hepatitis C virus; PDMS, poly(dimethylsiloxane); PEG, polyethylene glycol.

¶To whom correspondence should be addressed. E-mail: hermann.gaub@physik.uni-muenchen.de.

© 2003 by The National Academy of Sciences of the USA

containing 0.05% Tween 20 (VWR Scientific). Free reactive groups were blocked in PBS containing 2% BSA (Roth, Karlsruhe, Germany) overnight.

For the sandwich assay the HCV antigen (Johnson & Johnson) was diluted to a concentration of 500 ng/ml in PBS containing 0.4% BSA. This solution was incubated on the slide for 1 h before washing in PBS-Tween 20 (PBST) and PBS.

Immobilization of the DNA Force Sensor Complex on Poly(dimethylsiloxane) (PDMS) (Top Surface). Microstructured PDMS (Sylgard 184, Dow Corning) surfaces were fabricated by using structured 5' silicon wafers as templates, according to standard procedures (25). The PDMS structures consisted of $100 \times 100\text{-}\mu\text{m}$ pads separated by $25\text{-}\mu\text{m}$ -wide and $1\text{-}\mu\text{m}$ -deep grooves to allow for drainage of liquid during the contact process. After cross-linking, the PDMS was cut into $1 \times 1\text{-cm}$ pieces (thickness 1 mm) and activated by water plasma treatment. The PDMS was then derivatized with 3-aminopropyltrimethoxysilane (ABC, Karlsruhe, Germany) to generate free amino groups and coated with aqueous 18 mM NHS-PEG-COOH (5,000 g/mol; Shearwater Polymers) or 18 mM NHS-PEG-NHS (3,000 g/mol; Rapp Polymere). To bind the amino-labeled receptor oligonucleotide (5'-NH₂-AAA AAA AAA ATC TCC GGC TTT ACG GCG TAT-3'; MWG Biotech, Ebersberg, Germany) to the carboxy-modified surface, 50 mM EDC was added to the solution of the receptor oligonucleotide (25 μM) before it was spotted onto the PEG surface. Subsequently, the samples were rinsed with $1 \times \text{SSC}$ (Sigma) containing 0.5% SDS (Sigma) and incubated with an aqueous solution of 2% BSA, to reduce nonspecific binding. Cy3-labeled unzip oligonucleotides (5'-Cy3-ATA CGC CGT AAA GCC GGA GAC AGA TAA GAC GCT ACA TGA AAA AAA AAA AA-(haptene)-3'; metabion, Martinsried, Germany) were diluted to 2 μM in $5 \times \text{SSC}$ and then hybridized for 60 min under a cover slide at room temperature. For all experiments, where antibodies were connected to the DNA force sensor, streptavidin was used to connect biotinylated antibodies to a biotin label at the 3' end of the unzip oligonucleotide. After incubating the PDMS surface with the attached DNA in 1 $\mu\text{g/ml}$ streptavidin in PBS buffer containing 0.4% BSA for 1 h, the surface was rinsed with PBST and PBS. Then, 4 $\mu\text{g/ml}$ biotinylated antibodies were incubated for 1 h, followed by washing with PBST and PBS.

Contact Process and Fluorescence Readout. For the contact process a simple mechanical device was used to ensure that the two surfaces were aligned correctly and were parallel to each other. A force of $\approx 1.4\text{ N}$ was exerted to the 1-cm^2 PDMS surface for 10 min before the two surfaces were separated carefully, rinsed with double-distilled water, and dried with N₂. The bottom surface was then transferred to a GenePix 4000B microarray fluorescence scanner (Axon Instruments, Foster City, CA). Mean fluorescence transfer as well as background fluorescence intensities were determined by using NIH IMAGE software (National Institutes of Health, Bethesda; available at <http://rsb.info.nih.gov/nih-image>).

Results and Discussion

Fig. 1 schematically highlights the implementation of this format, which is similar to a microcontact printing setup (26–28), with the particular goal of discriminating specific from nonspecific interaction on a protein biochip. A short DNA duplex in unzip geometry served as a force sensor. One DNA strand was connected to a microstructured silicone elastomer surface (top surface) via a PEG spacer. The other DNA strand, which also carried the Cy3 fluorescence label, was attached to the ligand of the test complex, here a digoxigenin molecule. This particular type of force sensor was chosen for several reasons. It is known to provide a sequence-dependent force standard; 14 pN in this

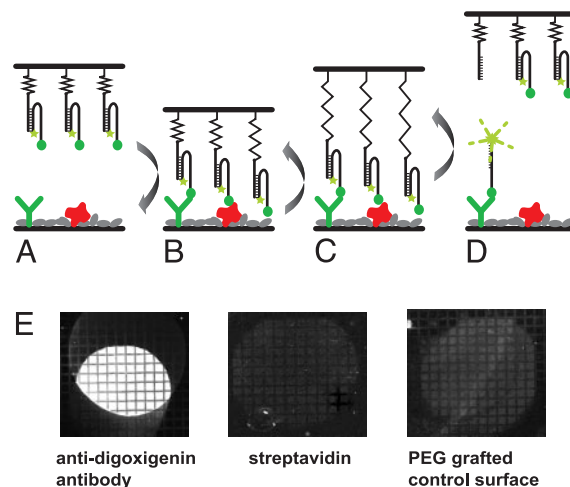


Fig. 1. Experimental realization of the differential force test. (A) DNA duplexes are connected to a microstructured silicone elastomer surface (top surface) via PEG spacers. The spacers are covalently bound to the silicone and in the next step are covalently attached to the 5' end of one of the DNA strands. The complementary DNA strand contains a fluorescence label at the 5' end and a 3'-digoxigenin label attached at the end of a poly(A) spacer sequence. (B) The PDMS surface is brought into contact with a second chip surface (bottom surface) containing spots of immobilized anti-digoxigenin antibodies, streptavidin proteins, or just the PEG passivation layer. (C) On separation of the two chip surfaces, the PEG spacers are extended and a force is built up in the molecular chains between the two surfaces. (D) As the two surfaces are further separated, the weakest molecular bond in each chain breaks, and the fluorescence label remains connected to the stronger bond. (E) After separation of the two surfaces, a fluorescence image of the bottom surface reveals strong fluorescence intensity on the spot carrying the anti-digoxigenin antibodies (Left), no fluorescence on the streptavidin spot (Center), and very little fluorescence on the PEG-coated control area (Right). The dark grids in the fluorescence images represent grooves of the microstructured PDMS. Note that in Left image the spots from the top and the bottom surface do not overlap entirely. Areas where the two spots do not overlap can be used as additional controls.

case (3, 29, 30). Because unzipping occurs in thermodynamic equilibrium, as long as the pulling velocity is kept below 200 nm/s, the unzipping force is independent of the separation rate and also independent of the duplex length (3, 30). The length may therefore be chosen according to the assay requirements such that the spontaneous off-rate is sufficiently slow to provide thermal stability (31). Note that the force threshold can easily be adapted by changing the base composition or the geometry of the DNA force sensor. To get to defined threshold forces above 65 pN, which corresponds to the shearing of long DNA duplexes (32, 33), nucleic acid derivatives like PNA or molecules such as streptavidin and biotin can be used as force sensors.

In Fig. 1B, the digoxigenin-bearing silicone surface was allowed to adhere to a piece of a protein biochip with one spot of covalently attached polyclonal anti-digoxigenin IgG, one spot of streptavidin, and an untreated area. To displace the liquid between the two surfaces and obtain a homogeneous contact, a pressure of 14 kPa was exerted on the silicone surface. If one assumes a grafting density of 10^{12} PEG molecules per square centimeter, 14 kPa corresponds to a force of 1.4 pN per PEG, still well within the range of entropic forces (34). It should be noted that the adhesion of the polymer-coated silicone, and thus the interaction of the molecules at the interface between the two surfaces, is governed by local forces rather than the external force. Therefore, local surface roughness and distortions are compensated to a large degree by the softness of the polymer-coated silicone. Although the mobility of the binding partners is reduced by their polymeric attachment to the surfaces, the

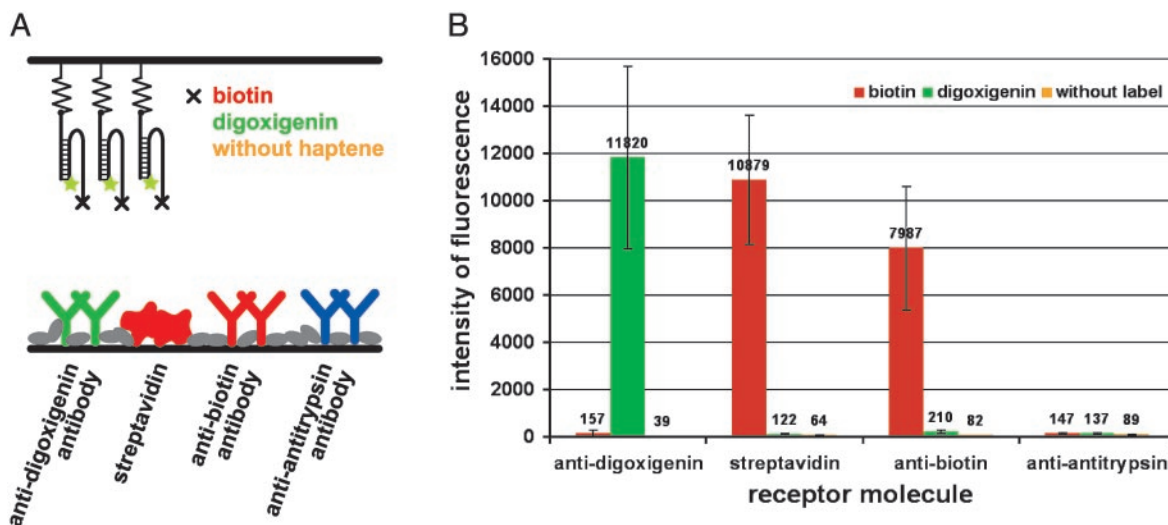


Fig. 2. Detection of specific haptene–protein interactions. (A) The transfer of two oligonucleotides coupled with different haptenes (biotin or digoxigenin) and one oligonucleotide without haptene label (top surface) onto spots containing the respective binding partners, as well as proteins not specific for the haptene (bottom surface), is determined. (B) Diagram showing the fluorescence intensities measured on (left to right) anti-digoxigenin, streptavidin, anti-biotin, and anti-antitrypsin spots on the bottom surface. Red bars correspond to biotin on the top surface, green bars correspond to digoxigenin, and yellow bars correspond to DNA without haptene. The ratio of specific to nonspecific transfer is always better than 50:1 for the two haptenes and their respective negative controls (transfer onto a specific binding partner versus transfer of the same haptene onto another “nonspecific” molecule).

reaction times are still faster than in corresponding conventional assays, because the local concentration of the binding partners in the gap between the two surfaces is extremely high. After 10 min in contact, the surfaces were separated (Fig. 1C), thereby stretching the polymeric anchors and gradually building up the force acting on the bonds and eventually rupturing the molecular interactions under investigation (Fig. 1D). The macroscopic force needed to pull the two surfaces apart is neither recorded nor analyzed. The interaction force is measured intrinsically and independently for each molecular bond. The asymmetry of the binding forces results in an asymmetry of the transfer of the reporter molecules, which is quantified, for example, by fluorescence imaging. Fig. 1E shows the anti-digoxigenin spot brightly illuminated by the Cy3 fluorescence. No fluorescence can be detected on the streptavidin spot, and only a faint pattern is recognizable on the untreated area. The dark grid stems from a trench pattern at the surface of the silicone, which allows for drainage of the liquid during contact formation and separation of the surfaces.

This sequence not only demonstrates the basic principle of the assay, but it furthermore helps to identify suitable reference force levels for the discrimination of specific and nonspecific interactions. This will play an important role in the following experiments. Obviously, the 14 pN, which we chose as reference force, are lower than this particular specific ligand–antibody binding force, resulting in efficient transfer of reporter molecules. At the same time this threshold is also high enough to overcome nonspecific interaction with the protein-coated surface of the streptavidin spot. The slight amount of transfer onto the untreated surface indicates a weak but measurable interaction, which, if needed, may be overcome by raising the threshold force. It might, however, also be caused by a few, but strongly interacting, molecules adhering to localized adhesion sites. In this case, improved blocking strategies might overcome this problem, as can be seen on the streptavidin spot.

Fig. 2 shows that the force threshold defined by the unzipping duplex is appropriate for a number of systems. Several small, haptene-like ligands were tested for their interaction with different proteins. The quantitative analysis (Fig. 2B) demonstrates the high discrimination ratio and the low level of nonspecific

transfer. The fact that more fluorescence is observed on the streptavidin spot than on the anti-biotin spot most likely reflects a difference in the number of accessible binding sites after immobilization, because streptavidin contains more binding sites for biotin than the anti-biotin antibody. Furthermore, the anti-biotin antibodies were polyclonal antibodies, and the batch used may have also contained antibodies, which are not specific for biotin. The anti-digoxigenin antibodies are also polyclonal antibodies. However, a quantitative comparison of biotin transfer levels to those of digoxigenin is not possible, because thermodynamic data are not available. Nevertheless, according to supplier specification the affinity-purified anti-biotin antibodies showed an activity level well below 100%, whereas the affinity-purified anti-digoxigenin antibodies showed 100% activity, which is consistent with the higher transfer onto the anti-digoxigenin spot.

Having demonstrated the functionality of this assay, protein–protein interactions were then investigated. A set of four different antibodies was coupled to the DNA force sensors (Fig. 3A). The setup was assembled sequentially by covalently attaching receptor oligonucleotides to the PEG-coated silicone surface, then hybridizing the biotinylated unzip oligos and treating the surface with streptavidin. Finally, the biotinylated antibodies were attached to this pretreated surface (see *Methods*). The four protein antigens were immobilized on the adjacent chip surface by covalent attachment. Each antibody was tested against all antigens. The fluorescent readings of the corresponding spots are plotted in Fig. 3B. At the chosen reference force of 14 pN, we generally found <13% of nonspecific interaction with other proteins. The anti-rabbit antibody, which was the only polyclonal antibody in this set of experiments, showed rather high nonspecific interactions with GFP and human serum albumin (HSA). Because polyclonal antibodies are obtained from immunized animals (in this case goat), they also may contain fractions of antibodies that are not specific for the target protein or fractions that are specific for other proteins, like GFP or HSA. This may then lead to nonspecific signals. Note, however, that in this case the level of specific transfer onto rabbit antibodies was also significantly higher than the specific signals of the other anti-

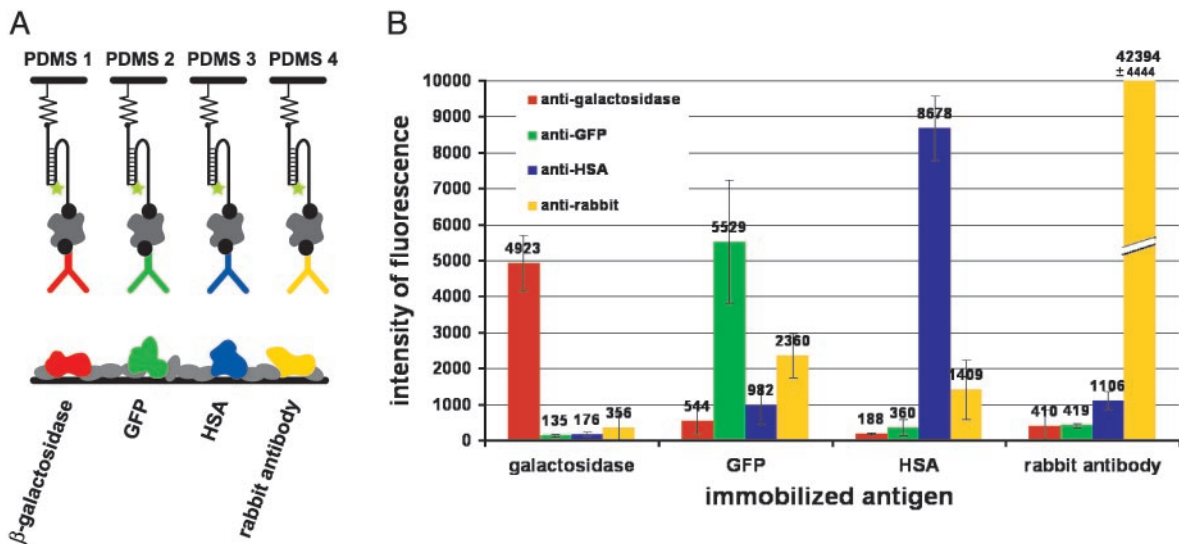


Fig. 3. Detection of specific antibody–antigen interactions. (A) The antibodies were coupled to the DNA force sensor (top surface) via biotin and streptavidin. Their corresponding antigens were immobilized on the bottom surface. Each antibody was tested against all antigens in the respective series (PDMS 1, monoclonal anti- β -galactosidase; PDMS 2, monoclonal anti-GFP; PDMS 3, monoclonal anti-HSA; PDMS 4, polyclonal anti-rabbit). (B) Fluorescence intensities measured on the bottom surface on spots containing (left to right) immobilized β -galactosidase, GFP, HSA, and rabbit antibodies. Red bars correspond to anti- β -galactosidase antibodies on the top surface, green bars correspond to anti-GFP, blue bars correspond to anti-HSA, and yellow bars correspond to anti-rabbit antibodies. The ratio of specific to nonspecific transfer is always better than 7:1 for the four antibodies and their respective negative controls (transfer onto a specific binding partner versus transfer of the same antibody onto another “nonspecific” molecule).

bodies, resulting in <6% background signal for the anti-rabbit antibody.

In the next step, we investigated the applicability of this differential force test to sandwich immunoassays (Fig. 4). Two different capture antibodies against a recombinant HCV antigen, as well as a mixture thereof, were covalently anchored at different spots on one chip surface (bottom surface). The HCV antigen was allowed to bind from solution, and the amount of bound antigen was then quantified by measuring the transfer of two different anti-HCV detection antibodies, as well as the mixture of both, from the second chip surface (top surface; assembly as in Fig. 3). The results are shown in Fig. 4B. The

highest fluorescence intensities are observed on the spots with the high-affinity capture antibody (C2). The lowest fluorescence intensities are observed on spots with the capture antibody with lower affinity (C1), whereas the spots with mixed capture antibodies lie between the two. Furthermore, the fluorescence intensities are always higher for the high-affinity detection antibodies (D1) than for the low-affinity detection antibodies (D2). However, here the maximum is observed for the mixed system. This scenario is plausible, if one considers that the two detection antibodies bind to two different epitopes of the antigen, and therefore up to two antibodies can be transferred to one bound antigen. A quantitative analysis of sample con-

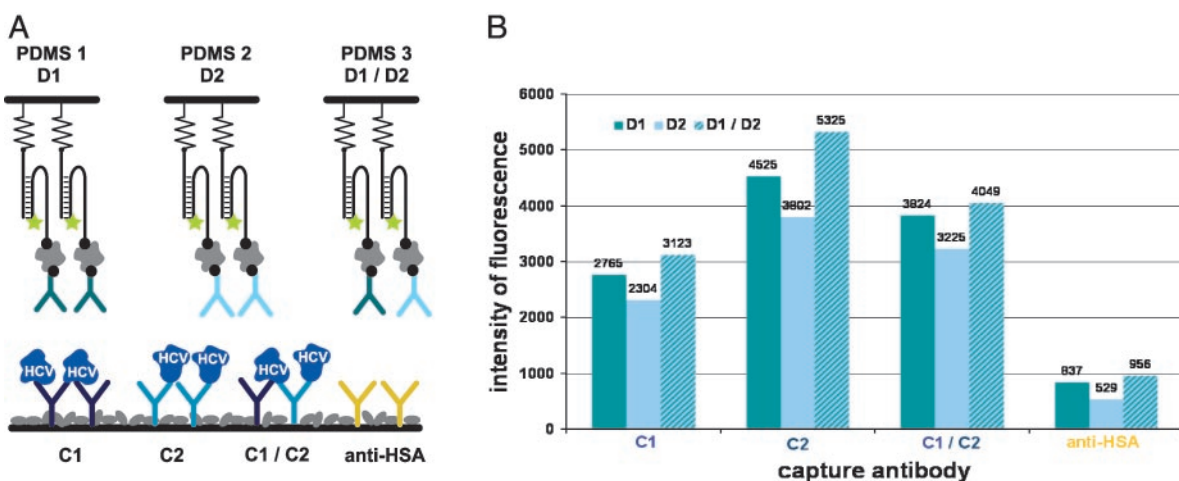


Fig. 4. An antibody sandwich assay for the detection of a hepatitis C virus antigen, based on the differential force test. (A) The detection antibodies are connected to the top surface via a DNA force sensor and a PEG spacer (PDMS 1, D1; PDMS 2, D2; PDMS 3, mixture of D1 and D2). Specific capture antibodies (C1, C2, and C1/C2), as well as one antibody binding human serum albumin as a negative control, are immobilized on the bottom surface. The antigen is bound by shaking the bottom surface in an antigen-containing solution. (B) Fluorescence intensities on the bottom surface on spots with (left to right) C1 capture antibodies, C2 capture antibodies, a mixture of C1 and C2 antibodies, and the negative control. Green bars represent D1 detection antibodies on the top chip surface, blue bars represent D2 detection antibodies, and striped bars represent a mixture of both. Specific to nonspecific ratios vary between 2.4:1 and 10.1:1 depending on the particular combination of sandwich antibodies, which were compared with the negative control.

centrations was also possible with this set-up, and the detection limit was comparable to a conventional sandwich setup, using the same type of capture surface and applying the detection antibodies from solution (data not shown).

In a more general context, this assay may be seen as a technology where a molecular species is brought to a certain position and delivered only if the interaction force at this position exceeds a chosen threshold, i.e., to probe whether a specific binding partner is present at a particular position. Here, we have only begun to exploit the potential of this new assay format. On the silicone surface (top), binding partners may be patterned in register to the pattern of molecules on the capture array (bottom); therefore, we have the option to probe each antigen bound to a capture array with a second antigen-specific binding partner. The second chip surface therefore allows for a second dimension of specific encoding. This is in sharp contrast

to existing multiplexing formats, which rely either on only one antigen-specific molecular interaction or apply the second binding partners in an arbitrary manner by incubation from buffer solution (35–37). As a consequence, in conventional assays, the nonspecific and false-positive signals grow geometrically with the number of different molecular species probed in parallel (38) and thus limit the multiplexing level that can be achieved (39–43). In our case, nonspecific and false-positive signals are independent of array size. This allows for a large number of molecular interactions to be assessed in parallel by reducing the complexity of a multimarker assay to the simplicity of a single-marker ELISA.

We thank Edith Potthoff, Boris Steipe, Andreas Lanckenau, and Claus Duschl for helpful discussions. Part of the project was supported by the Deutsche Forschungsgemeinschaft and the Bundesministerium für Bildung und Forschung.

1. Moy, V. T., Florin, E. L. & Gaub, H. G. (1994) *Science* **266**, 257–259.
2. Merkel, R., Nassoy, P., Leung, A., Ritchie, K. & Evans, E. (1999) *Nature* **397**, 50–53.
3. Rief, M., Clausen-Schaumann, H. & Gaub, H. E. (1999) *Nat. Struct. Biol.* **6**, 346–349.
4. Clausen-Schaumann, H., Seitz, M., Krautbauer, R. & Gaub, H. E. (2000) *Curr. Opin. Chem. Biol.* **4**, 524–530.
5. Williams, M. C. & Rouzina, I. (2002) *Curr. Opin. Struct. Biol.* **12**, 330–336.
6. Grandbois, M., Beyer, M., Rief, M., Clausen-Schaumann, H. & Gaub, H. E. (1999) *Science* **283**, 1727–1730.
7. Evans, E. (2001) *Annu. Rev. Biophys. Biomol. Struct.* **30**, 105–128.
8. Janshoff, A., Neitzert, M., Oberdorfer, Y. & Fuchs, H. (2000) *Angew. Chem. Int. Ed. Engl.* **39**, 3212–3237.
9. Hugel, T. & Seitz, M. (2001) *Macromol. Rapid Commun.* **22**, 989–1016.
10. Mehta, A. D., Rief, M., Spudich, J. A., Smith, D. A. & Simmons, R. M. (1999) *Science* **283**, 1689–1694.
11. Merkel, R. (2001) *Phys. Rep.* **346**, 343–385.
12. Binnig, G., Quate, C. F. & Gerber, C. (1986) *Phys. Rev. Lett.* **56**, 930–933.
13. Fritz, J., Baller, M. K., Lang, H. P., Rothuizen, H., Vettiger, P., Meyer, E., Guntherodt, H., Gerber, C. & Gimzewski, J. K. (2000) *Science* **288**, 316–318.
14. Arntz, Y., Seelig, J. D., Lang, H. P., Zhang, J., Hunziker, P., Ramseyer, J. P., Meyer, E., Hegner, M. & Gerber, C. (2003) *Nanotechnology* **14**, 86–90.
15. Minne, S. C., Yaralioglu, G., Manalis, S. R., Adams, J. D., Zesch, J., Atalar, A. & Quate, C. F. (1998) *Appl. Phys. Lett.* **72**, 2340–2342.
16. Albrecht, C., Blank, K., Lalic-Mülthaler, M., Hirler, S., Mai, T., Gilbert, I., Schiffmann, S., Bayer, T., Clausen-Schaumann, H. & Gaub, H. E. (2003) *Science* **301**, 367–370.
17. Florin, E.-L., Moy, V. T. & Gaub, H. E. (1994) *Science* **264**, 415–417.
18. Bustamante, C., Macosko, J. C. & Wuite, G. J. (2000) *Nat. Rev. Mol. Cell Biol.* **1**, 130–136.
19. Lavery, R., Lebrun, A., Allemand, J.-F., Bensimon, D. & Croquette, V. (2002) *J. Phys. Condens. Matter* **14**, R383–R414.
20. Viani, M. B., Schäffer, T. E., Chand, A., Rief, M., Gaub, H. E. & Hansma, P. K. (1999) *J. Appl. Phys.* **86**, 2258–2262.
21. Evans, E. & Ritchie, K. (1997) *Biophys. J.* **72**, 1541–1555.
22. Evans, E. (1999) *Biophys. Chem.* **82**, 83–97.
23. Schwesinger, F., Ros, R., Strunz, T., Anselmetti, D., Guntherodt, H. J., Honegger, A., Jermutus, L., Tiefenauer, L. & Pluckthun, A. (2000) *Proc. Natl. Acad. Sci. USA* **97**, 9972–9977.
24. Piehler, J., Brecht, A., Valiokas, R., Liedberg, B. & Gauglitz, G. (2000) *Biosens. Bioelectron.* **15**, 473–481.
25. Wilbur, J. L., Kumar, A., Kim, E. & Whitesides, G. M. (1994) *Adv. Mater.* **6**, 600–604.
26. Bernard, A., Renault, J. P., Michel, B., Bosshard, H. R. & Delamar, E. (2000) *Adv. Mater.* **12**, 1067–1070.
27. Bernard, A., Fitzli, D., Sonderegger, P., Delamar, E., Michel, B., Bosshard, H. R. & Biebuyck, H. (2001) *Nat. Biotechnol.* **19**, 866–869.
28. Xia, Y. & Whitesides, G. M. (1998) *Annu. Rev. Mater. Sci.* **28**, 153–184.
29. Essevaz-Roulet, B., Bockelmann, U. & Heslot, F. (1997) *Proc. Natl. Acad. Sci. USA* **94**, 11935–11940.
30. Bockelmann, U., Essevaz-Roulet, B. & Heslot, F. (1997) *Phys. Rev. Lett.* **79**, 4489–4492.
31. Strunz, T., Oroszlan, K., Schäfer, R. & Güntherodt, H.-J. (1999) *Proc. Natl. Acad. Sci. USA* **96**, 11277–11282.
32. Clausen-Schaumann, H., Rief, M., Tolksdorf, C. & Gaub, H. E. (2000) *Biophys. J.* **78**, 1997–2007.
33. Williams, M. C., Wenner, J. R., Rouzina, I. & Bloomfield, V. A. (2001) *Biophys. J.* **80**, 1932–1939.
34. Oesterhelt, F., Rief, M. & Gaub, H. E. (1999) *New J. Phys.* **1**, 6.1–6.11.
35. Ekins, R. P. (1989) *J. Pharm. Biomed. Anal.* **7**, 155–168.
36. Ekins, R. P. & Chu, F. (1994) *Trends Biotechnol.* **12**, 89–94.
37. Wagner, P. & Kim, R. (2002) *Curr. Drug Discov.* **5**, 23–28.
38. Abbott, A. (2002) *Nature* **415**, 112–114.
39. Mendoza, L. G., McQuary, P., Mongan, A., Gangadharan, R., Brignac, S. & Eggers, M. (1999) *BioTechniques* **27**, 778–788.
40. Huang, R. P. (2001) *J. Immunol. Methods* **255**, 1–13.
41. Mitchell, P. (2002) *Nat. Biotechnol.* **20**, 225–229.
42. MacBeath, G. (2002) *Nat. Genet.* **32**, Suppl. 2, 526–532.
43. Petach, H. & Glod, L. (2002) *Curr. Opin. Biotechnol.* **13**, 309–314.

P9

DNA: A Programmable Force Sensor

C. Albrecht, K. Blank, M. Lalic-Mülthaler, S. Hirler, T. Mai, I. Gilbert, S. Schiffmann,
T. Bayer, H. Clausen-Schaumann and H. E. Gaub

Science (2003) 301: 367-370

9. D. M. Wellik, P. J. Hawkes, M. R. Capecchi, *Genes Dev.* **16**, 1423 (2002).
10. G. M. Wahba, S. L. Hostikka, E. M. Carpenter, *Dev. Biol.* **231**, 87 (2001).
11. D. M. Wellik, M. R. Capecchi, data not shown.
12. S. L. Hostikka, M. R. Capecchi, *Mech. Dev.* **70**, 133 (1998).
13. Y. Harault, J. Beckers, M. Gerard, D. Duboule, *Dev. Biol.* **208**, 157 (1999).
14. P. Dolle, J. C. Izpisua-Belmonte, H. Falkenstein, A. Renucci, D. Duboule, *Nature* **342**, 767 (1989).
15. P. Dolle, J. C. Izpisua-Belmonte, J. M. Brown, C. Tickle, D. Duboule, *Genes Dev.* **5**, 1767 (1991).
16. B. Favier *et al.*, *Development* **122**, 449 (1996).
17. M. Suzuki, A. Kuroiwa, *Mech. Dev.* **118**, 241 (2002).
18. M. Hildebrand, *Analysis of Vertebrate Structure* (Wiley, New York, ed. 4, 1995).
19. E. B. Lewis, *Nature* **276**, 565 (1978).
20. M. J. Cohn, C. Tickle, *Nature* **399**, 474 (1999).
21. M. Kmita, B. Tarchini, D. Duboule, Y. Harault, *Development* **129**, 5521 (2002).
22. We are indebted to S. L. Hostikka for preparation of

the *Hoxc10* and *Hoxc11* mutant mice, and we thank J. F. Fallon, S. Sakonju, and B. W. Bisgrove for discussions of these data before publication.

Supporting Online Material

www.sciencemag.org/cgi/content/full/301/5631/363/DC1

SOM Text

References

14 April 2003; accepted 9 June 2003

DNA: A Programmable Force Sensor

Christian Albrecht,¹ Kerstin Blank,¹ Mio Lalic-Mülthaler,¹ Siegfried Hirler,¹ Thao Mai,¹ Ilka Gilbert,¹ Susanne Schiffmann,¹ Tom Bayer,¹ Hauke Clausen-Schaumann,^{1*} Hermann E. Gaub²

Direct quantification of biomolecular interaction by single-molecule force spectroscopy has evolved into a powerful tool for materials and life sciences. We introduce an approach in which the unbinding forces required to break intermolecular bonds are measured in a differential format by comparison with a known reference bond (here, a short DNA duplex). In addition to a marked increase in sensitivity and force resolution, which enabled us to resolve single-base pair mismatches, this concept allows for highly specific parallel assays. This option was exploited to overcome cross-reactions of antibodies in a protein biochip application.

Within the past decade, a variety of experimental tools based on applying and measuring piconewton forces between single molecules have been developed and have contributed to a better understanding of the mechanics of biomolecules and molecular bonds (1–4). Force measurements reveal detailed insights into binding-potential landscapes and into functional aspects of the molecules under investigation, and as a result, force has become a new structural and functional parameter in materials and life sciences. Receptor-ligand pairs (5–8), protein and nucleic acid structures (9–15), and even covalent bonds (16) have been investigated, and it has become evident that biomolecular processes are governed by piconewton forces. However, two major bottlenecks have hindered the widespread use of single-molecule mechanics: sizable instrumental effort and limited force resolution. To our knowledge, no single-base pair mismatch detection by single-molecule force measurements has been reported, despite numerous efforts. The best resolution to date has been 10 base pairs (bp), obtained by shearing and unzipping short oligomers by atomic force microscopy (AFM) (17, 18).

In conventional single-molecule force spectroscopy, inter- or intramolecular forces

are exerted and measured with microscopic force sensors like AFM cantilevers or beads in optical or magnetic traps (19, 20). With state-of-the-art instrumentation, the force resolution is limited only by thermal fluctuations that are detected by the force sensor. Arguments based on the fluctuation-dissipation theorem predict that a reduction of the sensor size should improve the signal-to-noise ratio (21). This has been verified in experimental studies using a new generation of small AFM cantilevers (22). The logical extrapolation is to replace the cantilever by a single elastic molecule. To increase the precision of the assay even further, we chose a differential measurement format, where rupture forces of two molecular complexes are directly compared with each other. This differential format offers several advantages. Because of the high symmetry of the assay, most external disturbances cancel out (23). In addition, for most applications, a precise measure of the difference is more valuable than two absolute values with their respective error bars, such as the ranking of binders or a single-base pair mismatch detection in a DNA sequence.

In our setup (Fig. 1), the cantilever spring was replaced by a polymeric anchor and a known molecular bond (reference bond) carrying a fluorescence label. The molecular bond under investigation was directly compared to this reference bond, which served as a molecular force standard. During separation of the two surfaces, the polymeric anchor was stretched, and the force acting along the mo-

lecular chain consisting of the sample and labeled reference complex built up gradually, until the weaker of the two bonds ruptured. The difference in the stability of the two bonds breaks the symmetry in this experiment. As a result, there is a higher probability that the fluorescence label will end up on the side of the stronger bond rather than on the side of the weaker bond. This process can be seen as a 1-bit analog-to-digital conversion broadened by thermal fluctuations (24). Many single-molecule force measurements can be performed simultaneously, using two congruent chip surfaces and different spots containing the molecules of interest. Counting the labels on each side, for instance, by single-molecule optics, provides a quantitative measure for the differences between the distributions of the bond rupture probabilities of the two molecular complexes. It is equivalent to measuring the fluorescence intensities, which are proportional to the densities of the fluorescence labels (25). Although a large number of molecules are probed simultaneously, the actual force measurement is still performed at the single-molecule level, because each sample bond is probed individually by a single reference bond.

Figure 1B illustrates the setup schematically. The rupture forces of two DNA strands with different hybridization lengths (a 20-bp duplex and a 25-bp duplex) are directly compared. Both oligonucleotides are bridged with a conjugated 65-base oligonucleotide, carrying a terminal Cy5 fluorescent label. The resulting 20-bp duplex is coupled to an activated glass surface, and the 25-bp duplex to a soft polydimethylsiloxane (PDMS) stamp (26–28), both by means of polyethylene glycol (PEG) spacers. Figure 1C shows fluorescence images of the glass surface containing the capture oligonucleotide and the labeled sample oligonucleotide before the two surfaces were brought into contact and separated again, and both glass (bottom) and PDMS (top) after the separation of the two surfaces. Because the PDMS stamp has a grid pattern of trenches to ease the water flux at the surface during separation, the transferred labels form a checkerboard pattern on the PDMS. No transfer occurred in the trenches, so that here the initial label density was maintained on the glass surface, whereas in the contact areas (squares), labels were transferred from the glass to the PDMS side.

¹Nanotype GmbH, Lochhamer Schlag 12, 82166 Gräfelfing, Germany. ²Lehrstuhl für Angewandte Physik and Center for Nano-Science, Amalienstrasse 54, 80799 München, Germany.

*To whom correspondence should be addressed. E-mail: hauke.clausen-schaumann@nanotype.de

REPORTS

A direct quantification of the fluorescent label density is limited by the different optical and chemical properties of the two surfaces—glass chip and PDMS stamp—which influence the quantum yield and the excitation efficiency of the label. In addition, the coupling efficiencies to the two chip surfaces may differ. However, the symmetry of the experiment can be restored by placing the two molecules of inter-

est on the same side of the assay and measuring both against a common reference on the other side (29). This is the format chosen for the following experiments, where single-base pair mismatches and different binding modes of DNA were investigated. A quantitative analysis of the experiment that is shown in Fig. 1 is provided in fig. S1.

To investigate the force resolution of the differential force test, we measured the reduction of the unbinding forces caused by a single-base pair mismatch in a 20-bp DNA duplex. Figure 2A illustrates the experimental setup and shows the superposition of the histograms of fluorescence intensities, obtained on the PDMS surface, after separating the two chips. The main peaks of the two histograms are clearly separated and are to a good approximation of Gaussian shape, indicating a homogeneous surface coverage with statistical distribution of the bond-rupture process. The spike (to the left) stems from the trenches of the grid and reflects the fluorescence background. The mean fluorescence intensities were determined by fitting Gaussian distributions to the histogram peaks. The ratio of these intensities, which directly represents the ratio of the bond-rupture probabilities of mismatch to perfect match was found to be 1.7. Because the half width of the two peaks is less than one-third of the difference of the peak values, a quantitative single-

nucleotide polymorphism assay with high precision is possible. The experiment was conducted in a buffer solution containing 150 mM NaCl at room temperature. Under these conditions, thermal off-rates are extremely low (30), and discrimination between mismatch and perfect match sequences is difficult to obtain in conventional equilibrium binding assays (31, 32). This high thermal stability ensures that in the force-based assay, the data are not obscured by spontaneous strand-separation events or differences in hybridization efficiencies (33).

On conventional DNA chips, single-base pair mismatches are detected by identifying differences in the thermal off-rate or the equilibrium constant. In both cases, stringent conditions are established by reducing the salt concentration (or alternatively increasing temperature) such that the DNA duplexes to be analyzed either dissociate at different time scales or bind with distinguishable binding ratios (34). Because both ionic strength and temperature are global parameters, a delicate compromise of these parameters has to be chosen to establish satisfactory ambient conditions for all the different spots on the chip. These global boundary conditions impose severe limitations on the sequences that can be tested in parallel on the same chip and require large numbers of additional control spots (35, 36). In contrast, in the differential force for-

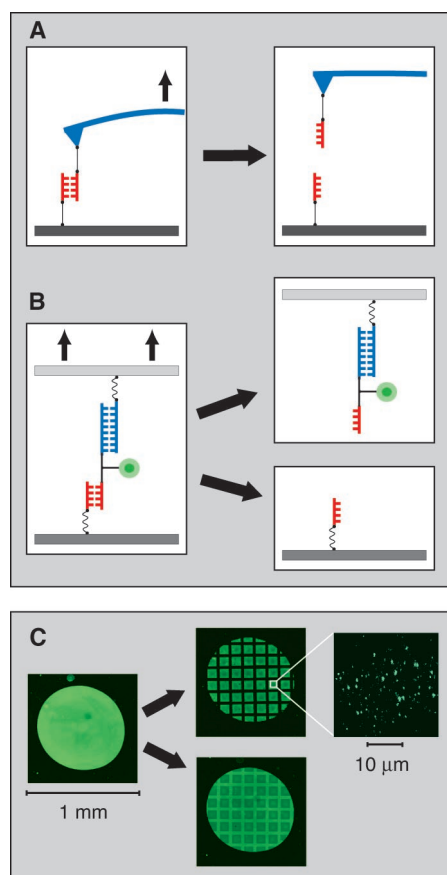


Fig. 1. (A) Conventional, AFM-based single-molecule force spectroscopy, in which the rupture force required to break a molecular bond, such as a DNA duplex (red), is measured with a cantilever spring (blue). (B) The differential force test, in which the rupture force of a sample bond (red) is measured by comparing it with a known reference bond (blue), which serves as a molecular force standard. Upon loading the chain of polymer spacers, sample bond, and reference bond, the weaker bond has a higher probability of rupturing than the stronger one. Consequently, most of the probed fluorescence labels (green) end up with the stronger bond after separating the two surfaces. (C) (left) Cy5 fluorescence image of a spot containing the molecular chains of polymer spacers, sample, and reference duplexes before connecting the biotinylated reference duplexes to the second chip surface. (middle) Cy5 fluorescence image of both chip surfaces—microstructured PDMS (top) and glass (bottom)—after separating them again. (right) PDMS surface at single-molecule resolution after separating the two surfaces. The image was obtained by TIRF.

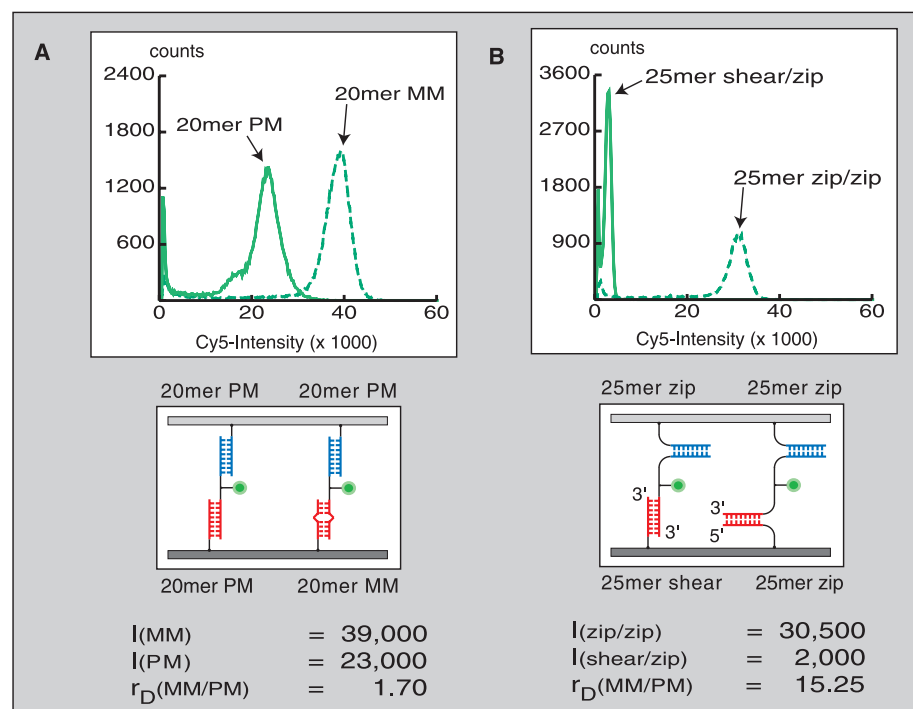


Fig. 2. (A) Histograms of a perfectly matching (PM) 20-bp DNA duplex (left) as compared with a 20-bp duplex that has a single-base pair mismatch (MM). Both duplexes were probed with a 20-bp reference complex that is reverse to the perfectly matching 20-bp duplex. Both sample duplexes are identical, except for a single base mutation (G \rightarrow C) that was introduced at position 13 of the capture oligonucleotide. (B) Histograms of identical 25-bp DNA duplexes in both shear (left) and unzip geometry (right), both of which have been probed with an identical 25-bp duplex in unzip geometry. I , mean fluorescence intensity; r_D , discrimination ratio.

mat, the stringency imposed by the reference complex is a local boundary condition. Both the sequence and the length of the reference complex on the stamp may be chosen for every sample spot on the chip accordingly, allowing optimum force resolution and background discrimination for every spot. Thermodynamic stringency is global, whereas mechanical stringency is local. The combination of maximum resolution and local stringency is desirable for the precise quantification of interactions.

Figure 2B highlights an additional and unique feature of force-based assays: the discrimination among energetically and kinetically equivalent interactions. Both hybrids, the one in shear geometry and the one in unzip geometry, have identical sequences and, therefore, have the same binding energy, as well as the same thermal on-rates and off-rates. However, upon forced dissociation, the complex in unzip geometry has a probability of rupturing that is more than 15 times as high as that of the

complex in shear geometry, as can be derived from the peak positions of the histograms in Fig. 2B. This pronounced difference is consistent with earlier measurements (13, 17, 37, 38) in which unzipping forces of 14 pN and values that were more than three times as high for the shear geometry were measured under comparable conditions (39).

The discrimination between different binding modes, as illustrated above, and the concept of mechanical stringency offer striking advantages when applied to the field of protein arrays. In this field, it is crucial to discriminate between specific and nonspecific interactions, and it is difficult to define a common set of stringent

ambient conditions for many different proteins (40, 41). Proteins typically interact with each other specifically over well-defined binding sites, whereas nonspecific interactions with other proteins and with surfaces occur over larger surface areas (42). As shown in Fig. 2B, discrimination between these two binding modes can then be reliably achieved using a low-force but high-affinity force sensor, such as a DNA duplex in unzip conformation. Figure 3 shows that the threshold force defined by such a DNA duplex in unzipping geometry is well suited to discriminate between specific and nonspecific binding for a variety of antibody-antigen interactions. At the same time, the affinity is high enough to provide a stable anchor. The antibodies can be safely “delivered” to their respective antigens. In addition, if needed, other threshold forces can easily be programmed into the DNA reference complex by changing the base composition or the binding geometry.

The advantages of the force-based delivery of antibodies become more apparent when applied to capture arrays based on a sandwich format. In conventional sandwich arrays, each detection antibody can interact with all spots of the array. Therefore, each analyte molecule that is bound to the array can be decorated by detection antibodies, even the ones that are bound nonspecifically or because of cross-reactive capture antibodies (43). Consequently, the nonspecific background and the number of false-positives grow geometrically with the number of spots on the chip, which severely limits the multiplexing capabilities of protein capture arrays (44). The differential force assay allows for the local application of specific detection antibodies, and the second chip surface therefore provides for a second dimension of specific encoding (45). Figure 4 shows an example of a cross-reactive capture antibody that is specific for both human and murine interleukin-5 (IL-5). In a conventional protein array, discrimination between human and murine antigens is not possible (Fig. 4A) with this capture antibody, and the assay generates false-positive results (46). In our assay, the second chip surface (top surface) allows the definition of two specific spots for the two different antigens, even if the same cross-reactive capture antibody is used in both spots of the capture surface (bottom). Specific detection and reliable discrimination of both antigens are now possible in a single step. This illustrates the potential of our assay to overcome a major bottleneck in the field of protein biochips, namely, the lack of specificity caused by nonspecific interactions and cross-reactions (47, 48).

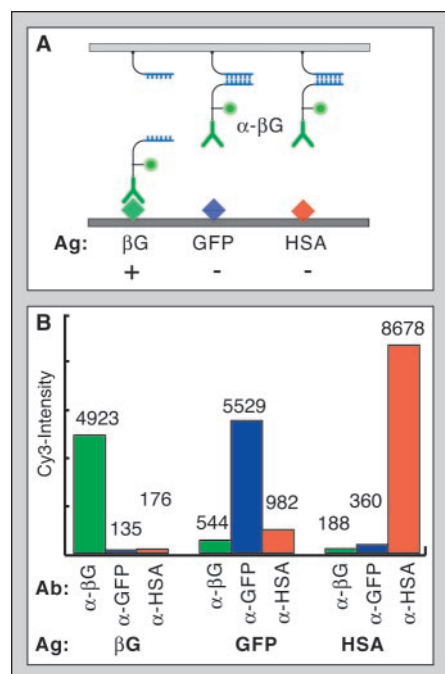


Fig. 3. Discrimination between specific and non-specific antibody-antigen interactions with a DNA force sensor. (A) Three spots with different proteins [β -galactosidase (β G), green fluorescent protein (GFP), and human serum albumin (HSA)] on the bottom surface were probed with antibodies to β -galactosidase, which were connected to the top surface by way of DNA force sensors in unzipping conformation. Upon separation of the two surfaces, only β -galactosidase, which was probed with its specific antibody, was decorated with the fluorescently labeled antibody. (B) Fluorescence intensities (arbitrary units) on three different antigens (on the bottom surface) after each antigen was probed with three different antibodies, which were connected to the top surface by way of DNA zippers. Ab, antibody; Ag, antigen.

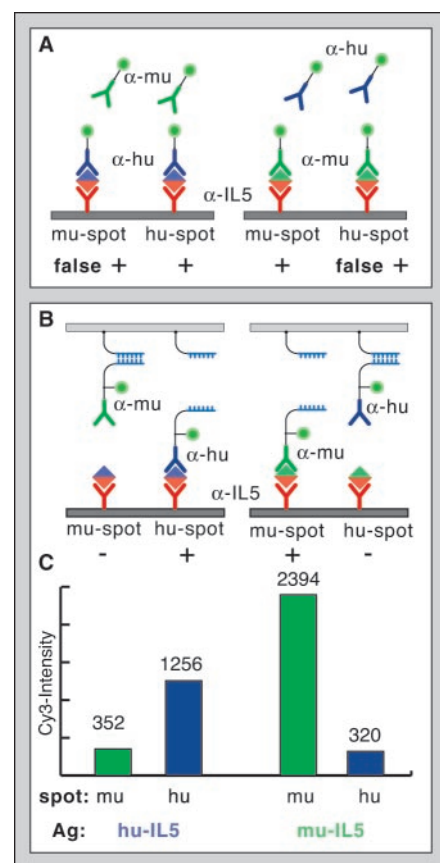


Fig. 4. Antibodies to IL-5, which bind both murine IL-5 and human IL-5, were used as capture antibodies in a sandwich immunoassay. The detection antibodies are specific for either murine IL-5 or human IL-5. (A) If both detection antibodies are applied simultaneously in buffer solution, as in a conventional protein array, the discrimination between murine (mu) and human (hu) antigens is not possible, because of the cross-reactivity of the capture antibody. (B) If the detection antibodies are coupled to the top surface by way of DNA force sensors, they can be applied locally. The second chip surface provides a second dimension for specific encoding, making it possible to define a murine and a human spot on the array and to discriminate between the two antigens. (C) Fluorescence intensities on the murine spots (green) and the human spots (blue) after incubation of human (left) and murine (right) antigen. Ag, antigen.

References and Notes

1. C. Bustamante, J. C. Macosko, G. J. Wuite, *Nature Rev. Mol. Cell Biol.* **1**, 130 (2000).
2. H. Clausen-Schaumann, M. Seitz, R. Krautbauer, H. E. Gaub, *Curr. Opin. Chem. Biol.* **4**, 524 (2000).

REPORTS

3. R. Merkel, *Phys. Rep.* **346**, 343 (2001).
4. R. Lavery, A. Lebrun, J.-F. Allemand, D. Bensimon, V. Croquette, *J. Phys. Cond. Matter* **14**, R383 (2002).
5. V. T. Moy, E.-L. Florin, H. E. Gaub, *Science* **266**, 257 (1994).
6. E.-L. Florin, V. T. Moy, H. E. Gaub, *Science* **264**, 415 (1994).
7. R. Merkel, P. Nassoy, A. Leung, K. Ritchie, E. Evans, *Nature* **397**, 50 (1999).
8. F. Schwesinger et al., *Proc. Natl. Acad. Sci. U.S.A.* **97**, 9972 (2000).
9. S. B. Smith, Y. Cui, C. Bustamante, *Science* **271**, 795 (1996).
10. M. S. Kellermayer, S. B. Smith, H. L. Granzier, C. Bustamante, *Science* **276**, 1112 (1997).
11. M. Rief, M. Gautel, F. Oesterhelt, J. M. Fernandez, H. E. Gaub, *Science* **276**, 1109 (1997).
12. A. F. Oberhauser, P. E. Marszalek, H. P. Erickson, J. M. Fernandez, *Nature* **393**, 181 (1998).
13. M. Rief, H. Clausen-Schaumann, H. E. Gaub, *Nature Struct. Biol.* **6**, 346 (1999).
14. F. Oesterhelt et al., *Science* **288**, 143 (2000).
15. T. Hugel et al., *Science* **296**, 1103 (2002).
16. M. Grandbois, M. Beyer, M. Rief, H. Clausen-Schaumann, H. E. Gaub, *Science* **283**, 1727 (1999).
17. T. Strunz, K. Oroszlan, R. Schafer, H. J. Guntherodt, *Proc. Natl. Acad. Sci. U.S.A.* **96**, 11277 (1999).
18. R. Krautbauer, M. Rief, H. E. Gaub, *Nano Lett.* **3**, 493 (2003).
19. A. Janshoff, M. Neitzert, Y. Oberdorfer, H. Fuchs, *Angew. Chem. Int. Ed.* **39**, 3212 (2000).
20. A. D. Mehta, M. Rief, J. A. Spudich, D. A. Smith, R. M. Simmons, *Science* **283**, 1689 (1999).
21. F. Gittes, C. F. Schmidt, *Eur. Biophys. J.* **27**, 75 (1998).
22. M. B. Viani et al., *J. Appl. Phys.* **86**, 2258 (1999).
23. In conventional force spectroscopy, molecular forces are measured as displacements against spring constants or trap slopes. Because the nature of intra- and intermolecular forces is fundamentally different from metal or silicon springs (or from optical or magnetic traps), all kinds of fluctuations or drifts, such as temperature and pH, will alter the measured signal. In the differential molecular format, each cancels out the effects of the other.
24. As long as the sample and reference complexes are similar, for example, consisting of two antibodies or two DNA oligomers (as in our case), the potential-energy landscape of the two complexes will be comparable. This means that the difference of the unbinding forces is approximately independent of the rate at which the force was built up. Consequently, this assay format is insensitive to variations of the spacer length or to separation velocity. Also, the force threshold of the common reference has to lie either within the force window defined by the molecular bonds under investigation, or close to one of these forces. The force distributions are broadened by thermal fluctuations on the order of $k_B T/l$, where k_B is Boltzmann's constant, T is temperature, and l is the characteristic width of the binding potential. Consequently, the window of possible reference forces is broadened by approximately the same amount (49, 50).
25. This is true as long as the lateral density is kept below the fluorescence resonance energy transfer limit.
26. A. Kumar, N. L. Abbott, E. Kim, H. A. Biebuyck, G. M. Whitesides, *Acc. Chem. Res.* **28**, 219 (1995).
27. Y. Xia, G. M. Whitesides, *Annu. Rev. Mater. Sci.* **28**, 153 (1998).
28. A. Bernard, B. Michel, E. Delamar, *Anal. Chem.* **73**, 8 (2001).
29. Different optical and chemical properties, as well as differences in coupling efficiencies to the two surfaces, are compensated in this way.
30. D. Pörschke, M. Eigen, *J. Mol. Biol.* **62**, 361 (1971).
31. C. Schildkraut, S. Lifson, *Biopolymers* **3**, 195 (1965).
32. P. Nollau, C. Wagener, *J. Int. Fed. Clin. Chem.* **9**, 162 (1997).
33. The discrimination between mismatch and perfect match could clearly be improved by decreasing the salt concentration or increasing the temperature and making use of both spontaneous and force-induced strand separation. However, in this study, we focused on forced unbinding events.
34. M. Chee et al., *Science* **274**, 610 (1996).
35. R. J. Lipshutz, S. P. Fodor, T. R. Gingeras, D. J. Lockhart, *Nature Genet.* **21**, 20 (1999).
36. F. Naef, D. A. Lim, N. Patil, M. Magnasco, *Phys. Rev. E* **65**, 040902 (2002).
37. U. Bockelmann, B. Essevez-Roulet, F. Heslot, *Phys. Rev. Lett.* **79**, 4489 (1997).
38. B. Essevez-Roulet, U. Bockelmann, F. Heslot, *Proc. Natl. Acad. Sci. U.S.A.* **94**, 11935 (1997).
39. The difference in the bond-rupture probabilities of the two chosen unbinding geometries is much larger than the difference in unbinding forces. Our assay measures the ratio of unbinding probabilities directly. Therefore, differences down to the order of the thermal force scale $k_B T/l$ can be resolved.
40. R. P. Ekins, *J. Pharm. Biomed. Anal.* **7**, 155 (1989).
41. R. P. Ekins, F. Chu, *Trends Biotechnol.* **12**, 89 (1994).
42. P. Mitchell, *Nature Biotechnol.* **20**, 225 (2002).
43. L. G. Mendoza et al., *Biotechniques* **27**, 778 (1999).
44. A. Abbott, *Nature* **415**, 112 (2002).
45. H. Petach, L. Glod, *Curr. Opin. Biotechnol.* **13**, 309 (2002).
46. C. Abrecht et al., data not shown.
47. G. MacBeath, *Nature Genet.* **32** (suppl. 2), 526 (2002).
48. P. Cutler, *Proteomics* **3**, 3 (2003).
49. E. Evans, K. Ritchie, *Biophys. J.* **72**, 1541 (1997).
50. P. Hänggi, P. Talkner, M. Borkovec, *Rev. Mod. Phys.* **62**, 251 (1990).
51. We thank M. Rief for kindly providing the total internal reflection fluorescence (TIRF) data showing single-molecule fluorescence, M. Benoit for technical support, F. Oesterhelt, C. Duschl, and D. Mendik for helpful discussions. Supported by the Nanobiotechnology and Proteomics program of the Bundesministerium für Bildung und Forschung (grants 13N8141 and O312821A) and the Bayerische Forschungsstiftung.

Supporting Online Material

www.sciencemag.org/cgi/content/full/301/5631/367/DC1

Materials and Methods

Fig. S1

19 March 2003; accepted 13 June 2003

Allosteric Activators of Glucokinase: Potential Role in Diabetes Therapy

Joseph Grimsby,¹ Ramakanth Sarabu,¹ Wendy L. Corbett,¹
 Nancy-Ellen Haynes,¹ Fred T. Bizzarro,¹ John W. Coffey,¹
 Kevin R. Guertin,¹ Darryl W. Hilliard,^{1*} Robert F. Kester,¹
 Paige E. Mahaney,^{1†} Linda Marcus,¹ Lida Qi,¹ Cheryl L. Spence,¹
 John Tengi,¹ Mark A. Magnuson,² Chang An Chu,¹
 Mark T. Dvorozniak,¹ Franz M. Matschinsky,³ Joseph F. Grippo^{1‡}

Glucokinase (GK) plays a key role in whole-body glucose homeostasis by catalyzing the phosphorylation of glucose in cells that express this enzyme, such as pancreatic β cells and hepatocytes. We describe a class of antidiabetic agents that act as nonessential, mixed-type GK activators (GKAs) that increase the glucose affinity and maximum velocity (V_{\max}) of GK. GKAs augment both hepatic glucose metabolism and glucose-induced insulin secretion from isolated rodent pancreatic islets, consistent with the expression and function of GK in both cell types. In several rodent models of type 2 diabetes mellitus, GKAs lowered blood glucose levels, improved the results of glucose tolerance tests, and increased hepatic glucose uptake. These findings may lead to the development of new drug therapies for diabetes.

Glucose homeostasis is lost in type 2 diabetes because of combined defects in both insulin secretion and insulin action (1, 2). The characterization of patients with abnormal glycaemic control due to either gain- or loss-of-function mutations in GK has provided new insights into the pathogenesis of type 2 dia-

betes. Loss-of-function mutations in the gene encoding GK have been linked to maturity-onset diabetes of the young type 2 (MODY2), an autosomal dominant form of diabetes mellitus characterized by early onset and mild chronic fasting hyperglycemia (3, 4). MODY2 patients display impaired glucose responsiveness of β cells, decreased net accumulation of glycogen, and increased hepatic glucose production after meals (5, 6). The GK mutations found in MODY2 patients result in decreased activity of this enzyme as a result of reduction in its V_{\max} and/or reduced affinity toward its substrates, glucose and adenosine triphosphate (ATP) (7–11). In contrast, gain-of-function GK mutations, which increase the catalytic activity of GK, cause persistent hyperinsulinemic hypoglycemia of infancy as a result of lowering the threshold

¹Department of Metabolic Diseases, Hoffmann-La Roche Inc., Nutley, NJ 07110, USA. ²Department of Molecular Physiology and Biophysics, Vanderbilt University, Nashville, TN 37232, USA. ³Department of Biochemistry and Diabetes Center, University of Pennsylvania School of Medicine, Philadelphia, PA 19104, USA.

*Present address: Lilly Research Laboratories, Lilly Corporate Center, Indianapolis, IN 46285, USA.

†Present address: Chemical Sciences, Wyeth Research, 500 Arcola Road, Collegeville, PA 19426, USA.

‡To whom correspondence should be addressed. E-mail: joseph.grippo@roche.com

11 Curriculum vitae

Kerstin Blank

Date of Birth 1st February 1974

Place of Birth Ochsenfurt

Nationality German

Education and professional experience

1980 to 1984 Elementary School, Markt Einersheim/Germany

1984 to 1993 Grammar School, Scheinfeld/Germany

09/1993 to 07/1996 Laboratory Assistant for Biology (vocational training)
Julius-Maximilians Universität, Würzburg/Germany

09/1996 to 01/2001 Diploma in Biotechnology
University of Applied Sciences, Jena/Germany

Thesis in the group of Prof. Dr. Andreas Plückthun
University of Zurich/Switzerland

Title: protein engineering of antibody scFv-fragments as
ligands for affinity chromatography

03/2001 to 09/2003 group leader and project manager “protein biochips”
nanotype GmbH, Munich/Germany

10/2003 to Present PhD in Physics
Chair for Applied Physics (Prof. Dr. Hermann Gaub)
Ludwig-Maximilians-Universität, Munich/Germany

12 Acknowledgements

Finally, I want to thank a lot of people who have contributed to the success of my projects either by sharing molecules, equipment, knowledge or data or even more important giving their support in many scientific and non-scientific problems:

Prof. Dr. Hermann E. Gaub

... for the opportunity to do my thesis in his group
... for the possibility to participate in many different projects
... for some stupid ideas (from a biologist's view) leading to two publications finally

Ludmila Mendelevitch and Anna Schmitz

... for help in preparing some of the molecules
... for the work on the antibody project, which is not part of this thesis

Hermann Gump and Elias Puchner

... for the very good collaboration on the lipase project
... for the time sitting in the dark in front of the screen to see the dirt blinking
... and for your helpful suggestions regarding this thesis

Stefan Kufer and Thomas Nicolaus

... for the collaboration on the hAGT project
... for the many helpful discussions about immobilizing biomolecules

Dr. Gregor Neuert, Dr. Ferdinand Kühner, Dr. Martin Benoit and Dr. Dieter Braun

... for answering all my stupid questions about basic physics
... for the many inspiring discussions

Dr. Kay Gottschalk

... for the discussions about antibody on-rates
... for the calculations of the antibody on-rates
... and for your help in interpreting the antibody data and writing the publication

Angelika Kardinal and Verena Thalhammer

... for the perfect organization of the chemistry lab
... for the background music when doing boring work

The rest of the gambicrew

... for many inspiring discussions
... for the very good atmosphere
... and for all the Weisswüschtl lunch breaks...

The Bioscope project partners

... for sharing knowledge about lipases and coupling chemistry
... for many interesting discussions and a lot of helpful ideas
... and last but not least for the fantastic meetings

Prof. Dr. Andreas Plückthun, Dr. Christian Zahnd and Dr. Beatrice Luginbühl

... for providing the clones of the antibody fragments
... for sharing their data
... and many helpful ideas

My former colleges at nanotype

... for the very productive time
... for the good collaboration on the protein biochip project
... for the excellent atmosphere until the bitter end

Hauke & Danielle

... for the many constructive discussions about the protein biochip project
... for the credit and the freedom in how to reach the goals of the project
... and thank you for still being valuable support and good friends

Julia

... for the extremely constructive collaboration in all our projects THANK YOU!!!
... for all the coffee and lunch breaks helping to solve almost every problem
... you have become a very good friend

Alan

... for your advice in many scientific and non-scientific problems
... for all the encouraging and inspiring discussions
... and most importantly: YOU ARE A CONSTANT SOURCE OF MOTIVATION